MODELING OF SPARK PLASMA SINTERING PROCESS

BY

MOHAMED ABDELMAGEED MOHAMEDZEIN

A Thesis Presented to the

DEANSHIP OF GRADUATE STUDIES

KING FAHD UNIVERSITY OF PETROLEUM & MINERALS

DHAHRAN, SAUDI ARABIA

In Partial Fulfillment of the
Requirements for the Degree of

MASTER OF SCIENCE

In

MECHANICAL ENGINEERING

MAY, 2016

KING FAHD UNIVERSITY OF PETROLEUM & MINERALS

DHAHRAN- 31261, SAUDI ARABIA

DEANSHIP OF GRADUATE STUDIES

This thesis, written by **MOHAMED ABDELMAGEED MOHAMEDZEIN** under the direction his thesis advisor and approved by his thesis committee, has been presented and accepted by the Dean of Graduate Studies, in partial fulfillment of the requirements for the degree of **MASTER OF SCIENCE IN MECHANICAL ENGINEERING**

Dr. Abul Fazal Arif
(Advisor)

Dr. Zuhair M. Gasem
Department Chairman

Dr. Sohail Akhtar
(Member)

Dr. Salam A. Zummo
Dean of Graduate Studies

Dr. Abbas Hakeem
(Member)

15/6/16
Date

Dedicated to my parents, who always encourage and support me in every step on my life, to my sisters and brothers

ACKNOWLEDGEMENT

I am deeply grateful to Professor Abul Fazal Arif for his guidance. He supported me and gave me a great help throughout my master program, and I really appreciate his perfect guidance. Thanks a lot to Dr. Hakeem Abbas for his great help and guidance in all the experiments I have conducted during this thesis work, and for his permission to use the lab facilities. I would like to thanks Dr. Sohail Akhtar for his guidance and advices, especially on the experimental part.

I would (particularly) like to thank Usama Siddiqui. His knowledge and experience played a great role in this work, he was always available for the help and corrections. I owe my deepest gratitude to Homam Jomaa. Without him this work would not have been possible, me and him worked as a team.

I would like to show my greatest appreciation to Abba Abdulhameed Abubakar for his great help and guidance. I received generous support from Kareem and Mohamed Elhady and discussion with them have been illuminating.

Advice and comments given by Dr. Khalid Alathel had been a great help during the progress presentations and monthly meetings. I have greatly benefited from Mr. Latif, he was very supportive and helpful whenever I need to use the material science lab facilities.

I would like to show my greatest appreciation to all Sudanese students in KFUPM and Sudanese faculties also, they helped a lot by support and relieving the pressure of the study, they gave the help whenever I needed.

TABLE OF CONTENTS

LIST OF TABLES

LIST OF FIGURES

LIST OF ABBREVIATIONS

CAPAD	:	Current Activated Pressure Assisted Densification
SPS	:	Spark Plasma Sintering
EM	:	Electro Migration
ST	:	Surface tension
DL	:	Diffusion under Load
PM	:	Powder Metallurgy
DC	:	Direct Current
γ_s	:	Surface free energy
μ	:	Shear modulus
PECS	:	Pulsed Electric Current Sintering
PDS	:	Pulse Discharge Sintering
PAS	:	Plasma activated sintering
FAST	:	Field Activated Sintering Technique
ECAS	:	Electric Current Assisted Sintering
HP	:	Hot Pressing

HIP	:	Hot Isostatic Pressing
FEM	:	Finite Element Method
$\dot{\varepsilon}$	:	Strain Rate
MMC	:	Metal Matrix Composite
XRD	:	X-Ray Diffraction
EDS	:	Energy Dispersive Spectroscopy
SEM	:	Scanning Electron Microscope
RGB	:	Red-Green-Blue
HV	:	Vickers Pyramid Number
BHN	:	Brinell Hardness Number
$\boldsymbol{\rho_{th}}$	:	Theoretical Density
$\boldsymbol{\rho_r}$	:	The ratio between the powder density and $(\boldsymbol{\rho_{th}})$
$\boldsymbol{\rho}$	:	Density
θ	:	Porosity
$\dot{\boldsymbol{e}}$	:	Shrinkage rate
J	:	Current density
E	:	Electric field strength

C_p	:	Heat capacity
K	:	Thermal conductivity
gb	:	Grain Boundary
$\dot{\varepsilon}_x$	:	Strain rate in (x) direction
$\dot{\varepsilon}_{crx}$	:	Power law creep strain rate
$\dot{\varepsilon}_{gbx}^{dl}$	:	Strain Rate resulting from (dl) through (gb) in (x) direction
$\dot{\varepsilon}_{gbx}^{em}$	:	Strain Rate from (em) through (gb) in (x) direction
$\dot{\varepsilon}_{gbx}^{st}$	:	Strain Rate from (st) through (gb) in (x) direction
G	:	The average grain size
α	:	Surface Tension
A_o	:	Power law creep frequency factor constant
Q_{cr}	:	Activation energy for power law creep
m	:	Power law creep exponent
R	:	Ideal gas constant
$\delta_{gb}D_{gb}$	:	Grain boundary diffusion frequency factor
Ω	:	Atomic volume
r_p	:	Pore size

$Z * e_q$	:	Effective charge
ec	:	Electric currents [Comsol abbreviation]
ht	:	Heat transfer in solids [Comsol abbreviation]
solid	:	Solid mechanics [Comsol abbreviation]
dode	:	Domain ODEs and DAEs [Comsol abbreviation]
ε_r	:	The emissivity constant

ABSTRACT

Full Name : [Mohamed Abdelmageed Mohamedzein Abdelhameed]

Thesis Title : [Modeling of spark plasma sintering]

Major Field : [Mechanical Engineering]

Date of Degree : [may, 2016]

CAPAD (Current Activated Pressure Assisted Densification) is a powder consolidation technique, where electric current is used to generate heat due to material electric resistivity. Pressure is applied simultaneously with the electric current to assist the densification process. Spark Plasma Sintering (SPS) is a CAPAD process in which the current is a pulsed direct current. It is a multi-physics process as it involves electrical-thermal-mechanical actions. Some of the fundamental mechanisms which are occurring during the SPS namely; creep, electro-migration, surface tension, and diffusion under load are responsible for the densification during the process. In the current work, a multi-physics model that simulates the SPS process has been developed, considering all the four densification mechanisms mentioned above. This model allows the investigation on the effect of different process parameters such as voltage, pressure, holding time, and heating rate on the quality and properties of the product like porosity, strain, and residual stress. The model also allows investigating the contribution of each densification mechanism on the process. The computational results are validated against experimental results by comparing temperature and porosity distribution. The validated model is used to conduct a parametric study. Some experimental investigation about the process parameters was conducted by producing aluminum/alumina composite samples and varying the pressure and temperature. Some properties were measured on the samples

such as the hardness to study the effect of changing the SPS parameters on the properties. Results of the model show that porosity is higher at the outer radius than the center of the sample. Creep is found to have the major effect in densification and electro-migration has considerable effect during the holding time.

ملخص الرسالة

الاسم الكامل: **محمد عبد المجيد محمد زين عبد الحميد**

عنوان الرسالة: **تصميم برنامج لمحاكاة طريقة الشرارة والبلازما للتشكيل من البودرة**

التخصص: **قسم الهندسة الميكانيكية**

تاريخ الدرجة العلمية: **مايو، 2016**

عملية التصليب بإستخدام التيار الكهربائي المباشر وبمساعدة الظغط، هي أحد عمليات تصليب البودرة. حيث يستخدم التيار الكهربائي لتوليد الحرارة، نتيجة لمقاومة المادة لمرور التيار الكهربائي من خلالها. يطبق الضغط علي البودرة بالتزامن مع مرور التيار الكهربائي، مما يساعد في عملية التصليب. تصليب شرارة البلازما هو فرع من عملية التصليب المذكورة أعلاه، يكون فيه التيار مباشر ومتقطع، وهي عملية تحتوي علي أكثر من فيزياء، حيث أنها تحتوي جانب حراري وجانب كهربائي وجانب ميكانيكي. تتسبب بعض العمليات الأساسية في عملية التصليب أثناء تصليب شرارة البلازما. من هذه العمليات؛ الزحف، الإنتقال الكهربائي، الشد السطحي، وإنتقال المادة بسبب الإجهادات. في هذا البحث تم إنشاء نموذج محاكاة رقمي يحتوي علي أكثر من فيزياء، بغرض محاكاة عملية تصليب شرارة البلازما. العمليات الأساسية الأربعة المذكورة أعلاه، تم إعتبارها في نموذج المحاكاة. يسمح النموذج بدراسة بعض العوامل المؤثرة في عملية تصليب شرارة البلازما، وتأثيرها في جودة المنتج. من هذه العوامل الجهد الكهربائي، الضغط، و المدة الزمنية التي تبقي فيها درجة الحرارة عند أعلي قيمة. من الخصائص التي يمكن قياس جودة المنتج من خلالها، الكثافة والإجهادات الساكنة. يسمح نموذج المحاكاة أيضا بدراسة مدي تأثير كل من العمليات الأساسية الأربعة المذكورة أعلاه في عملية التصليب وتماسك حبيبات البودرة. تم التأكد من إعتمادية نموذج المحاكاة، وذلك بمقارنة نتائج النموذج مع بعض قياسات التجارب المعملية، مثل درجة الحرارة، وتوزيع الكثافة في العينة المنتجة. في هذه الدراسة أيضا، تم إجراء بعض التجارب المعملية، لدراسة تأثير بعض عوامل عملية تصليب شرارة البلازما علي جودة المنتج. هذه التجارب تمت علي مادة مركبة من الألومنيوم وأكسيد الألومنيوم. وذلك بقياس بعض الخصائص في العينات المنتجة مثل الصلابة.

أظهرت النتائج المستخرجة من نموذج المحاكاة أن الكثافة في مركز العينة أعلي بقليل من الكثافة في المناطق المجاورة للأسطح الخارجية. كما أظهرت النتائج أن عملية الزحف لها التأثير الأكبر من بين العمليات الأساسية الأربعة التي تؤدي إلي عملية التصليب المذكورة أعلاه, وأن الإنتقال الحراري مؤثر بدرجة ملحوظة. خصوصا خلال فترة إبقاء درجة الحرارة عند أعلي قيمة لها

CHAPTER 1

INTRODUCTION

Powder metallurgy (PM) [1] is a type of manufacturing process in which engineering components are made from metallic powder. Thus PM has an advantage over conventional removal process, that it has lower cost, because the waste material is less in PM. It is a suitable manufacturing technique for high melting point material, such as ceramics. Because the maximum temperature in this process is lower than melting temperature. Design flexibility is also an advantage of PM, as it is used for producing tools and products with controlled porosity or nearly fully dense products, as parts can be produced in complex geometry like net shape. Other advantages of PM process are:

- Permits a wide variety of alloy systems
- Produces good surface finish
- Provides materials, which may be heat treated for increased strength, or increased wear resistance
- Provides controlled porosity, for self-lubrication, or filtration
- Facilitates manufacture of complex or unique shapes, which would be impractical or impossible with other metalworking processes
- Is suited to moderate- to high-volume component production requirements
- Offers long-term performance reliability in critical applications

Generally PM consist of three basic processes: powder blending, compaction, and sintering. Powder blending is done using a mixer to get good powder homogeneity, especially in case of composite materials. In compaction process most of the powder particles come into contact and stresses are developed inside the material. Compressed material is called green part. In sintering stage the high temperature lead the powder to form metallurgical bond between individual particles.

1.1 Sintering

Sintering can be defined as a thermal treatment of fine-grained material, at a temperature below the melting point of that material. As a result, the powder particles will bond together at the contact points, to form the desired solid piece. There are many types of sintering, like hot pressing, pressure less sintering, and SPS, in SPS technique, a uniaxial force is applied to the powder, and a pulsed (on-off) direct electric current (DC) passes through the powder, at a low atmospheric pressure. This technique has some advantages over other conventional techniques, like, the very high heating and cooling rates, which enhances densification over grain growth, and as a result maintaining the properties of the nanopowders in their fully dense product. When all densification is achieved by changing the powder particles shape, without the ability for particles to move freely, and arranged in the presence of liquid, in this case the sintering is called solid state sintering. But when some liquid presents as sintering temperature get high, this will help in rearranging the particles, and make it easy for them to slip over each other. This way, better compaction is achieved. Usually, the liquid amount will not be enough to fill all porosity at the initial

state. This small amount of liquid may be added as impurities during powder mixing and preparation. The physical phenomenon happened during the sintering process are complicated, and the interaction between them is not well understood.

At first stages of the process during the compaction, densification takes place by a combination of particle rearrangement, by sliding at grain boundaries, or by particle fracture. And grains change shape by plastic flow. After these stages, particles start to bond to each other. Interatomic forces act between them, and atoms or molecule start to feel attraction force at the region of contact. Material elastically deform forming a neck. the reason for this interatomic force, is the decrease in surface free energy, due to replacement of solid-vapor interface, which has high energy by solid-solid interface with lower energy [2] Figure 1.

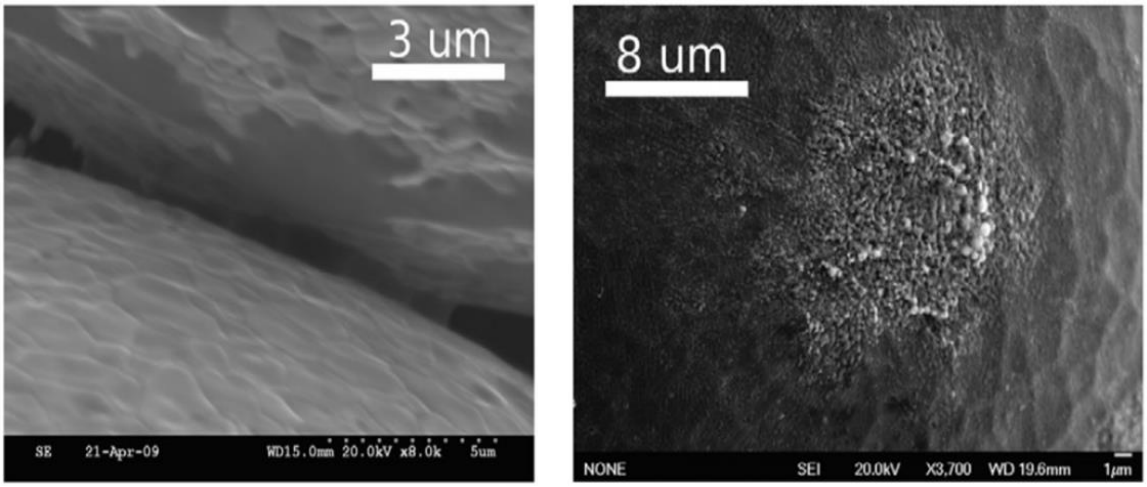

Figure 1. Neck Initiation [3]

By considering two particles after small neck formed, it starts to grow due to interatomic forces. The neck growth rate is governed by the equation

$$\dot{X} = \frac{C\,a^2}{x} \quad for\ X < \frac{\gamma_s\,a^2}{10\,\mu} \qquad 1\text{-}1$$

Where X is the radius of contact disc of two particles, γ_s is surface free energy, μ is the shear modulus, C is the velocity of sound, and a the radius of both particles in case they have the same radius. when this neck reaches a considerable size, (Figure 2) assumed by the above equation 1-1 by the limit of X, the surface energy of these two particles start to act as a driving force, which is trying to change the shape and reach a shape of the minimum surface area, which theoretically sphere. Because of the high-temperature, material find enough energy to diffuse, in order to accommodate the change in shape.

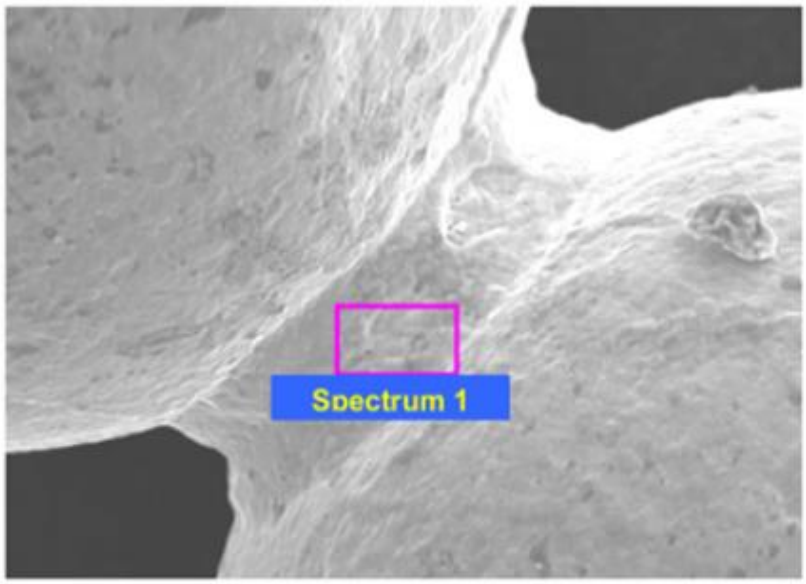

Figure 2. Neck growth [3]

If the material is amorphous, then matter flows just like a viscous liquid with high viscosity. The diffusion process is described completely by the stocks equation, and the continuity equation for an incompressible fluid.

$$\mu \nabla^2 u - \nabla p + f = 0 \qquad 1\text{-}2$$

$$\nabla . u = 0 \qquad 1\text{-}3$$

Where u is the velocity of the material, ∇ p is the gradient of the pressure μ is the dynamic viscosity, and f is an applied body force.

In case of crystalline particles, material is difficult to flow like in amorphous material, due to the ordered arrangement of the atoms. In this case, diffusion process, can be described by vacancy diffusion. Equilibrium condition in crystalline material is characterized by huge number of vacancies. Concentration of these vacancies on the surface of particles depends on the curvature. When there is a difference in the curvature vacancies concentration become unequal throw the surface (vacancy is an absence of an atom or molecule). In the presence of temperature, vacancies find the required energy to diffuse, trying to achieve the equilibrium of vacancies concentration. Diffusion of vacancies in one direction means diffusion of material in the opposite direction. Depending on material properties and some factors the diffusion takes place through many paths as shown in Figure 3. All these diffusion mechanisms may happen simultaneously depending on material properties and temperature. The driving force is surface energy. In the class of the pressure assisted sintering types like hot pressing and (SPS), the driving force for diffusion is more than surface energy alone. Adopting

Nabarro-Herring and Coble creep may lead to more accurate results for the contribution of applied pressure.

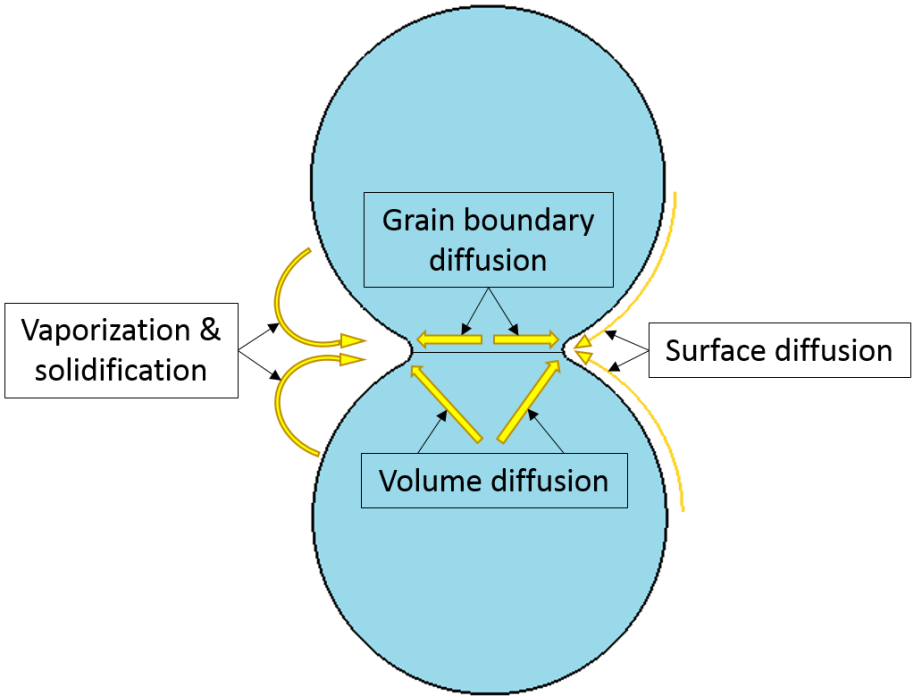

Figure 3. Diffusion Mechanisms

Material diffuse towards neck surface from other surface positions in case of surface diffusion, and from the interior lattice in case of volume diffusion. The grain boundary diffusion term, refer to the diffusion at the grain boundaries in the contact region between the two particles. This region is a preferable destination for the vacancies located at the neck surface. As a result the accumulation of vacancies in the boundary between the two particles create a phenomena often called Plating (Figure 4), where vacancies form a shape of disc in this region. Material tend to fill this region through an inward movement of both particles in a rigid body motion leads to shrinkage and densification.

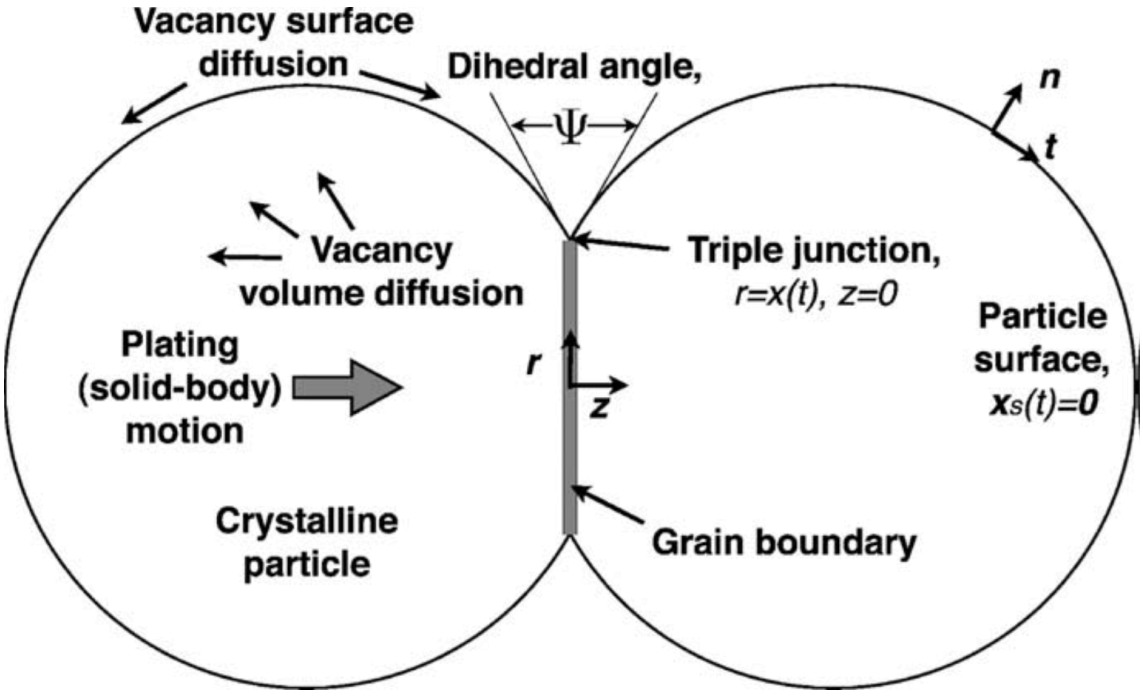

Figure 4. Grain boundary diffusion and plating by [4]

1.2 CAPAD and SPS

CAPAD is one of sintering techniques, where electric current is used to generate heat due to material electric resistivity. Pressure is applied simultaneously with the electric current to assist the densification process. CAPAD is one of the advanced sintering methods in which the heating rate is very high as well as the cooling rate, leading to reduce the grain growth [5]. Unlike the conventional methods, as a result the intrinsic properties of the powder is maintained in the dense product. SPS is a CAPAD process in which the current is a pulsed direct current with high frequency. The pulsed direct current leads to the formation of sparks between powder particles. These sparks is claimed to be one of the reasons of superior properties in the products of SPS. It is claimed also plasma is formed

in the contact region between the particles, and this is the reason for the name Spark Plasma sintering. But there is no experimental evidence on that [6].

1.2.1 (SPS) system and components

The SPS system [7] (Figure 5), consist of upper and lower punches, the die, pulsed direct current generator, and a thermocouple to control temperature. All these components are placed in a vacuum chamber. The pressure is applied through the upper and lower punches by a pneumatic system. The pulsed direct current flow in the die, punches, and the powder. The whole system is heated up by the effect of joule heating.

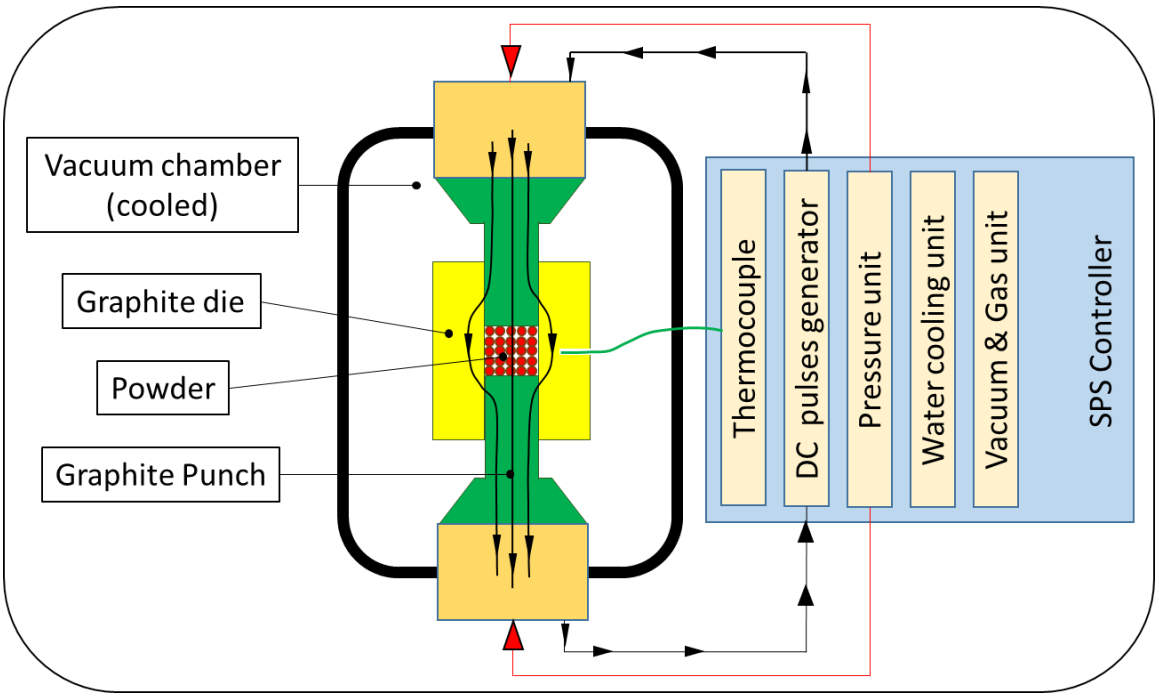

Figure 5. SPS components

In this system heat is generated exactly at the contact points between the particles, where the heat is needed, as these are the locations of bonds formation (Figure 6). The enhanced mechanical properties of products produced by these advanced sintering methods are reported in many scientific articles, for instance, the tensile strength of SPS sintered objects was found greater than those objects produced by the isostatic press with the same density.

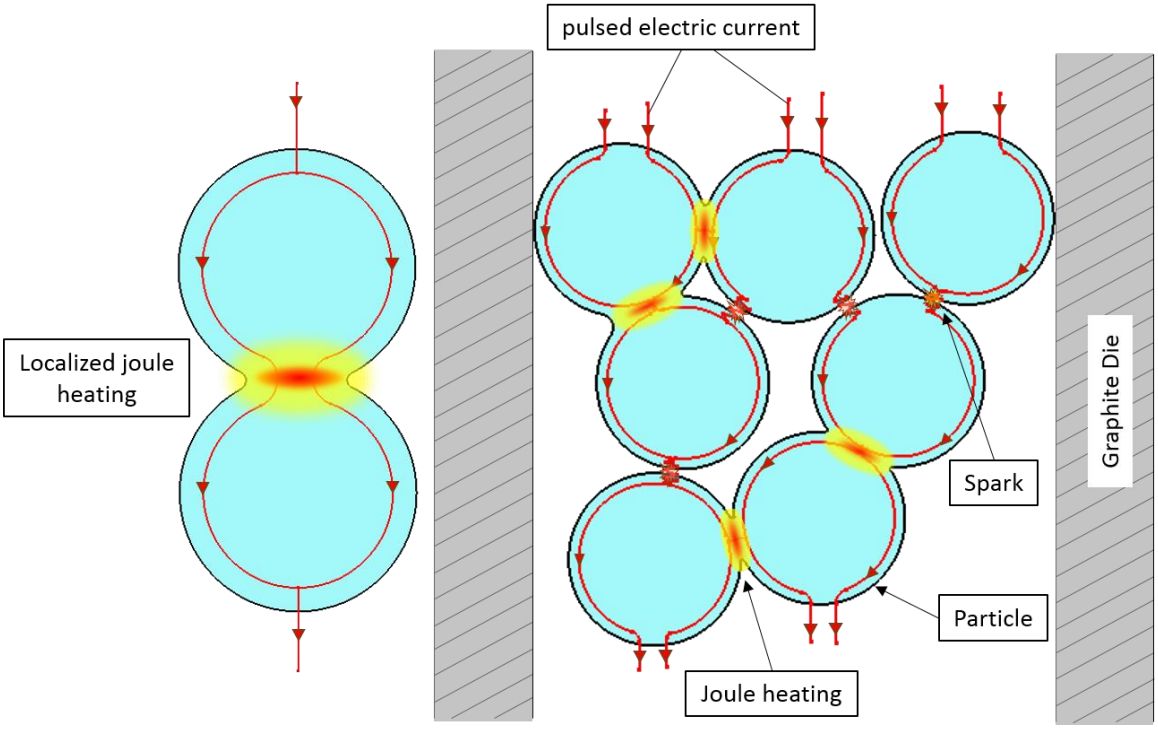

Figure 6. Joule heating & sparks generated between particles

For achieving high density and good bonding between metallic powder particles the temperature of the powder should be high enough. Usually resulted density at the center of the sample is high due to high temperature in this region; also there a tendency for high density at the two ends of the sample. SPS is also called resistive sintering, according to electric current cycles and the machines commercially produced a variety of

names and acronyms were designated for each type, SPS is the most produced type among them (Figure 7)

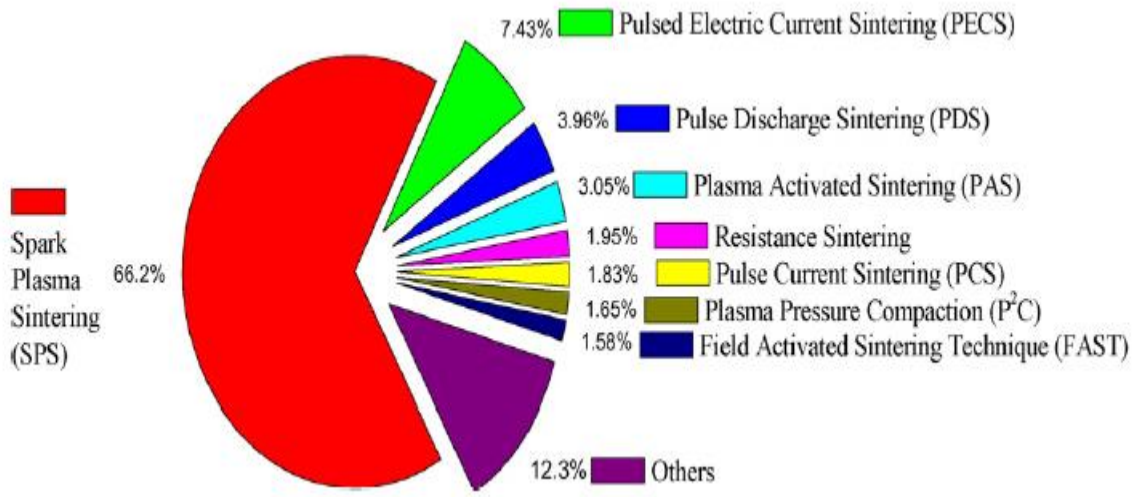

Figure 7. Different Commercial CAPAD apparatus developed [8]

1.2.2 Advantages of (SPS) and advanced sintering methods over conventional methods

As mentioned above, advanced methods improve properties and facilitate the process allowing more production with high quality. Some of these advantages are listed below

- Possibility of producing advanced ceramics, composite material, and advanced metal based composite

- Specific and tailored properties can be produced for some advanced technology objects
- Reducing sintering time dramatically from hours to minutes
- Produce high density with lower temperature than conventional sintering temperature
- Lower pressure
- Reducing grain growth and give fine microstructure
- High homogeneity in products because it reduces temperature gradient
- High density
- High densification rate
- Good electrical properties
- Good bioactivity

Some of the claimed reasons for these advantages in SPS and resistive sintering techniques is not convincing for some researchers, as it has no experimental evidence. Joule heating effect is well understood and proved. But others like spark formation between particles, and plasma formation, and pulsed current also claimed to remove oxides at the contact regions leading to cleaning effect and facilitate bonds formation, no evidence reported on them.

1.3 Motivation

- Although SPS has very good properties, but still there is a room for improvement, by reducing porosity gradient of the final product and, hence improving the quality.
- Also, this process results in some stresses inside the products at the end of the process, which may reduce the life of the product and, cause unpredictable failure.
- The gradients of the final porosity, may results from the variation of temperature and stresses inside the sample during the process.
- So, there is a need for a comprehensive study about temperature and stresses fields while densification is happening during the process. In another word in-situ monitoring, which very difficult or impossible to be carried out during the SPS process.
- A finite element model could be an effective tool to study temperature and stress inside the sample during the process. The model should capture the densification during SPS process considering its most effective fundamentals densification mechanisms.
- This model could also be used to study the densification mechanisms, and enhanced our understanding of the fundamentals aspects of SPS process, which is still not well understood.
- Objects produced using SPS process maybe produced in a desired porosity value. Using the reliable model, one can set the necessary process parameters to achieve the desired porosity value.

- A reliable model could be used to set the process parameters to get a controlled prosoty. In some application porous objects are desired, for instance in some cases presence of pores may enhance the fracture toughness [9], [10], and [11]

1.4 Objectives

- Develop a constitutive model for SPS process, considering most effective densification mechanisms.
- Validate the model experimentally.
- Use the model to predict some properties, like thermal gradient, residual stresses, and strains.
- Use the model to design the process parameters and the die to produce cutting tool inserts having a net shape and some necessary properties for its usage.

1.5 Thesis outlines

- In chapter two, there is a discussion on the previous work done in this area, and discussing finite element models and their considerations.
- Chapter three contains a description of the experimental work being done to validate and calibrate the model. This work played a great role in developing a good constitutive model that gives results close to reality. The chapters also discusses some experimental study results.

- Chapter four describes the mathematical formulation of the developed model and densification mechanisms considered. Implementation of the model inside Comsol software environment is also discussed. At the end of this chapter calibration and validation of the model is described.
- Chapter five includes the results and the discussion.
- Chapter six include recommended work, and the improvements which can be done on the model.

CHAPTER 2

LITERATURE REVIEW

PM [1] is a widespread process used for the production of many engineering objects and tools. Because of the advantages of this process mentioned in chapter one, there is a lot of research and published work in this area. Especially CAPAD process as it is an advanced process, publication in that area increased dramatically in the past three decades as shown in Figure 8.

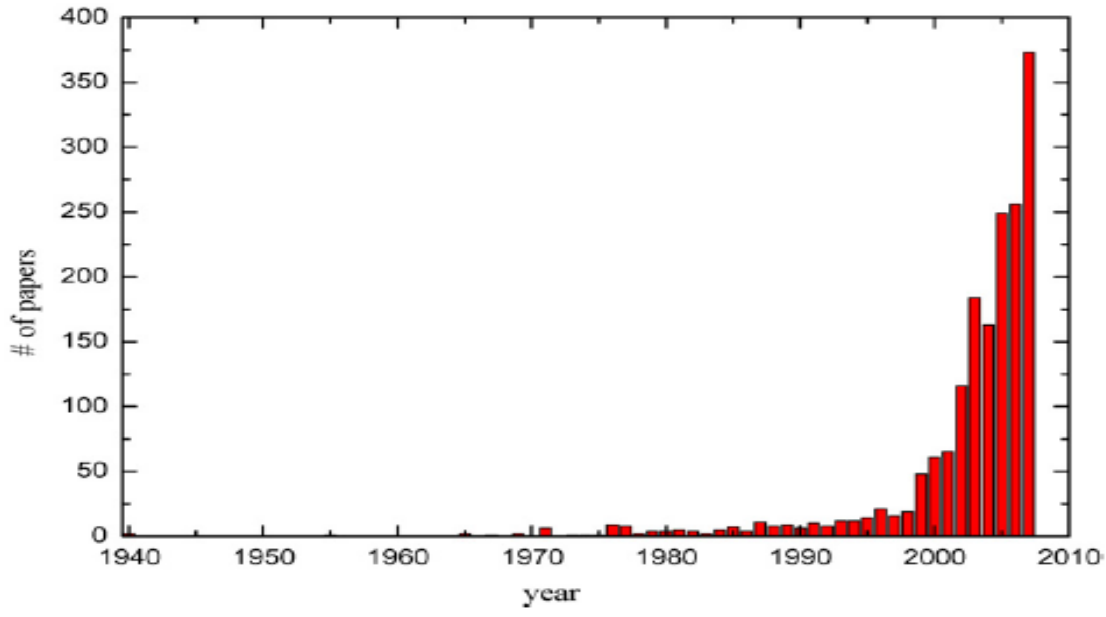

Figure 8. Number of publication on CAPAD by years [8]

This types of sintering were first to appear commercially in japan, and it still used there and in eastern of Asia more than other places. It makes sense that majority of published work is coming from japan and Korea as shown in Figure 9

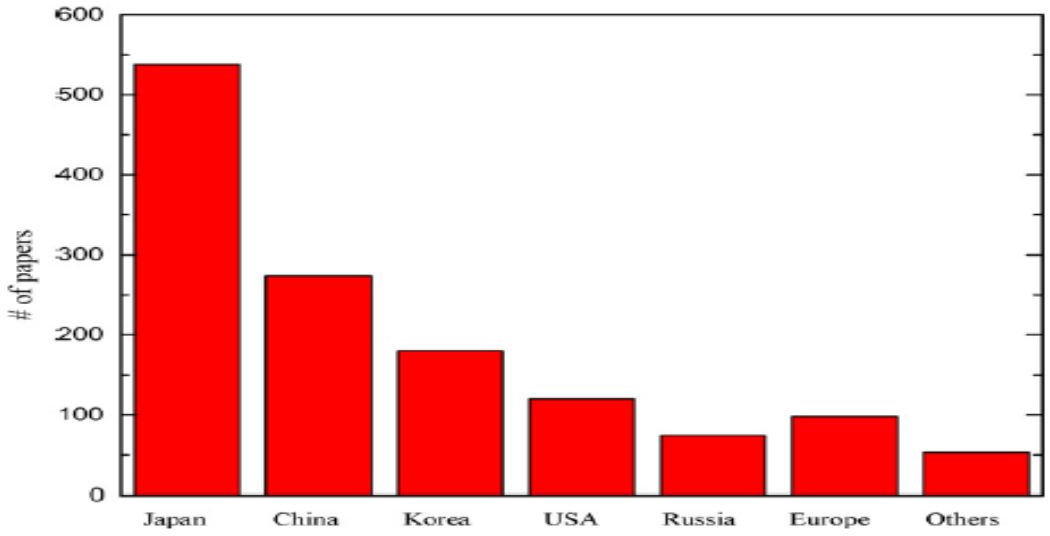

Figure 9. Publications by countries [8]

Regarding modeling and simulation in this area, a lot of models tried to capture the densification process on a very small scale, to the size of the powder particles. Generally, in these models, there is a focus on diffusion paths, like surface diffusion, volume diffusion, and grain boundary diffusion. Very few authors consider evaporation.

2.1 Meso-scale modeling

Robert L. Coble [12] developed an analytical model for initial intermediate and final stage of hot pressing sintering densification under pressure. Which explicitly include both, the surface energy and applied pressure as driving forces. He also used Nabarro-Herring creep and coble creep models to approximate densification rates for lattice and boundary diffusion models respectively. For the final stage when density reaches high-value about 95% he used an alternative model depending on the material diffusion transport because the model for the intermediate stage is not valid.

In the last stage, when pores are isolated, achieving theoretical density may become difficult if some non-diffusing gas is present inside the pore [13]. In most case near fully dense material can be produced, but it is difficult to get fully dense product.

M.F ASHBY [2] constructs two forms of diagrams, these diagrams include six mechanisms, which contribute to the sintering process, and he did not include the applied stress. The diagrams show at a given temperature, particle size, and neck size, the dominant mechanism and show the rate of sintering that all the mechanisms acting together produce. But the six mechanisms considered in his work were resulting from only one driving force, which is the surface tension. This is one of the most important charts in sintering related to conventional sintering by just heating the green powder by a normal conduction heating. The six mechanisms are;

1. surface diffusion

2. volume diffusion, considering the source of the material is the surface of the particles
3. vapor transport
4. grain boundary diffusion, with the material source is the grain boundary itself
5. another volume diffusion, but from a different material source, which is the grain boundary
6. A third volume diffusion, with the material sourced from dislocations.

Material from all these sources is sinking into the neck.

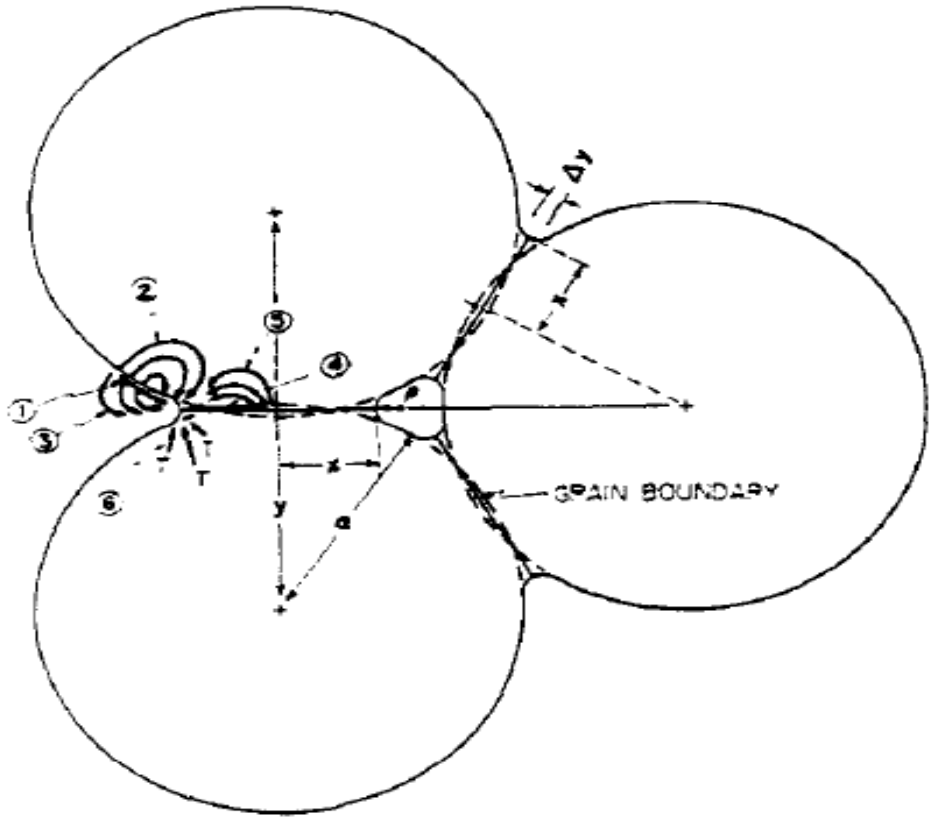

Figure 10. The six possible paths for diffusion [2]

Figure 10 describes the six diffusion paths. There are two mechanisms, No (4) and No (6), resulting in the centers of the particles becoming closer to each other during the sintering process, the other four contribute only to the growth of the neck.

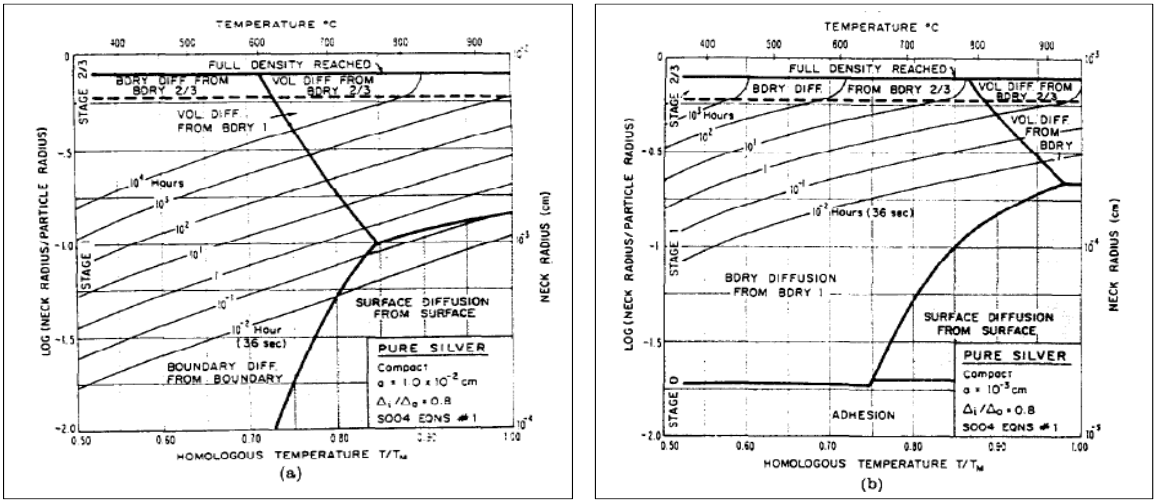

Figure 11. Sintering diagrams for silver spherical particles [2]

Figure 11 shows the sintering diagram for tungsten (a) indicating the dominant mechanisms, and (b) shows the neck size for a given time and temperature.

F.B SWINKELS and M.F ASHBY [14] add new ideas to the first sintering diagram, like the coupling of boundary diffusion and surface diffusion. New criteria for the stages of sintering. An approximate treatment of particles rearrangement. The diagrams show how both, the neck size and the density of compact of wires and spheres, change with time and temperature. They illustrated the usage of these diagram by analyzing sintering data for the two types, wires and spheres of stainless steel, Cu, Ni, NaCl, Fe, and W. In this work they describe two approaches for assembling the sintering model in the diagrams that can

be used to obtain useful information, like the neck size, and the density, as they varied with time and temperature. In 2009 Olevsky [15] extend the MSC concept using constitutive formulations. This approach is useful to obtain material properties in numerical models A.JAGOTA and P.R DAWSON [16] studied the compaction of particles by developing a micromechanical model for a unit problem (Two particles). The objective of the developed model is to study the interaction behavior of the particles. As the general trends of these small scale models they considered only the surface tension between the particles. So the model is not suitable for hot pressing sintering type. In this case, the effect of the pressure on the diffusion should be considered. To describe the state of densification in hand, he used the contact area as a variable which change with the process time and represents the densification at the moment. A.JAGOTA and P.R DAWSON [17] develop a numerical model to simulate the viscous sintering for amorphous material in 2D. In this case, material will not flow in the different diffusion paths separately as mentioned earlier, instead, material will flow from every location in the particle towards the neck, just like a fluid, but with high viscosity.

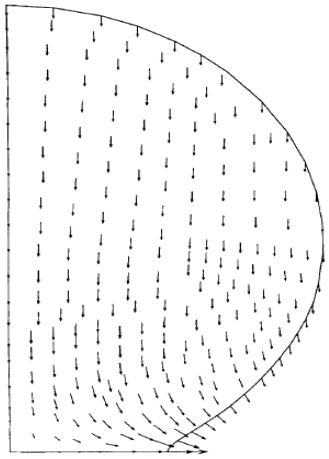

Figure 12. Velocity field [17]

Figure 12 shows the velocity field. The simulation shows that, velocity near the neck region is very high relatively when compared to other locations, because the energy of the driving force is high due high curvature.

J. PAN and A.C.F. COCK [18] coupled the finite element method with finite difference method to develop a numerical model that simulates the surface diffusion coupled with grain boundary diffusion, he simulates the sintering of a closed packed array of cylinders with the same sizes and with different sizes. In his routine the surfaces locations are determined from the two diffusion processes. This method has potential to simulate other phenomena rather than sintering, like void growth resulting from diffusion and creep crack propagation.

$$\bar{v}_{s,ip} = -\frac{\bar{J}_{s,ip+p} - \bar{J}_{s,ip-p}}{\Delta s_{ip}} \qquad 2\text{-}1$$

This formula determined the velocity of the each point, but not for the tip and two neighbors point. The picture shows the discretization of the free pore surface.

JORGE I. MARTINEZ et al [19] developed a 3 dimensional axisymmetric particles finite element model for viscous sintering of amorphous material. They considered several initial configuration. The basic of this work was the previous model of A.JAGOTA and P.R DAWSON [17]. The model cannot capture the case of particles with different materials. The advantage of this model is the study of the effect of different initial configuration, he studied two spherical particles with different sizes, four particles

different ratio is considered [(1:1), (1:4/3), (1:2), and (1:4)] he found (1:4) has high densification in shorter time when compared to the other ratios as shown in Figure 13.

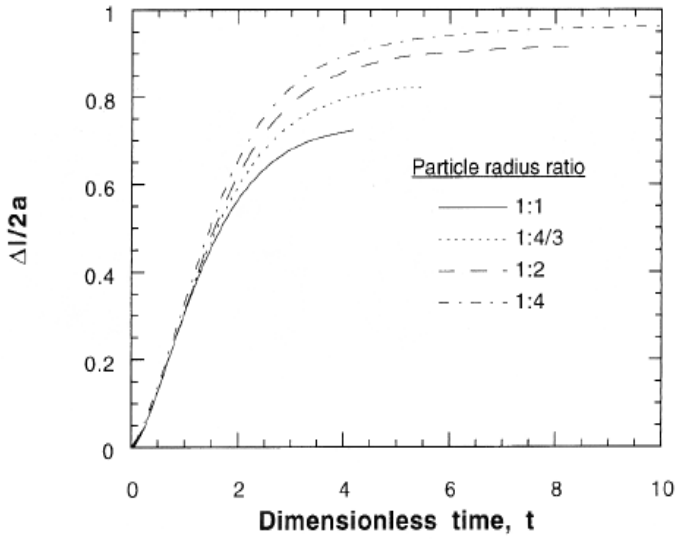

Figure 13. Densification for different particles radius ratios [19]

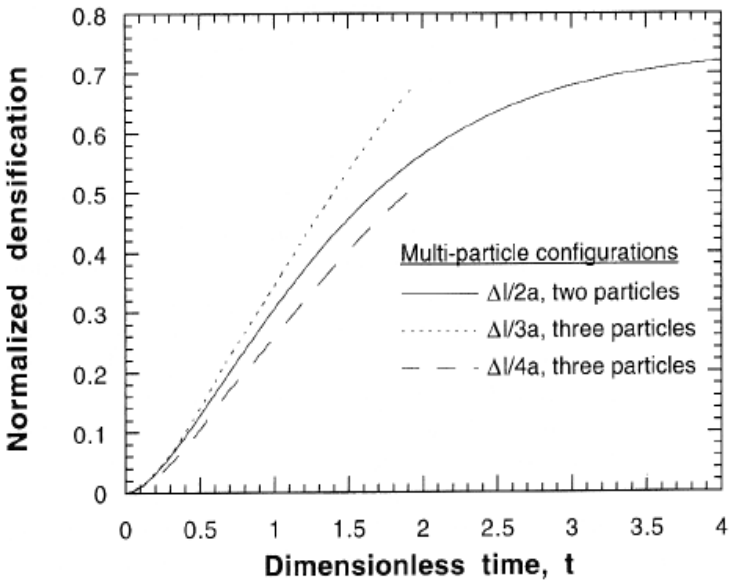

Figure 14. Densification for different particles configurations [19]

Also for the case of three particles compared to two particles shrinkage calculated in the axis of the particles, results are shown in Figure 14. HADRIAN DJOHARI [20] developed a finite element model for diffusion process in the crystalline material without considering applied pressure. The model considers two particles. Surface diffusion is coupled with volume diffusion and grain boundary diffusion. Vaporization and condensation are neglected. A balance equation in dimensionless according to Fick's law,

$$\nabla^2 c = 0 \qquad 2\text{-}2$$

And relation between curvature and vacancies concentration given by

$$c_x(1-c) = k \qquad 2\text{-}3$$

Then the balance equation for surface diffusion can be written in the form

$$n.\dot{X}_s = n.\nabla c + \alpha\nabla_s^2 \ along\ x = x_s \qquad 2\text{-}4$$

Maximenko and Olevsky [21] introduced the idea of the effective diffusion coefficients, which are grain boundary coefficients taking into account the volume diffusion. Using this technique, allows simulating a three dimensional problem into two dimensional problem. YU U. WANG [22] developed a phase field model for solid state sintering. The model treats rigid body translation and rotation of powder particles, grain growth through boundary migration, and various diffusion mechanisms including surface diffusion, grain boundary diffusion, volume diffusion, and evaporation and condensation. Phase field modeling is very powerful tool and effective technique. This model consider all possible

material paths possibility, two based equations are used, Cahn-Hilliard equation for nonlinear diffusion, and Allen-Cahn equation for structural relaxation. M.M.Ristic, and S.Dj.Milosevic [23] presented Frankl theory which was the first theory explaining sintering process physically, it describes the process in two consecutive stages of a viscous flow of crystalline material, due to the surface tension. In the first stage, contact area between particles increase gradually, after the pores become isolated. In second stage pores tend to disappear totally.

DUSTIN M. HULBERT [6] and others, conducted an experimental study regarding the presence of momentarily generated plasma between particles during SPS process, as it is proposed earlier that, plasma in one of the reasons of enhanced sintering abilities of SPS process. The study advocates the absence of plasma during SPS. HADRIAN DJOHARI [24] developed a 2D finite element model for sintering process, considering two particles and ignoring the applied pressure. He compares the results of viscous sintering of amorphous material with the sintering of crystalline material. He also compared surface diffusion with volume diffusion, and when they are coupled. Results show that, the viscous flow of amorphous particles, leads to the growth of the neck and shrinkage, by shortening the distance between centers of the particles at the same time. For crystalline material neck growth happened more than shrinkage, due to material diffusivity nature. Unexpectedly, the simulation shows that, when considering the surface vacancy diffusion alone, the system will elongate instead of shrinkage

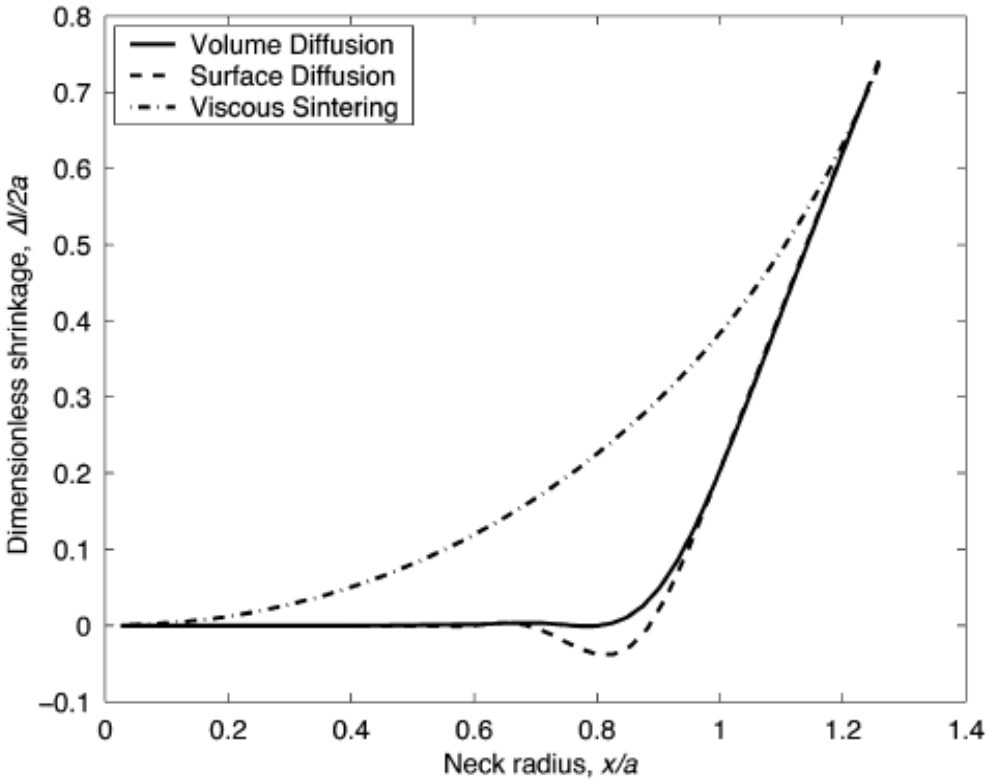

Figure 15. Shrinkage of two particles considering different diffusion paths [24]

Figure 15 describes the difference between the three categories, as the little pump in surface diffusion shows the strange behavior discussed above. HADRIAN [4] developed a 2D finite element model for two particles of crystalline material, by adding the effect of grain boundary diffusion and compared it with the previous case, when he excluded the grain boundary diffusion. As a result, he found a great shrinkage in the onset of the sintering process, when including the grain boundary condition. This effect is referred to the plating effect, resulting from diffusion of the material to the grain boundary, exactly at the neck. JULIAN BRUCHON [25] and others developed a numerical strategy to simulate the material diffusion by surface diffusion and volume diffusion, based on two ideas, using eulerian description and using level set function. The change in the external

shape can evolve through a fixed mesh. This approach removes the restriction in the number of particles used in the model. In this study it is applied on a granular packing. DMYTRO DEMIRSKYI [3] and others conduct an experimental study on the neck growth kinetics of free packed spherical shaped without binders of tungsten carbide particles during microwave and SPS sintering. The surface diffusion is a primary mass transport mechanism for microwave sintering, and the grain boundary diffusion and power low creep was the main mechanisms for neck growth in SPS sintering. Also, in both sintering types, the neck growth rate is faster than in conventional sintering by up to 100 times.

2.2 Macro-scale and continuum modeling

Olevsky [26] developed a continuum theory of sintering, which predict the macroscopic behavior of porous bodies during sintering. Because the models which discuss the sintering behavior into the scale of individual particles and the interactions and bonds between them does not give the full picture of the process. But there are macroscopic behavior affecting the process and the quality of sintered product, for instance, the applied load and the constraints of the powder by die and punches. Also the properties of powder in this macroscopic scale, will not be uniform, due to distribution of the powder before the sintering process. This approach based on non-linear deformation for porous material and the plastic deformation. The porous body is considered as a body consisting of two phases, one is the bulk material itself, and the other is the pores. He considered

very wide assumptions relating to the real application. For example, the constitutive parameters are depending on porosity. The application of uniaxial pressure is common in many application like SPS and hot pressing. Plastic deformation and diffusion resulting from the external load are considered which is essential in SPS. The shape of pores also has a great effect on the kinematics of sintering, for this reason, he considered two different morphology and the distribution of these pores. First, he proposed a circular shape with two different sizes most small size and few of bigger size. The effect of the pores shape on anisotropy during the sintering process, it is a well-known phenomenon, take for instance the case of sintering of wires, the cylindrical shape will cause the densification in the axial direction to differ from the radial one.

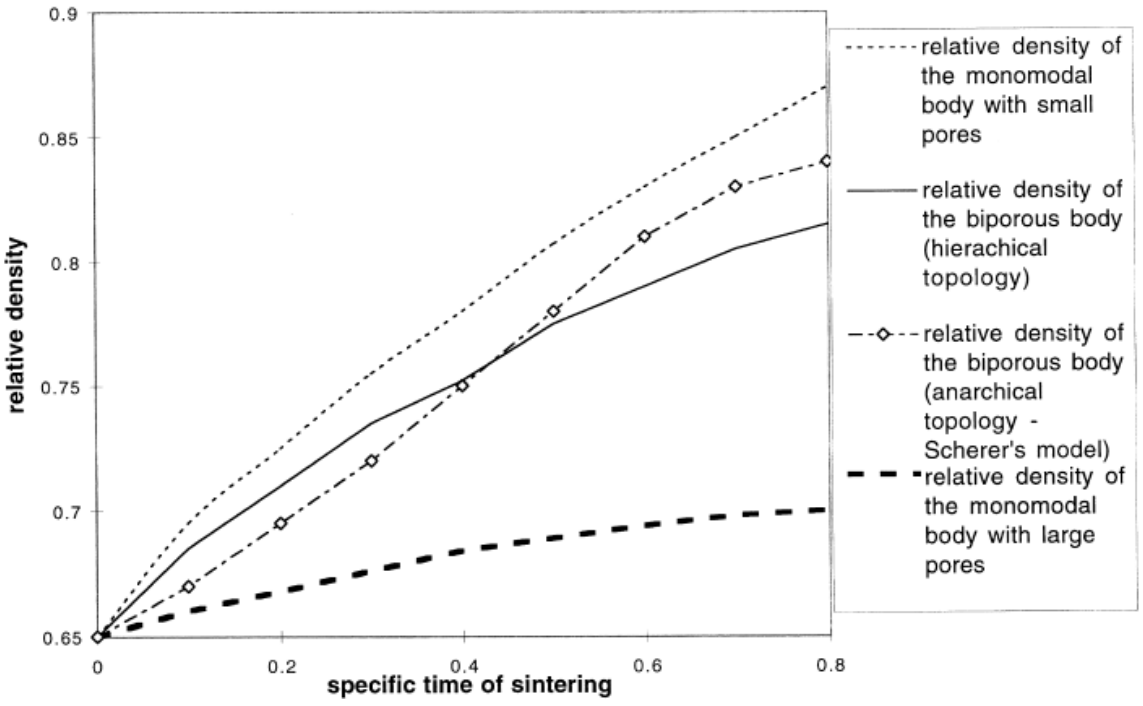

Figure 16. Comparison between calculations done by Sherer's model & Olevsky for bi-porous topology [26]

For this case an ellipsoid pore shape is considered with the same size distributed uniformly, the nature of this shape results in anisotropy in the densification process. Figure 16 shows the differences between Olevsky's model and Sherer's model for bi-porous topology.

Olevsky [27] also developed a constitutive model for SPS, considering the conductive materials. This model covered many types of diffusion mechanisms, the power law creep which is found to be a dominant mechanism, electro-migration resulting from the high direct current used in SPS system, the effect of the external pressure from upper and lower punches on the diffusion process, and the diffusion resulting from surface tension force. Power law creep is consisting of dislocation glide and climbing at the time, the strain rate is the lower rate in the two mechanisms, climbing is considered a diffusional process. The other three considered mechanisms are diffusional, which in reality take place through many paths like surface diffusion, volume diffusion, grain boundary diffusion, and evaporation then condensation in the neck region, due to the fact that grain boundary diffusivity is much larger than other paths, and the difference is high between the values he considered grain boundary diffusion only. The work is based on his continuum theory, by considering that densification will happen in one direction along the axis of external pressure, which is the direction of direct current flow. The ellipsoid pore shape distributed uniformly. His model shows that powder particles size and pores size are greatly affecting which diffusion mechanism is dominant, for 40 micron particle size the dominant mechanism is the power low creep, but with time when pores become small and if particle size is very small electro-migration become dominant, if the powder become in nano-size surface tension will play great role. Strain rate calculated from each

mechanism in one direction is added together and used to calculate the relative density for aluminum powder. His results are validated against experimental data from literature with very good agreement. He used the study of densification mechanisms dominance to construct a map for aluminum powder shown in Figure 17. The map is divided into three main regions according to the powder particle size and porosity, when porosity is high creep is always dominants.

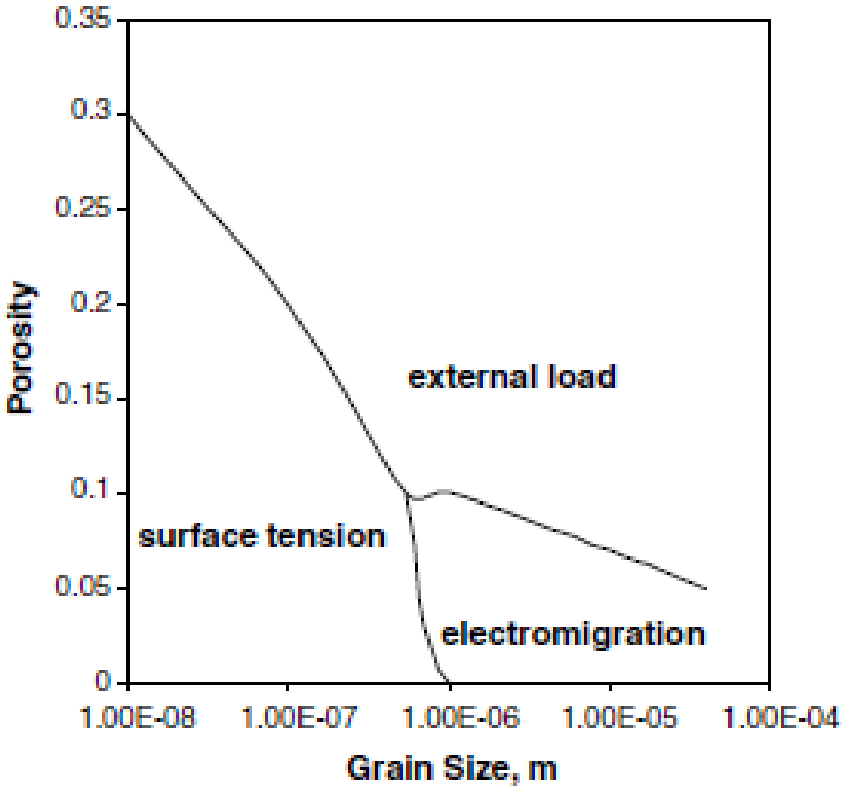

Figure 17. Aluminum densification map [27]

Z. A. Munir & U. Anselmi-Tambarini [28] in a review of SPS showed the effects of the pressure on sintering as a driving force besides the surface energy. Also, when the size of

the particle related to surface energy is small, then the relative contribution of the pressure is small. But becomes significant as the particle size increase. Regarding the effect of the pulsing of direct current during the process, and it's claimed advantage of producing plasma and sparks between the particles resulting in improved final properties, Xie et al. investigated this effect experimentally by producing many samples of aluminum with different pulse frequencies, they did not found any effect on porosity or electrical conductivity or elastic modulus. Results on the effect of heating rate on properties of the final product show that when sintering the powder without applying any pressure, densification is enhanced. When studying the on grain growth as well as densification some experiments show no effect on grain size for MoSi2, but for alumina results indicate an inverse relationship. Shen et al reported that heating rate has a small effect on densification of alumina up to certain value 350 ℃/min, after this value, density will decrease by increasing heating rate. also, there is a strong dependence of grain size on low heating rate as the grain size decrease by increasing the heating rate.

ROBERTO ORRU [8] and others conduct a review study on synthesis and consolidation of materials by Electric Current Assisted Sintering ECAS. They reviewed more than a 1000 published papers. The review shows that through ECAS technique one can fabricate advanced ceramics, metal based and composite materials. And give the possibility to fabricate high tech parts, by tailoring properties that cannot be achieved by conventional sintering. Some advantages of ECAS technique over Pressure Assisted Sintering technique PAS like hot pressing HP or HIP are the shorter sintering time, lower temperature and pressure, fine and homogeneous microstructure, higher density and densification rate, improved mechanical properties, and improved electrical properties

and bioactivity. Each property mentioned above were mentioned in the literature in some specific material. Some of the explanations for the advantages of ECAS like the spark between particles, momentary plasma formation, removing the oxides and cleaning of particles surfaces, they were not confirmed experimentally. Wang [29] and others conducted a finite element simulation for the distribution of temperature in the axial direction and radial one. The heat flux and electric flux pass through the whole device and the sample during SPS. Some of their results that during the SPS process the temperature gradient in the sample depends on the thermal conductivity of the powder, time, and electric power. The temperature gradient is high if the powder conductivity is low or the time is short. The temperature distribution in the conductive material is found to be different from the distribution of a non-conductive material as shown in Figure 18, which is making sense because electric current will differ resulting in more uniform temperature in a non-conductive material. In both cases, the temperature at the center is higher than the temperature at the outer radius. But generally, the gradient is not high.

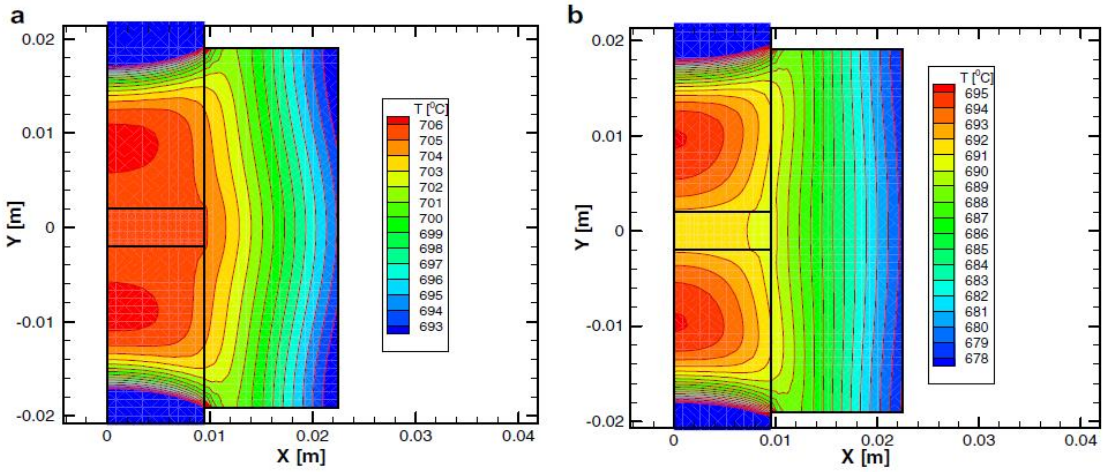

Figure 18. Temperature distribution for copper & alumina [29]

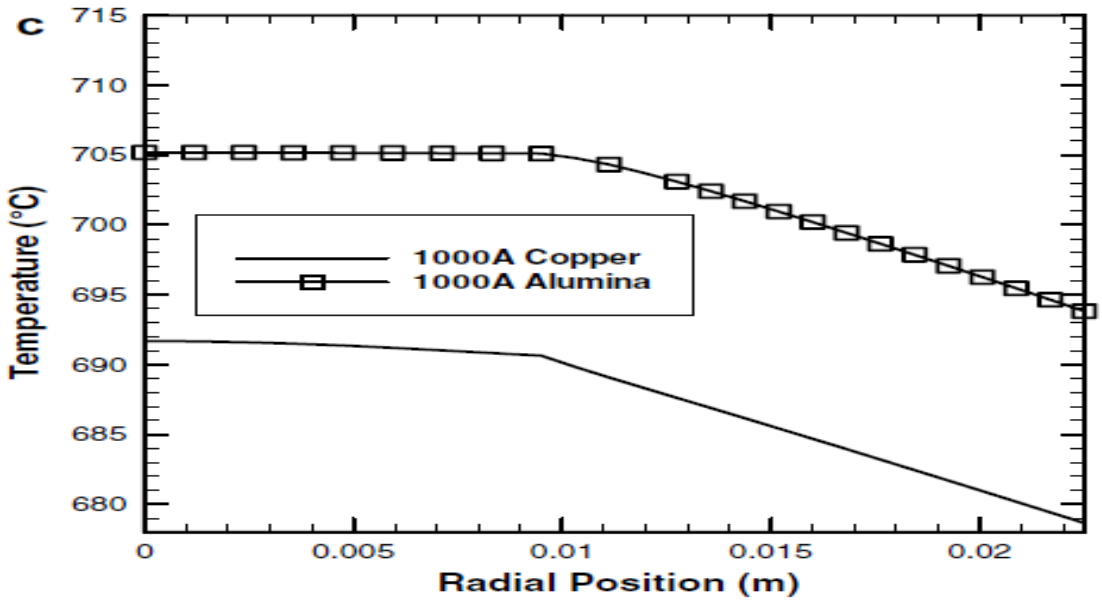

Figure 19. Temperature distribution [29]

The stress gradient is higher than temperature gradient which is shown in Figure 19, and the only high stress is the vertical stress as shown in Figure 20

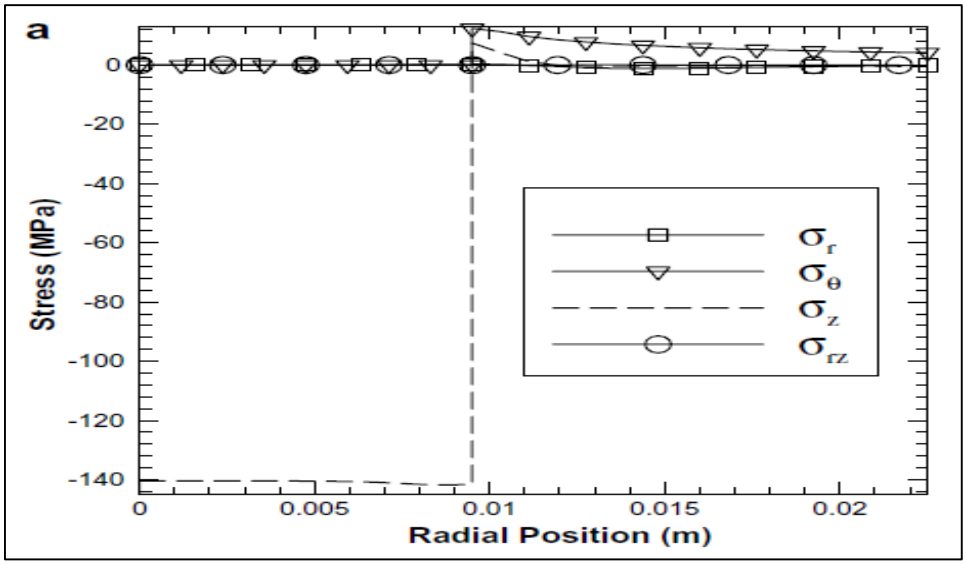

Figure 20. Stresses distribution for alumina [29]

CAO WANG [30] and others developed a thermal-electrical-mechanical coupled, dynamic FEM to study the temperature and the stress distribution in the specimen in SPS process. They also studied the densification by using a moving mesh. COMSOL was used to develop the model. The temperature profile for alumina, shows the same trend resulted from previous work of Devesh Tiwary [31]. But the vertical stresses is much lower as it reaches 50 MPa.

PAMELA MONDALEK [32] and others conduct a 3D finite element analysis, for electrical-thermal-mechanical coupled simulation and dynamic for SPS process, based on CEMLIB, using monolithic approach. For densification, they took into account the change in porosity during the process, the strain rate is considered a sum of four components as in the equation

$$\dot{\varepsilon} = \dot{\varepsilon}(pl) + \dot{\varepsilon}(dl) + \dot{\varepsilon}(em) + \dot{\varepsilon}(st) \qquad 2\text{-}5$$

Where $\dot{\varepsilon}(pl)$ represent the strain rate due to plastic deformation, results from the pressure during the process, $\dot{\varepsilon}(dl)$ strain rate due to material diffusion occurred because of the pressure, $\dot{\varepsilon}(em)$ is the strain rate due to electro-migration results from the direct current, and $\dot{\varepsilon}(st)$ is the strain rate results from material diffusion due to surface tension. In their study, they considered the plastic deformation only, and neglect the others three terms as plastic deformation has the largest value. Some of the results that, in alumina the increase of electrical conductivity leads to the high-temperature gradient in the powder. Results show that geometry of the sample, die, and punches are strongly affecting the electric current and temperature distribution in the compact powder. Also, the temperature distribution in the vertical direction is not quite symmetrical, because not all condition are

symmetrical in this direction. They used the model to a different shape rather than the simple disc, porosity distribution in the new shape has high gradient, due to change in stresses and temperature profile, resulting from the new contact area between powder and the die.

JING ZHANG & ANTONIOS ZAVALIANGOS [33] create a simulation of thermos-electric behavior in SPS. They studied the effect of the DC pulses frequencies on the temperature distribution and heating rate. Results show that pulsed current is better than direct current, as it gives higher heating rate and more uniform temperature distribution. Another results, that due to applied uniaxial pressure the thermal and electric conductivity shows higher value in the same direction and lower value in the normal direction.

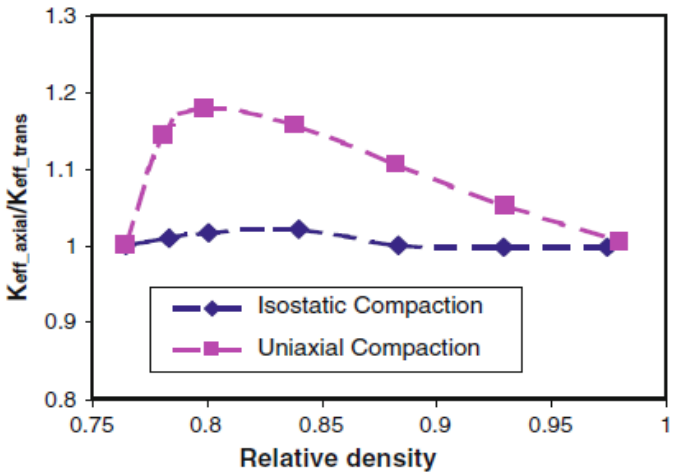

Figure 21. The ratio between axial and radial values for thermal conductivity [33]

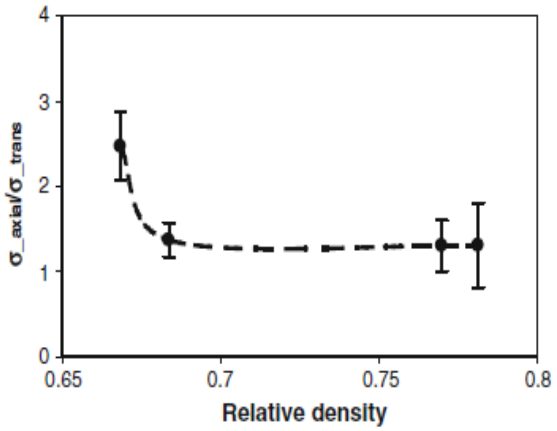

Figure 22. The ratio between axial and radial values for electric conductivity [33]

Figure 21 shows the simulation results for the evolution of the thermal conductivity, by taking the ratio in the axial direction and the radial direction. In the case of uniaxial pressure the ratio become high before high density is achieved. But when reaching high relative density, effective thermal conductivity tend to become equal in both directions. Figure 22 shows experimental measurement for electric conductivity, and it shows the same trend of thermal conductivity.

McWilliams and Zavaliangos [34] have run a two-part FEM, to obtain a fully coupled model, that is a thermal-electric simulation, where the temperature history was fed to a thermal displacement simulation. That model was run using ABAQUS on a rectangular compact, with an initial density, which required them to consider the variation of material properties depending on the variation of both, temperature and density throughout the process. Their work was only considering thermal sintering without the use of pressure or die to constrain. Coupling meso-scale and continuum model [35] by using the meso-scale to approximate the sintering stress and the bulk viscosity, and using these properties in the continuum model to simulated changing in dimensions during the sintering process.

McWilliams et al. [36], enhanced their previous work [34], where they have added the die and the punches and externally applied a load, to study their effect on the sintering process. As an improving attempt to, C. Wolff et al [37], have considered applying the effect of plastic work to the generated heat using ABAQUS packages software in a sequential manner

LUGMAN [38] developed a thermal-electrical-mechanical coupled finite element model to study the distribution of the temperature in the sintered material, the device, and stresses. He found that in the case of alumina, the residual stress developed in the sample is higher than in the case of aluminum. The maximum radial stress is found at the top and the bottom surfaces of the sample. In the case of sintering, the material properties is affected by temperature and porosity, which are changing during the process, and Lugman model was lacking some accuracy in material properties.

K. Sairam [39] and others, conduct an experimental study of the densification behavior of boron carbide produced by SPS, with a temperature between 1100℃ and 1800℃. The mechanical properties which are affected by the porosity are measured, specifically hardness, fracture toughness, and elastic modulus. The pulsed direct current was found to be the main reason to achieve near theoretical density at a temperature lower than in conventional sintering.

Olevsky [40] and his coworkers have conducted a fully coupled FEM analysis to study the tooling geometry size and heating rate influence in SPS process using COMSOL. Giuntini et al [41] also, used COMSOL to analyze the SPS geometry aiming to resolve tooling overheating problem. From this literature review, we can see that there was

almost no attempt to investigate the sintering operating parameters, particularly the holding temperature and pressure applied, aiming to optimize the final product for a particular material. In the present study, a fully coupled simulation was validated and conducted to identify optimized operating parameters, namely holding temperature and pressure, in consolidating pure aluminum powder using CAPAD technique. Residual stresses evaluated using the model as well as experimentally.

2.3 Literature review summary

Table 1. Summary of the previous work on SPS (with considerations of each model)

paper title	author	Volume vacancy diffusion	Surface vacancy diffusion	grain boundary vacancy diffusion	coupling volume and surface	grain boundary and surface diffusion	grain boundary surface and volume diffusion	vaporization & solidification	Electro-migration effect on diffusion	pressure effect on diffusion
"Diffusion Models for Hot Pressing with Surface Energy and Pressure Effects as Driving Forces[1970]"	"Robert l. Coble"	an analytical model for (surface energy & pressure as driving forces)								
"A first report in sintering diagrams[1974]"	"M. F. Ashby"	yes	Yes	yes				yes		
"A second report in sintering diagrams[1980]"	"F. B. Swinkels and m. E ashby"	yes	Yes	yes		yes				
"Micromechanical modeling of powder compacts-i. Unit problems for sintering and traction induced deformation[1988]"	"A. Jacota and p. R. Dawson"	(Micromechanical FEM for the compaction process)								
"Simulation of the Viscous Sintering of Two Particles[1990]"	"A. Jacota and p. R. Dawson"	(FEM for viscous sintering)								
"A numerical technique for the analysis of coupled surface and grain-boundary diffusion[1994]"	"J. Pan and a.c.f. cock"					yes				
"Viscous Sintering of Spherical Particles via Finite Element Analysis[1995]"	"Jorge i. Martinez – herrera and jeffry"									
"A FEM for theSintering of Crystalline Particles[2004]"	"Hadrian Djohari"	yes	Yes	yes	yes	yes	Yes			

paper title	Author	Volume vacancy diffusion	Surface vacancy diffusion	grain boundary vacancy diffusion	coupling volume and surface	grain boundary and surface diffusion	grain boundary surface and volume diffusion	vaporization & solidification	electro-migration effect on diffusion	pressure effect on diffusion
"A discussion on the absence of plasma in spark plasma sintering[2009]"	"Dustin m. Hulbert and others"	(through experimental study, no evidence found for plasma formation)								
"Transport mechanisms and densification during sintering- I Viscous flow versus vacancy diffusion[2009]"	"Hadrian Djohari,JorgeI.M, and others"	yes	yes		yes					
"Transport mechanisms and densification during sintering: II. Grain boundaries[2009]"	"Hadrian Djohari,JeffreyJ.Derby"						Yes			
"Finite Element Simulation of Mass Transport During Sintering of a Granular Packing. Part I. Surface and Lattice Diffusions[2011]"	"Julian bruchon"	yes	yes		yes					
"Peculiarities of the neck growth process during initial stage of spark-plasma, microwave and conventional sintering of WC spheres[2012]"	"dmytro demirskyi"	(experimental study on the neck growth kinetics)								
"Finite Element Simulation of Mass Transport During Sintering of a Granular Packing. Part I. Surface and Lattice Diffusions[2011]"	"Julien Bruchon, Daniel Pino-Mun˜ oz, and others"				yes					working on this effect
(Modeling sintering at different length scales[2003])	(Pan, Jingzhe)	review about modeling (include the effect of pressure)								

paper title	author	Volume vacancy diffusion	Surface vacancy diffusion	grain boundary vacancy diffusion	coupling volume and surface	grain boundary and surface diffusion	grain boundary surface and volume diffusion	vaporization & solidification	electro-migration effect on diffusion	pressure effect on diffusion
"A finite element analysis of the motion and evolution of voids due to strain and Electromigration induced surface diffusion[1997]"	"L. Xia, A.F. Bower, Z. Suo, C.F. Shih"		yes						yes	
"Computer modeling and simulation of solid-state sintering: A phase field approach[2006]"	"Yu U. Wang"	Yes	Yes	Yes	Yes	Yes	Yes	Yes		
"Constitutive modeling of spark-plasma sintering of conductive materials[2006]"	"Eugene Olevsky & Ludo Froyen"			Yes					Yes	Yes
"Effect of interface behavior between particles on properties of pure Al powder compacts by spark plasma sintering[2001]"	"Guoqiang Xie et. Al"	(Experimental investigation of the properties and behavior of Al powder compacts by different process parameters)								
"Densification mechanisms during hot pressing of ZrB2–20 vol.% Sic composi`te[2013]"	"Manish Patel et. Al"	(Experimental investigation of the dominant densification mechanisms during hot pressing of ZrB2–20 vol.% SiC composite)								
"Fundamental Aspects of Spark Plasma Sintering II. Finite Element Analysis of Scalability[2012]"	"Eugene Olevsky et.al"	(Developed a three-dimensional fully coupled thermo-electro-mechanical finite element framework)								Yes
"Fundamental Aspects of Spark Plasma Sintering I. Experimental Analysis of Scalability[2012]"	"Eugene Olevsky et.al"	(Experimental analysis of scalability for SPS using different sample of alumina)								

paper title	Author	Volume vacancy diffusion	Surface vacancy diffusion	grain boundary vacancy diffusion	coupling volume and surface	grain boundary and surface diffusion	grain boundary surface and volume diffusion	vaporization & solidification	electro-migration effect on diffusion	pressure effect on diffusion
"the mechanical properties of porous aluminum using Finite element method simulations and compression experiments[2013]"	"Max Larner and Lilian P. Dávila"	(A finite element model that predict the properties of porous metals)								
"Multi-phenomena simulation of electric field assisted sintering[2008]"	"Brandon mcwilliams , Antonios Zavaliangos"						yes			
"Phenomenological analysis of densification kinetics during sintering application to WC–Co mixture[2000]"	"O. Gillia, D. Bouvard"	Developed analytical formula for densification under surface tension effect					yes			
"Densification simulation of compacted Al powders using multi-particle finite element method[2009]"	"Kyung-Hun LEE"	(multi-particle finite element model for aluminum powder compaction)								
"Finite element simulation of powder forming and sintering[2005]"	"K. Mori"						yes			yes
"Influence of spark plasma sintering parameters on densification and mechanical properties of boron carbide[2014]"	"K. Sairam et. Al"	(experimental study on the effect of porosity on mechanical properties)								

CHAPTER 3

Experimental study

For the sake of building a reliable numerical model that could be used to study the SPS processو and improve understanding of the effects of its parameters on the quality of products, the model should be built combined with enough experimental data. First, a pure aluminum powder is used to produce three samplesو having disc shape of a diameter of 20 mm diameter and the thickness is 6 to 8 mm. The powder is characterized using the SEM imaging technique to see the particle shape. Particles size analyzer is used to know the average size of the particles, because particle size has a great effect in the numerical calculations of densification, and also affecting the contribution of each densification mechanism in the process.

(MMC) metal matrix composite material by using aluminum as the matrix and alumina as the reinforcement component. This study to investigate more in the process parameters as well as the effect of adding Nano- size alumina powder and micro size alumina powder on the properties of aluminum. Microhardness is measured for the composite and the residual stress using hole drilling method, XRD (X-ray Diffraction) technique is used to analyze the elements in the powder and check the purity. A similar technique which is EDS (Energy Dispersive spectroscopy) is also used for elemental analysis.

Usually, in SPS machine the load start to increase gradually, before the pulsed direct electric current start to pass in the system. The temperature begins to rise after applying the current, and the densification will start to occur when the temperature reaches a certain value. At this moment, the powder is already compressed. The powder in this moment is called the green piece, and it has initial relative density value, or in other word value initial porosity value. This value is needed for the numerical calculations. To determine this initial value, a compression test is conducted for the powder using punches with the same diameter of the one that used in SPS machine. Different forces are applied in the compression test, to get an empirical relation between pressure and porosity. Archimedes principle is used to measure porosity, also, volume and weight of the green piece is used.

3.1 Powders preparation

XRD is used to check the powder purity. Results show that, aluminum is dominant by comparing the peaks (Figure 23). SEM also used to see the particles shapes (Figure 24, 25), because in the mathematical formulation the surface tension driving force is assuming a spherical shape for powder particles. The SEM images were taken using 20 KV power, in different scales and many locations, to make sure it will represent the powder.

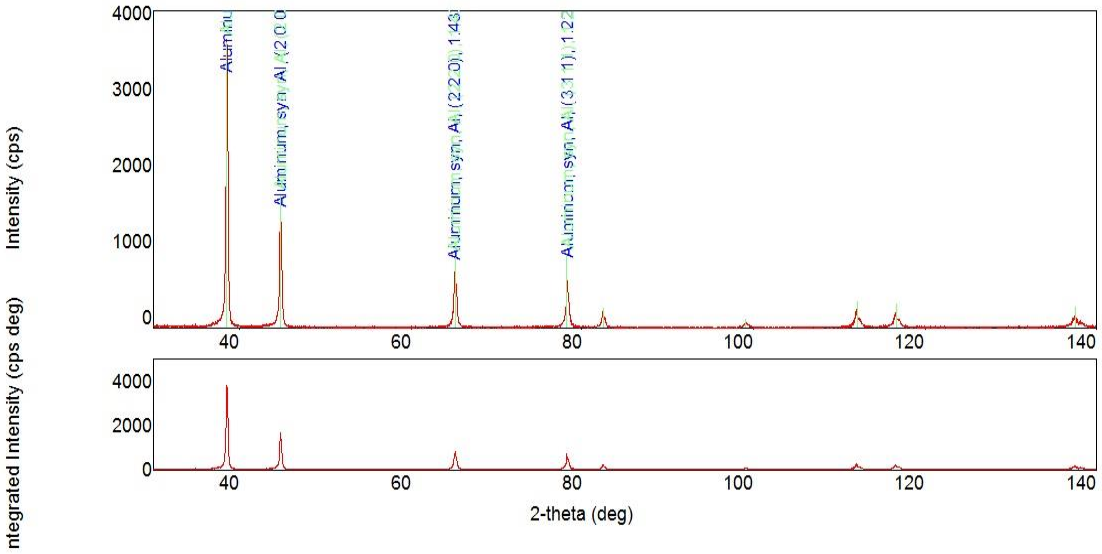

Figure 23. XRD results for aluminum powder

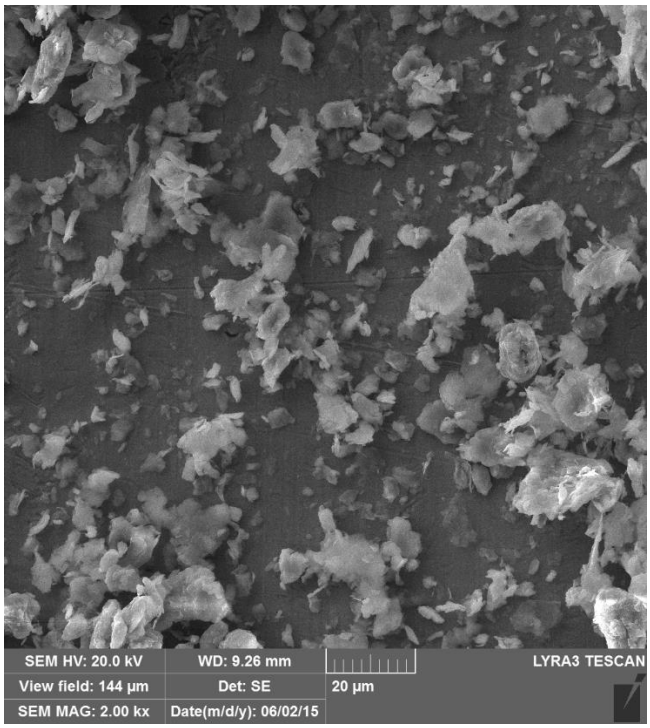

Figure 24. SEM Images for aluminum powders view field 144 µm

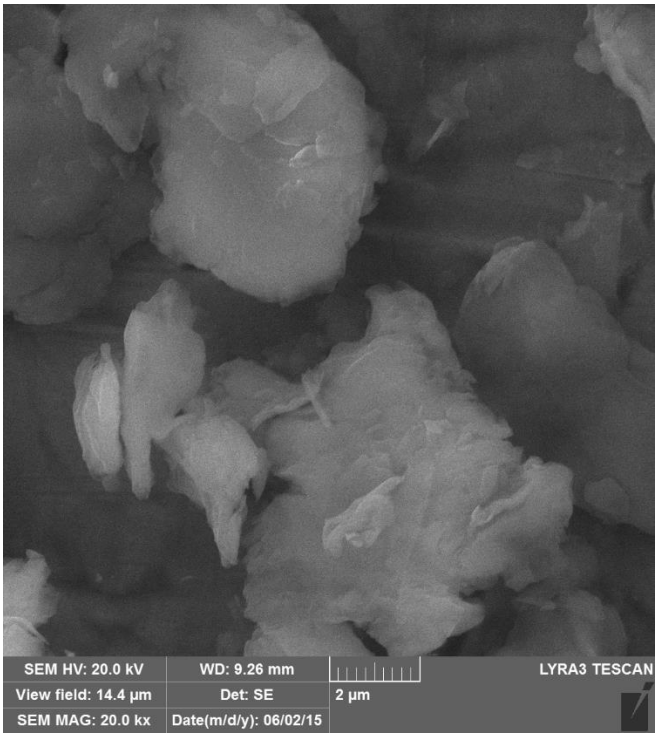

Figure 25. SEM Images for aluminum powders. View field 14.4 µm

SEM images show that powder particles are not spherical in shape. It has random shape, sometimes close to spherical. Still the model can give good results by assuming that decrease and increase in energy resulting from surface tension will cancel each other due to randomness. EDS is also used to detect all elements in the sample. It shows aluminum mainly and a small amount of oxygen, this oxygen is negligible as shown in Figure 26.

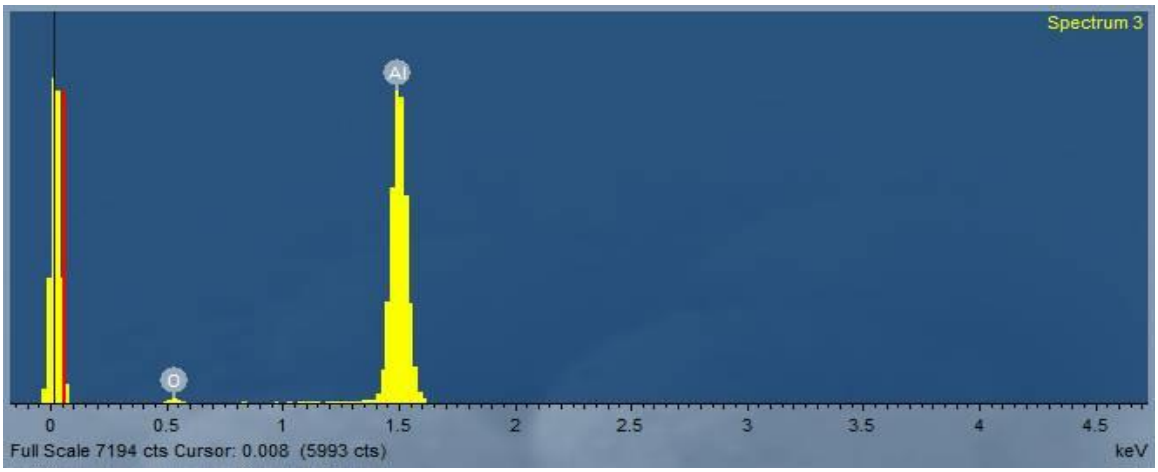

Figure 26. EDS analysis for aluminum powder

3.1.1 Particles size analyzer

The Particles size analyzer is used on the powder to know the average particles size, it is a necessary data for the model. We found a range from 3µm to 25µm, most of the particles has about 12µm size (Figure 27)

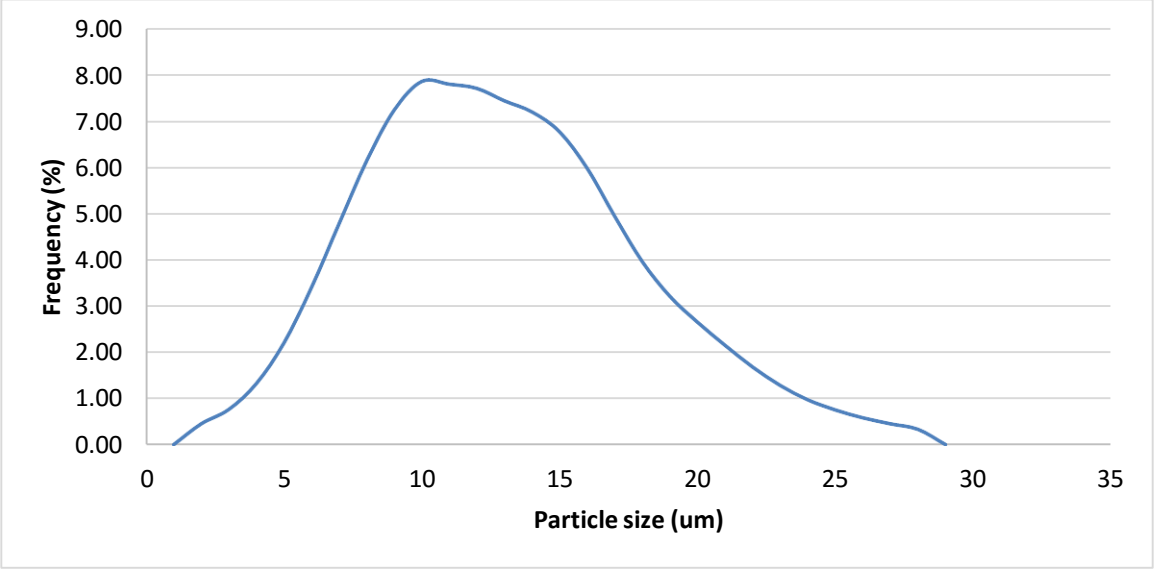

Figure 27. Aluminum particles size

3.1.2 Powder mixing

An experimental study was conducted on MMC using aluminum and alumina produced by SPS technique. For that, a mixture of the two materials should be prepared so that a good homogeneity is achieved. To mix the powder, ball milling machine is used by applying low speed 200 rpm for only 1 hours. Ball to powder weight ratio used was 5:1, 2 wt % of Stearic acid is added to prevent cold welding and agglomeration of the powder. EDS technique is used to check for mixture homogeneity by detecting aluminum in one Image and detecting Oxygen in another image. Oxygen will give a good indicator for the locations of alumina particles. This check is conducted for the mixture of micro size alumina as well as nano size alumina, and it shows very good homogeneity in the mixture. EDS test is conducted for the following samples:

1- 10% Alumina micro size
2- 15% Alumina nano size

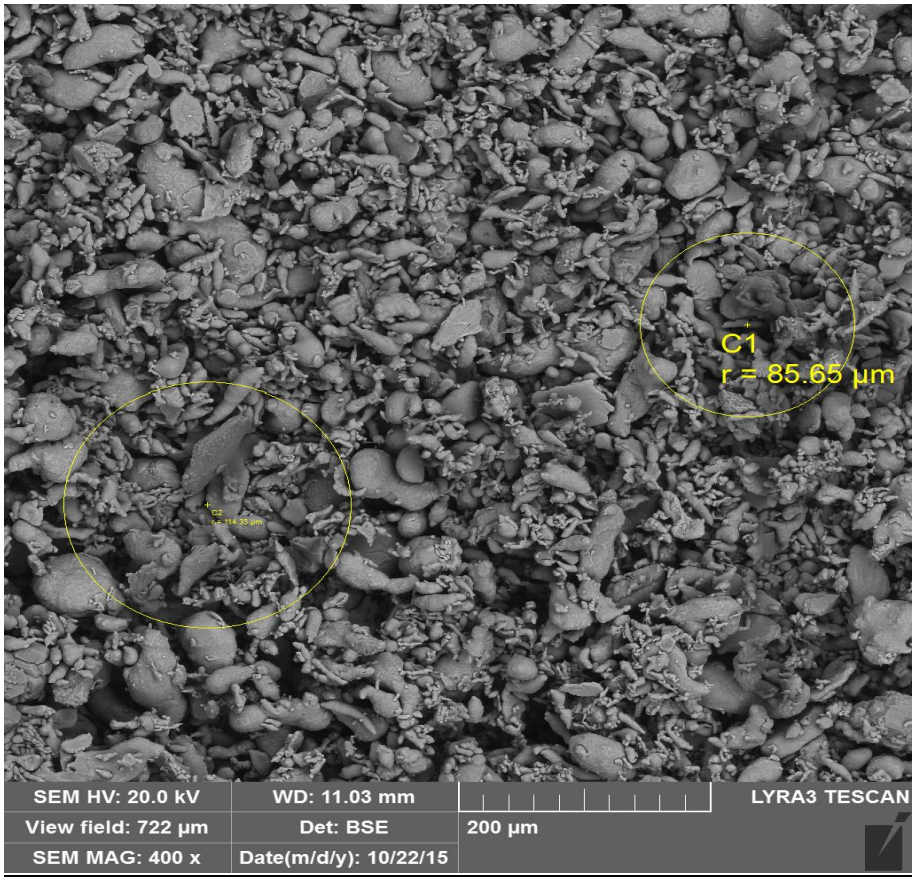

Figure 28. Locations of EDS analysis in 10% micro-size alumina

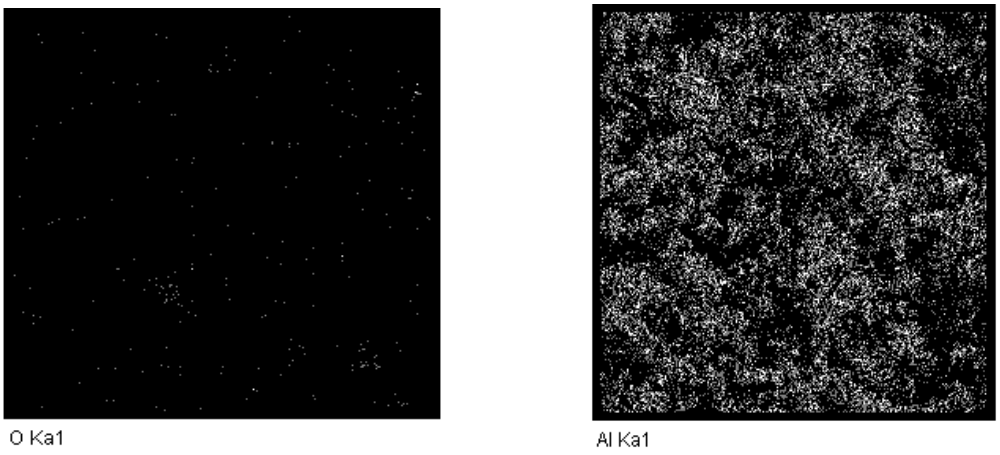

Figure 29. Distribution of oxygen in aluminum (in 10% micro-size alumina sample)

Locations of oxygen atoms in Figure 28 appear in Figure 29 the right picture by white dots and aluminum in the left one. The distribution of oxygen which indicating alumina locations is homogenized and uniform in all the area.

Second powder sample with 15% nano size (150 nano) alumina particles. Because alumina particles are small when compared with Aluminum particles, they tend to stick uniformly around aluminum particles as shown in figure 30 and 31. The EDS results show good homogeneity in this mixture, with good distribution of oxygen in aluminum (Figure 32)

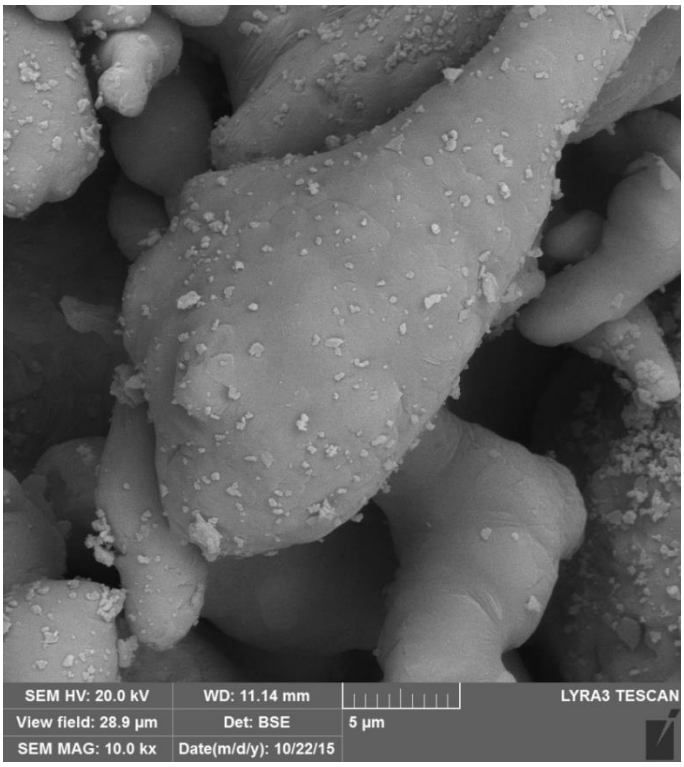

Figure 30. Nano alumina particles sticking on Micro aluminum particles

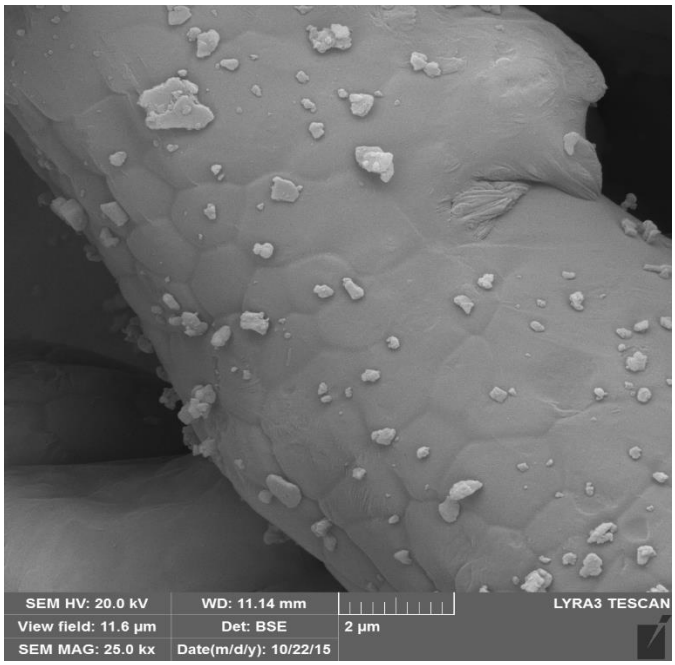

Figure 31. Nano alumina and aluminum mixture (view field 11.6 µm)

Figure 32. Distribution of oxygen in aluminum (in 15% nano-size alumina sample)

Above figure shows good distribution of alumina in aluminum in this mixture

3.2 Initial porosity (before beginning of densification)

The pure aluminum powder is compressed using automatic hydraulic compression machine by setting the desired force. The process is repeated nine times using nine values for the force including the value used in SPS machine. The volume and weight of green piece (Figure 33) resulting from the compression are measured, knowing the theoretical density of powder allow to calculate the relative density.

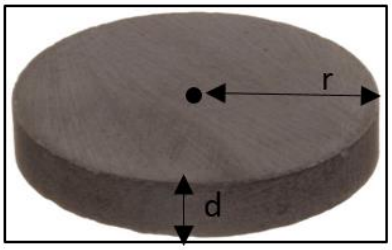

Figure 33. Green piece after compression test

$$V = \pi r^2 * d \qquad 3\text{-}1$$

$$measured\ density = \frac{measured\ weight}{V} \qquad 3\text{-}2$$

$$relative\ density = \frac{Measured\ density}{theoretical\ density} \qquad 3\text{-}3$$

$$Porosity = 1 - relative\ density \qquad 3\text{-}4$$

Each time a green piece is produced, its porosity is calculated using the above-mentioned procedure. Below graph in Figure 34 shows the results of compression test and the empirical equation relating porosity and pressure.

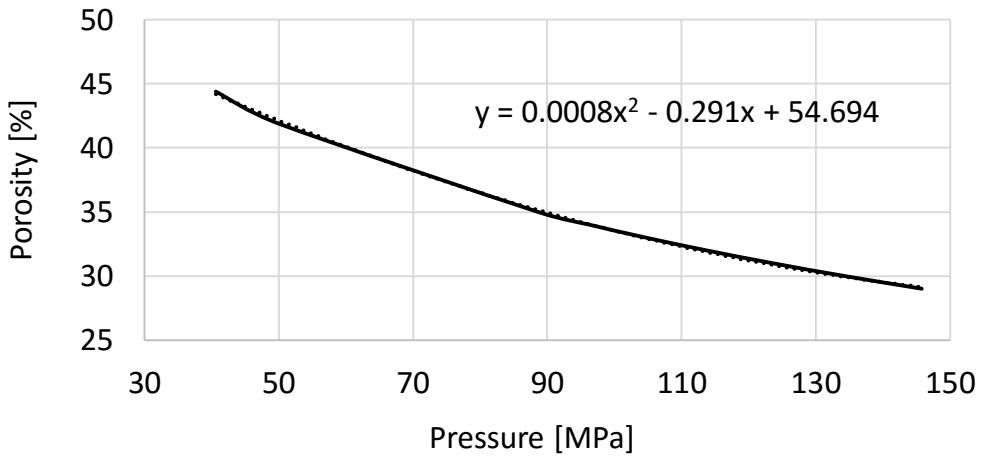

Figure 34. Pressure vs porosity (compression test using 20 mm diameter die)

In this equation y represent porosity as a percentage of one hundred, and x represent the pressure applied in MPa unit. The duration of the applied pressure is five minutes before releasing the pressure and do porosity measurement. 41 % initial porosity can be achieved using 55 MPa, this value is suitable for the die so that it will not break. Before sintering the powder we pressed it with 55 MPa using the same SPS machine to achieve the desired initial porosity, SPS process started after that.

3.3 Sintering the powder using SPS

After preparing the powder and have the initial porosity curve, a three samples of pure aluminum are made using the SPS machine Type HP D-50, FCT Systeme, Rauenstein, Germany. Each sample is made using a unique combination of temperature and pressure, holding time is fixed for 10 minutes and heating rate is fixed in 100 ℃ / s for all three

samples. Two values for temperature 550, and 450℃. Table 2 shows the three samples parameters

Table 2. Samples prepared by SPS

	Temperature (ºC)	Pressure (Mpa)
Case-1	550	41
Case-2	550	25
Case-3	450	41

The voltage input is varying with process time using the controller installed in the machine to achieve the desired temperature profile in the process. The desired temperature is measured from a point in the die as it is difficult to measure the temperature inside the powder or on the surface. That's why one should be careful when setting the desired temperature because sometimes sample temperature may be higher than the measured one.

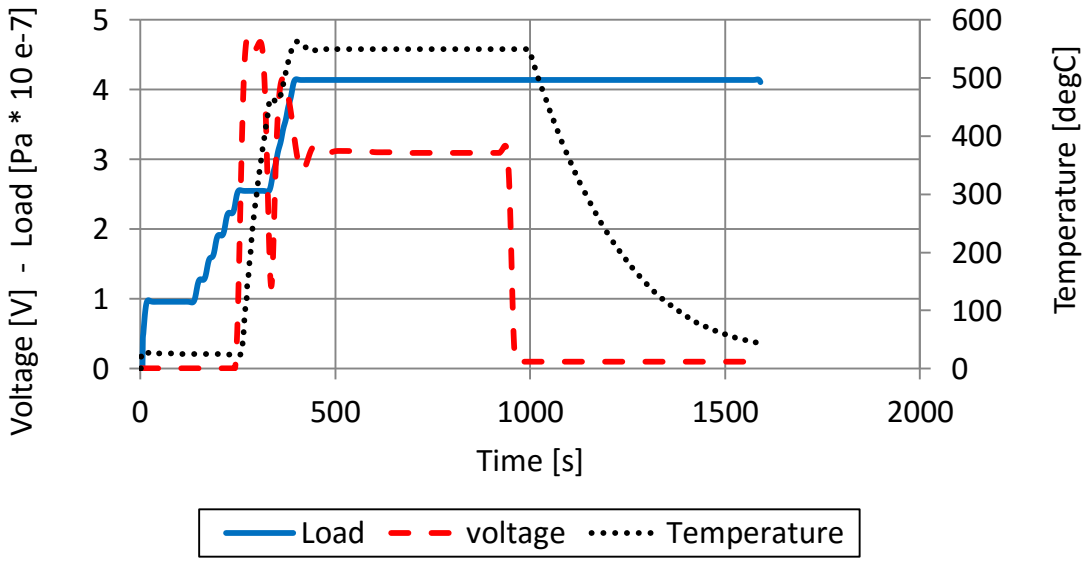

Figure 35. SPS parameters for the first case

Figure 35 above shows how the pressure is increased gradually to reach the maximum 41 MPa, at the same time the voltage increased rapidly to give high heating rate and reach the desired temperature, which is indicated by the green line. There is a visible fluctuation in the voltage resulting from the controlling system, to reach the maximum temperature with the minimum overshoot. The response in temperature is delayed after the change in voltage, because, heat needs time to be generated in the system then a variation in temperature in the punches and the die occurs due shape change and different cross-section in different height. The temperature difference between the sample and the die & punches happened because materials are different, the temperature needs time to reach equilibrium. After heating period comes the holding time period, voltage is maintained constant and also the temperature for about ten minutes followed by cooling down period. Voltage is dropped immediately to zero as any current pass in the system will generate some heat, but as mentioned before temperature took longer time to be reduced to room temperature. Because the process is done in a vacuum chamber leading to very low cooling rate by means of conduction and convection on the surface of the die and punches. During all this process the upper and lower rams are continuously cooled by cold water to reserve the systems from the high temperature usually generated inside the chamber, as temperature goes very high in some other material like alumina may reach 1700℃. Some temperature is dissipated from the outer surface of the die and the punches by means of radiation. Most data relating to SPS parameters mentioned above is recorded by the machine and can be taken out in excel file. The porosity of the three samples was measured using Archimedes principle. Micro-hardness is also measured in many points

in the section of the sample, SEM images were taken in different locations in the section in each sample the see the variation of the density of the sample.

3.4 Measuring porosity

Archimedes principle is used to measure the average porosity in the sample, SEM images and image processing technique utilizing Matlab software is used to check the variation of porosity in the section of the sample.

3.4.1 Archimedes principle

Pores inside the sample are of two kinds; closed pores and opened pores. There is some access for pure water to reach the open pores from the surface of the sample, but water cannot reach the closed pores inside the sample. Using pure water three accurate weight measurements is needed in order to measure porosity in the sample, the dry sample weight, the soaked weight, and the suspended weight they are all illustrated in Figure 36 below.

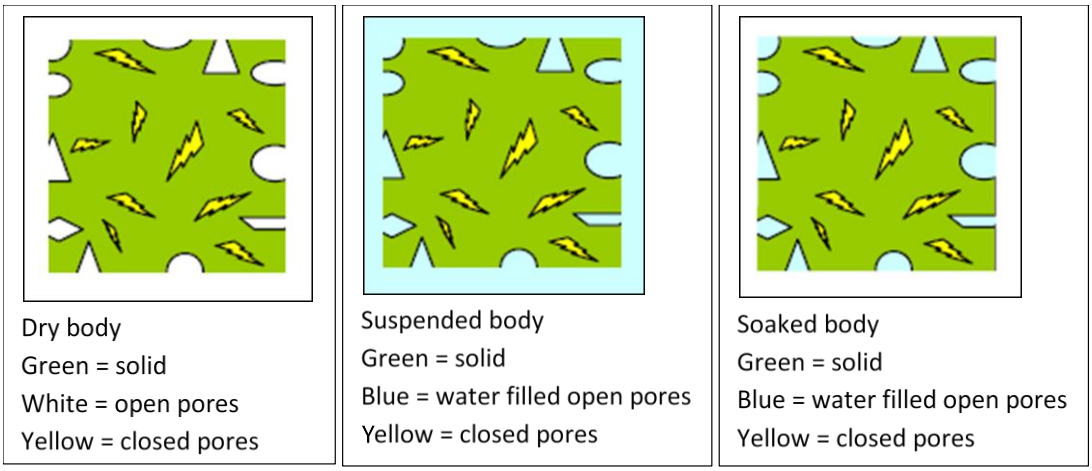

Figure 36. Weight measurements for porosity calculations [42]

Bulk volume is defined as the volume of solid and open pores and also closed pores, then the bulk density is the mass divided by the bulk volume.

$$Bulk\ density = \frac{Dry\ weight}{Soaked\ weight - Suspnded\ weight} \qquad 3\text{-}5$$

By taking the three weight measurements for the three sample relative density is calculated for the three cases, Table 3 below shows the relative density values

Table 3. Measured relative density

	Temperature (^{o}C)	Pressure (Mpa)	Relative density (%)
Case-1	550	41	94.13
Case-2	550	25	92.22
Case-3	450	41	88.8

3.4.2 Porosity variation

To check variations in porosity inside the sample 9 SEM images were taken in different locations on the section of the sample. It is expected that properties are axisymmetric due to the disc shape, may be that properties are not symmetric axially around the center line, because the upper punch is moving and the lower punch is not during the process, which leads to different mechanical contact pressure between the powder and the die wall. But this variation is very small and can be neglected, because sample thickness is very small 6 mm. For this reason, images are taken in one-quarter in the section, Figure 37 shows the locations of the images on the section. It can be evaluated visually as there is a clear variation in the images. Images in Figure 38 are ordered in the same way shown in Figure 37. Density at the center is higher than other locations in the sample but the variation is not that much because the sample is small and has a disc shape which leads to more uniform properties.

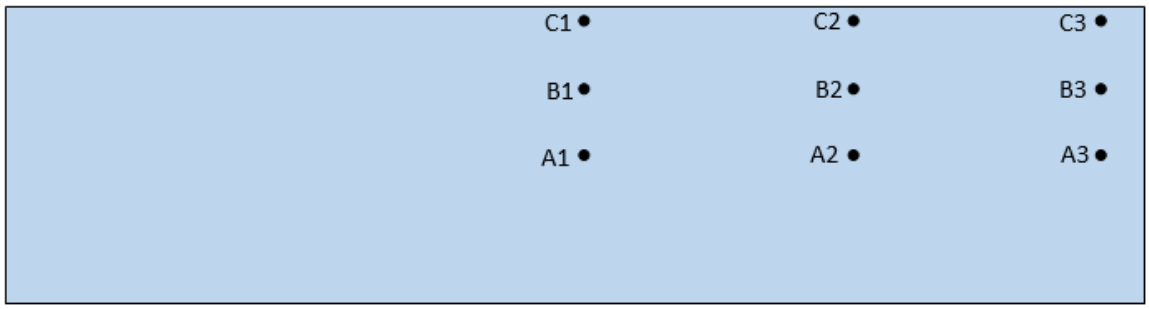

Figure 37. SEM images locations in one-quarter on the section

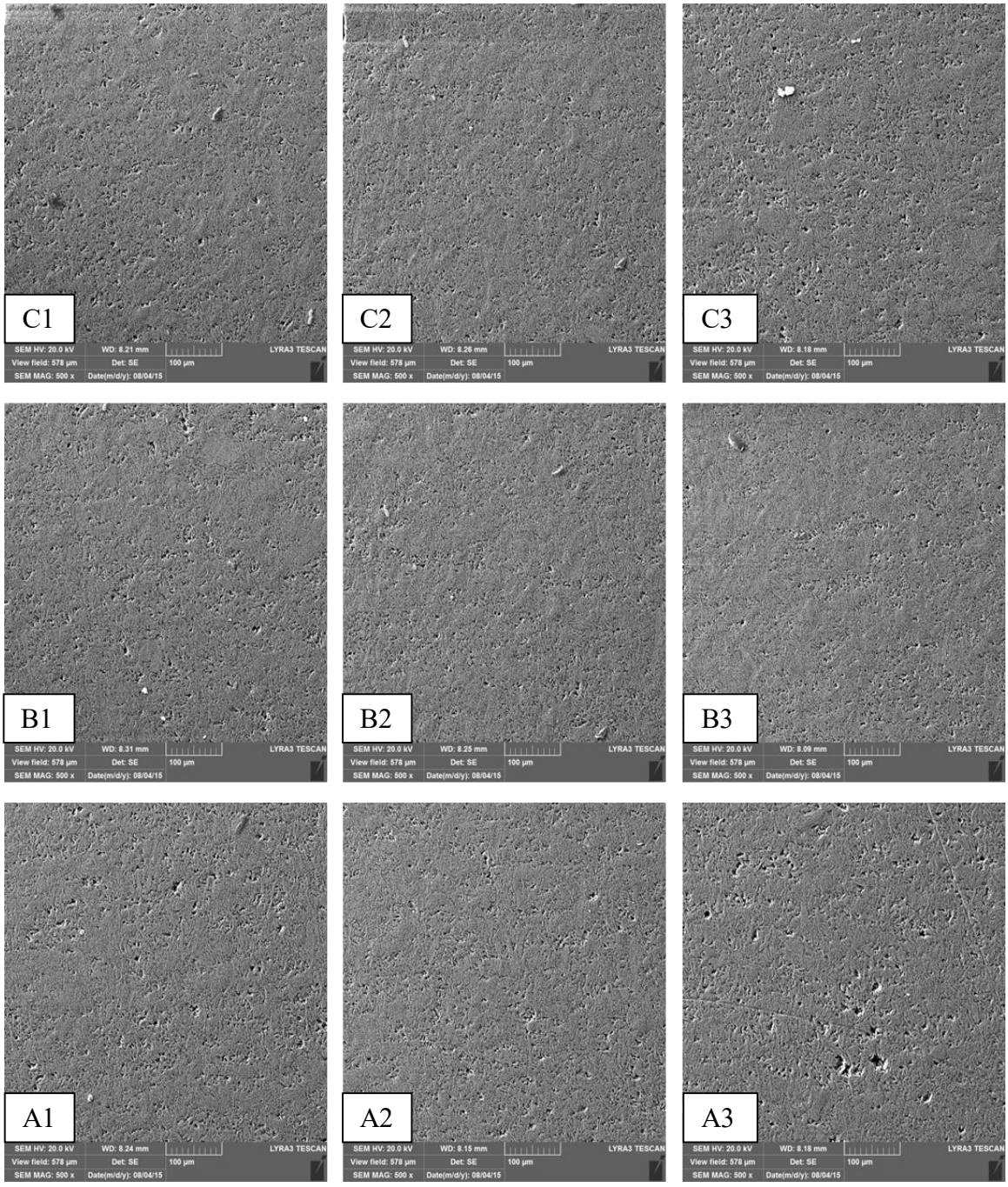

Figure 38. SEM Images in sample case-1

Approximated values for porosity in each image is evaluated using MATLAB, by reading the image as RGB style, then convert it to grayscale image which means all the pixels in the image are in the range between black (having a zero number) and white (having a one number). Setting a certain number between zero and one is required to be the gray value after which any pixel with darker color is considered as a pore, if it is more than that value then it is considered as a dense pixel. By calculating the total number of pixels in the images and the pores pixels, porosity is determined for this image. This technique is used for the nine images, and results in Figure 39 shows that high porosity at the outer radius and more density at the center of the sample, axially there is no noticeable difference because of the small thickness

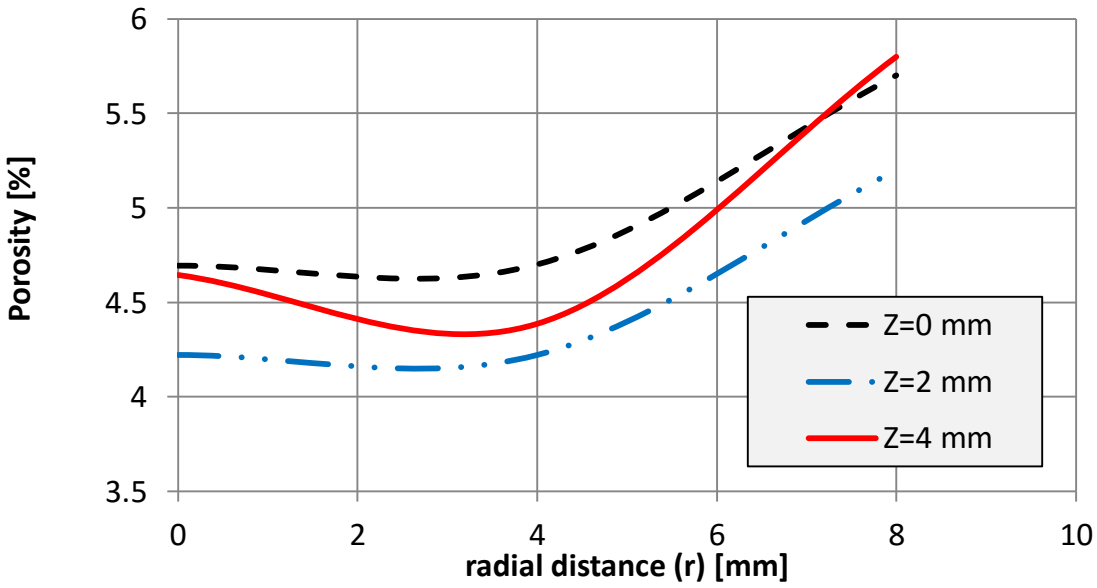

Figure 39. Porosity profile evaluated from SEM images

3.5 Relating hardness, microstructural, and porosity

Vickers hardness test is one of simplest hardness tests, it uses the same indenter for all materials because it uses diamond, and it also had one of the widest scales among hardness tests. The principle is simple, it measure the ability of the examined material to resist the plastic deformation resulting from applying pressure on the surface, using very small pyramid shape diamond indenter. The device can apply a range of forces, the value should be chosen according to the material. For hard material a high force should be used and for soft material a law force should be used. By applying the force, resulting indentation area (Figure 40) will differ from material to another according to the hardness value, measuring this area and using force value, hardness value can be determined. The unit used usually in this test is called Vickers Pyramid Number HV or Diamond Pyramid Hardness DPH.

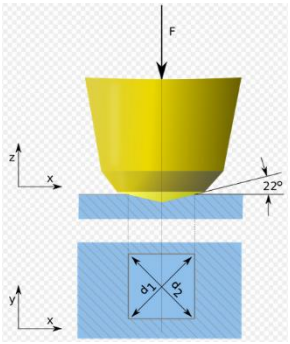

Figure 40. Vickers hardness test

Micro-hardness is measured for the sample using (BUEHLER, Vickers hardness machine), 100 gf is used, because aluminum is soft, and the test was conducted in the section of the sample.

The process begins by cutting the sample into two halves, after mounting the sample grinding process was done using silicon carbide paper of 120, 400, and 600 grit. The sample was polished using 9-micron diamond past, the section is divided into nine different regions (Figure 41), and five indentations are done in each region to see the hardness variation in the sample.

C1	C2	C3
B1	B2	B3
A1	A2	A3

Figure 41. Regions on the sample section where micro-hardness is measured

Results show very small variation as the maximum value out of 45 indentations is 33.9 HV Figure 46 and the minimum value is 27.4 HV Figure 47. Average value for the hardness in the middle is higher than the average values in the outer regions, this hardness profile is agreeing with the porosity profile Figure 39. Optical microscope images were taken to check the microstructure for each region of the cross-section after etching the surface using hydrofluoric acid (2%).

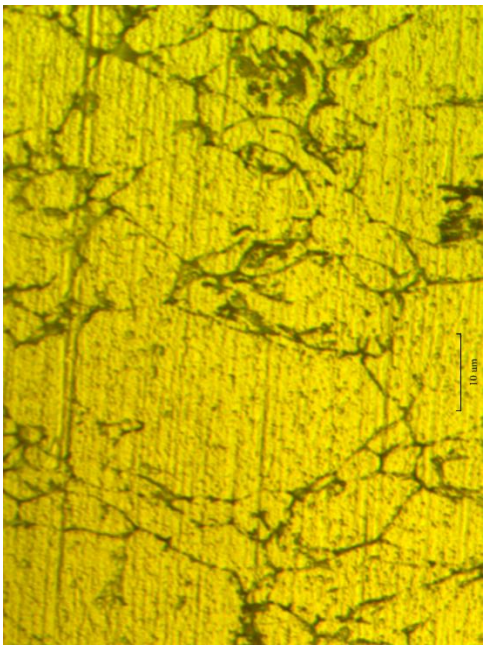

Figure 42. Region A1, microstructure and microhardness values [max = 30.2, min = 29.1, average = 29.95 HV]

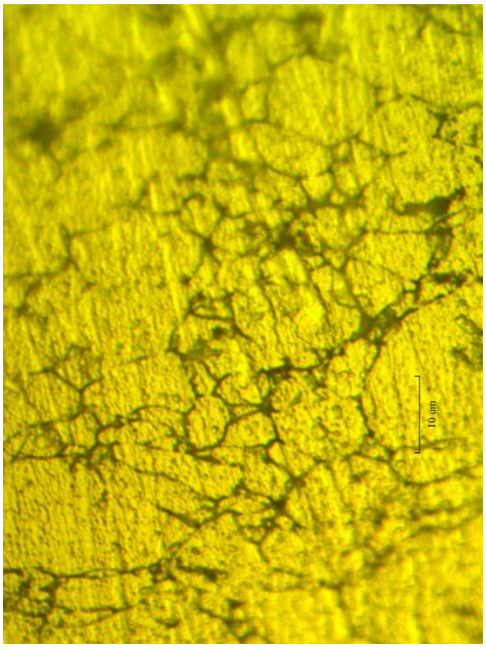

Figure 43. Region A2, microstructure and microhardness values [max = 32.7, min = 29.9, average = 31.7 HV]

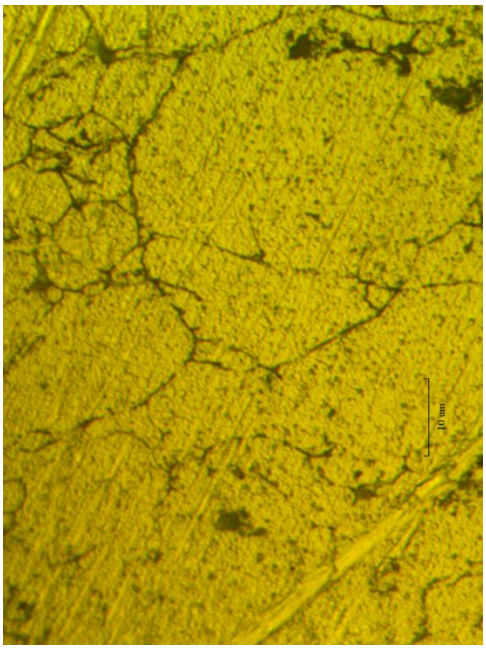

Figure 44. Region A3, microstructure and microhardness values [max = 31.9, min = 30.1, average = 31.1 HV]

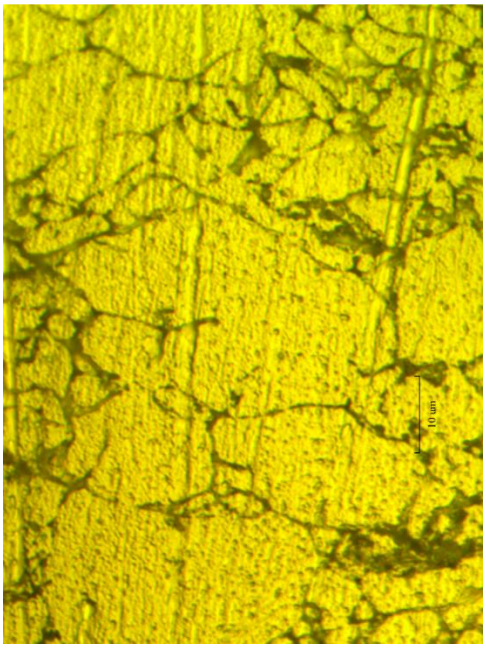

Figure 45. Region B1, microstructure and microhardness values [max = 31.7, min = 30.7, average = 31.68 HV]

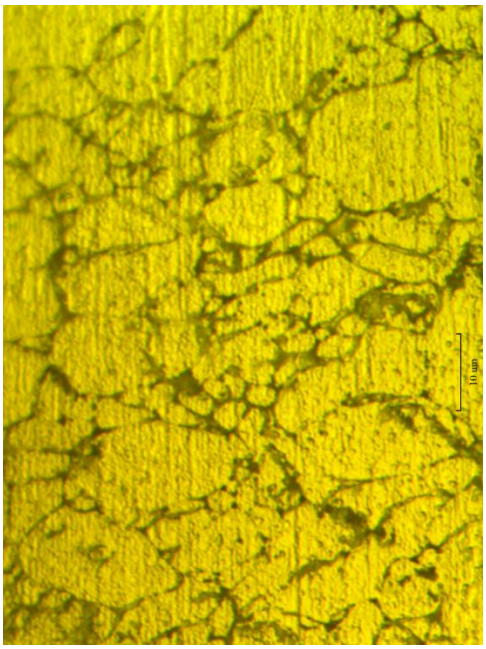

Figure 46. Region B2, microstructure and microhardness values [max = 32.8, min = 32.3, average = 32.57 HV]

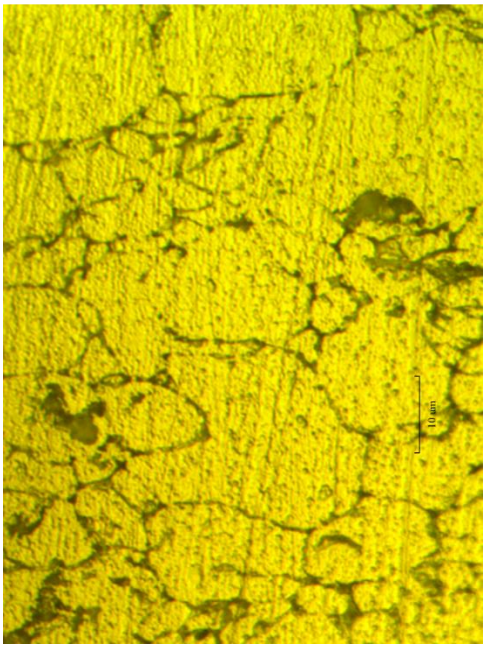

Figure 47. Region B3, microstructure and microhardness values [max = 32.7, min = 27.4, average = 31.04 HV]

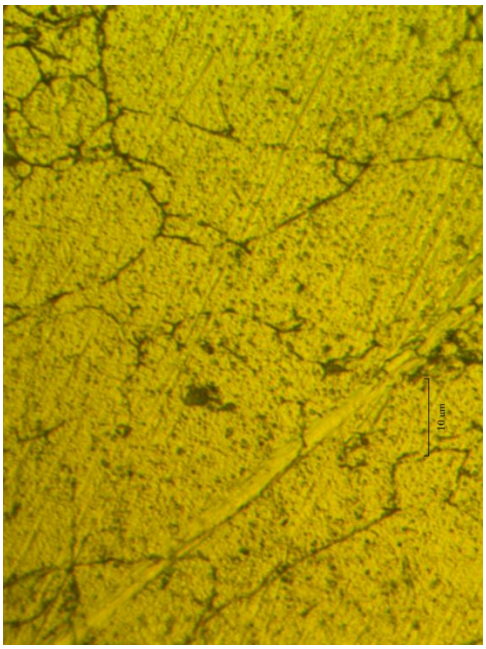

Figure 48. Region C1, microstructure and microhardness values [max = 32.1, min = 30.4, average = 31.16 HV]

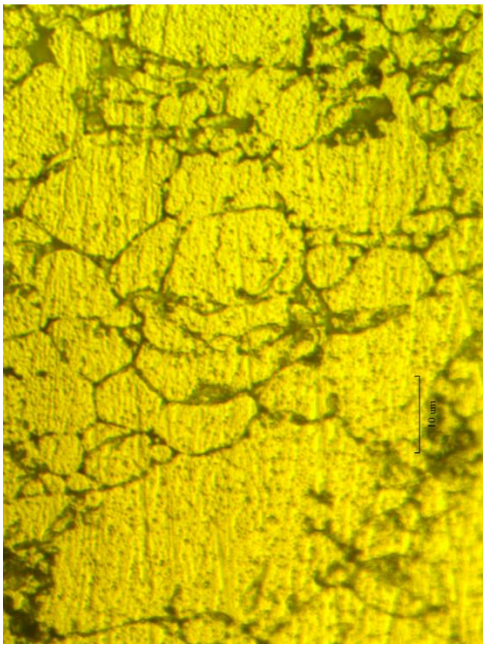

Figure 49. Region C2, microstructure and microhardness values [max = 33.9, min = 29.7, average = 31.68 HV]

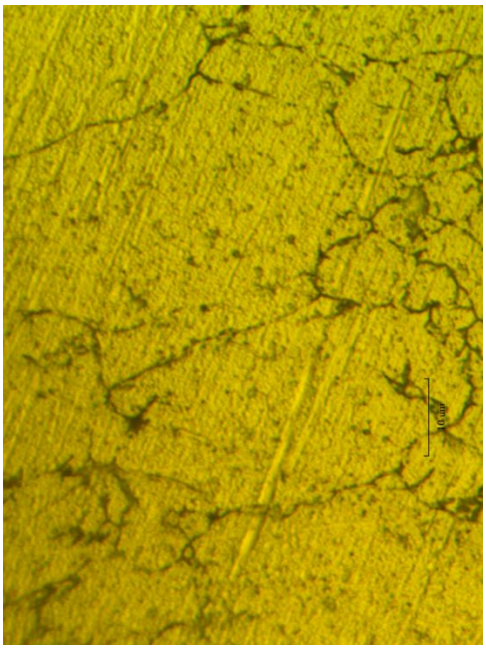

Figure 50. Region C3, microstructure and microhardness values [max = 32.3, min = 29.9, average = 31.21 HV]

Below observations were concluded from the images:

- At the center of the sample, there are more grain boundaries than the outer radius.
- All the grains are aligned with the direction of the uniaxial pressure which leads to a kind of orthotropic properties.
- This behavior can be explained by two parameters (Temperature & stress)
- A high cooling rate at the center of the sample results in hindering the grain growth process which means small grains size.
- A lower cooling rate at the outer radius areas resulting from many factors likes the shape of the sample and the die and the difference in the thermal properties between them.
- This low cooling rate results in a higher grain growth than that at the center which means bigger grains.

- Stress at the center is higher than outer radius resulting from thermal expansion and applied pressure.
- This two parameters (temperature & stress) cannot be checked experimentally, but using the reliable model is a good approach to study them, a detailed discussion is mentioned in chapter four (modeling).
- Locations, where hardness is high, is the same where there are more grain boundaries because these grain boundaries hinder dislocations from moving and slipping which is the mechanisms for the plastic deformation.
- On the other hand, fewer grain boundaries mean less hardness.
- The same pattern is found in porosity, where there is high temperature, lower cooling rate, high stress, a high number of grain boundaries, and high hardness value. At this location there is low porosity meaning more densification.

3.6 Residual stress measurement

The hole-drilling method is used to measure the residual stress in the aluminum sample using the set-up from the (measurements group Vishay). A configured strain gage rosette is bonded to the surface of the sample, and a small, shallow hole is introduced into the structure, through the center of the gage, with a precision drilling apparatus (Figure 51). Strains in the immediate vicinity of the hole are measured, and the relaxed residual stresses are computed from these measurements. The measured stresses by this method are parallel to the direction of the strain gage surface as shown in Figure 52

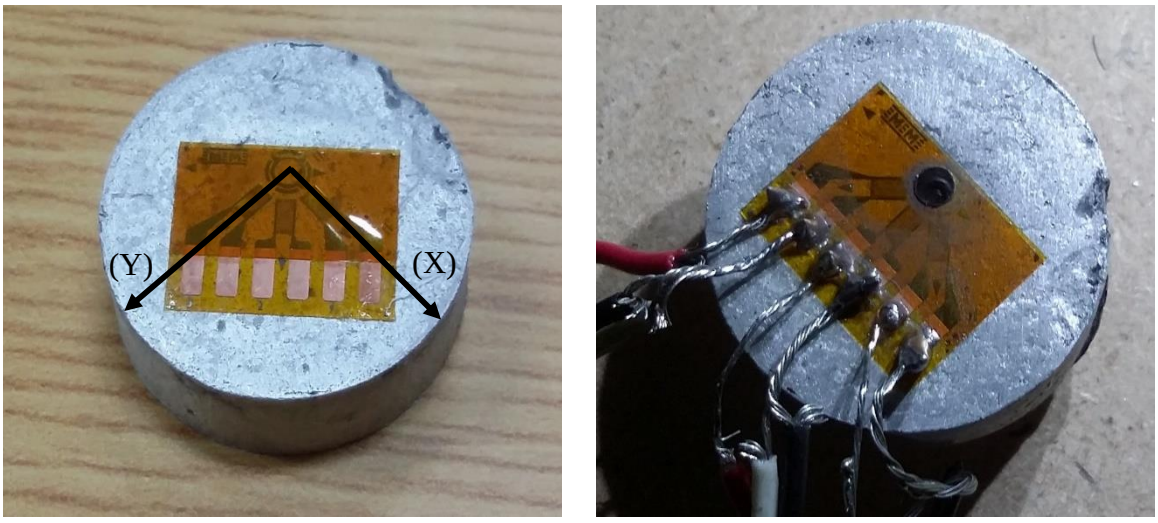

Figure 51. Strain gage bonding, wiring, and the drilled hole

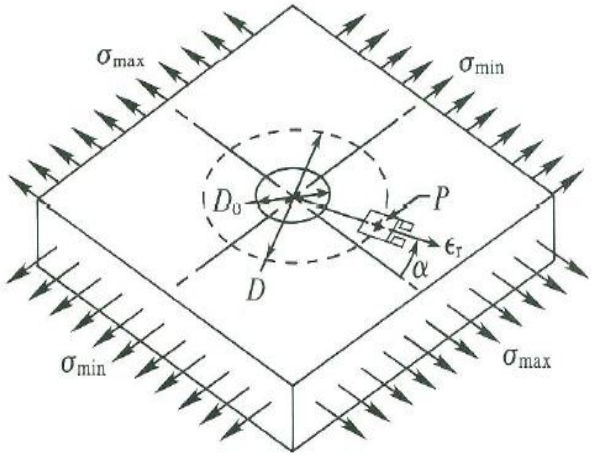

Figure 52. Measured residual stresses by the hole-drilling method

The experiment start by preparing the surface, first by wiping the surface with CSM degreaser, then the surface is abraded with 320 grid silicon carbide paper. After that a conditioner (M-prep), M-prep neutralizer 5–A is wiped on the surface to provide proper surface PH value for strong bond with most strain gage adhesive. The strain gage is bonded to the prepared surface, and the wires are soldered to the strain gage. After

checking the wires connections using volt-meter a hole is drilled to 2 mm depth and 1.8 mm diameter, by increments of 0.25 mm. the strain reading were recorded after each increment, then a software (H-drill) owned by the same company is used to calculate the uniform residual stress. Results of the measurement is shown in Table 4 below.

Table 4. Residual stress measurement results

X-stress [MPa]	Y-stress [MPa]	XY-shear [MPa]
-40	-32	-9

3.7 Study (A) [Effect of alumina particles size on the properties of the MMC]

In this study, three different weight percent aluminum alumina powder mixture and two alumina particle size are used. Table 5 and 6 below shows samples produced with different SPS parameters.

Table 5. Micro alumina samples

Alumina wt %	T(℃)	P(MPa)	Alumina size
0	550	50	NA
5	550	50	Micro
10	550	50	Micro
15	550	50	Micro

Table 6. Nano alumina samples

Alumina wt %	T(°C)	P(MPa)	Alumina size
0	550	50	NA
5	550	50	Nano
10	550	50	Nano
15	550	50	Nano

In these seven samples, the temperature and pressure are the same, only alumina percentage is changing and there are two different sizes for the alumina.

3.7.1 Effect on hardness

Aluminum is soft material with very low-density value that is why it is used in many applications like aerospace and automobile but for many purposes one may need to increase the hardness. In this experimental study alumina particles with 200 microns average size was added to aluminum and 150 nanometer average particles size with different weight percentage (5%, 10%, 15%) for both of the two sizes. Aluminum-alumina composite has light weight and wear resistance, and could be used at high temperature [43]

Brinell hardness test with 2.5mm ball diameter is used this time instead of Vickers test, because in case of micron alumina particle size the small indenter of Vickers make a very

small indentation, and it will not cover enough area containing aluminum as well as alumina.

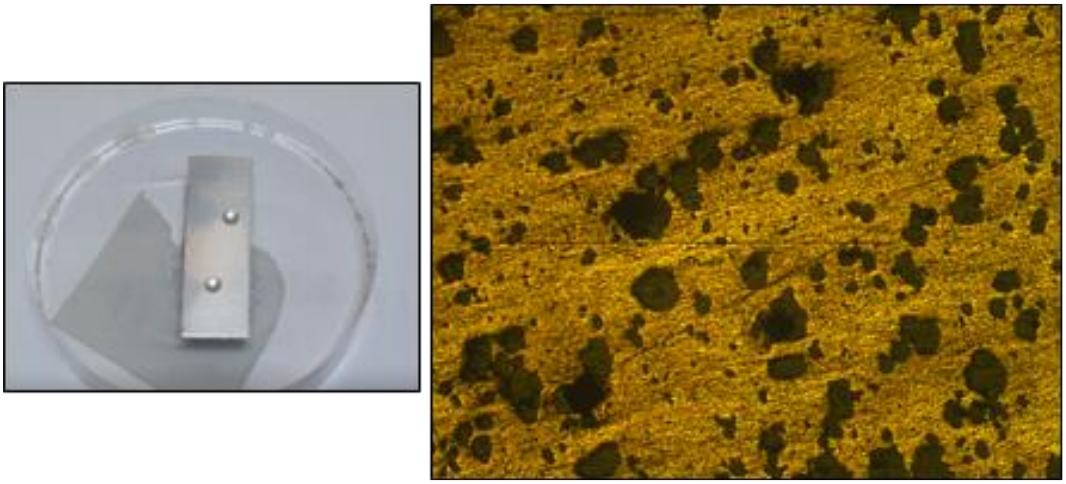

Figure 53. Brinell indentation

In Figure 53, the optical microscope image to the right shows the sample with 10% micron alumina, the micrometer inside the image shows 1 mm and it covers a good area which represents the composite, Brinell indentation is shown to the left is about 1mm. Ball material is tungsten carbide and the test force is 62 kgf for 35 seconds. Compared to the other hardness test methods, the Brinell ball makes the deepest and widest indentation, so the test averages the hardness over a wider amount of material, which will account more accurately for multiple grain structures and any irregularities in the uniformity of the material. This method is the best for achieving the bulk or macro-hardness of a material, particularly those materials with heterogeneous structures. The calculated value is converted from BHN to HV to compare the values with the Vickers

test conducted earlier. Generally results (Figure 54) show higher hardness values for the micron size alumina particles than Nano-size particles, both of them with the same weight percentage.

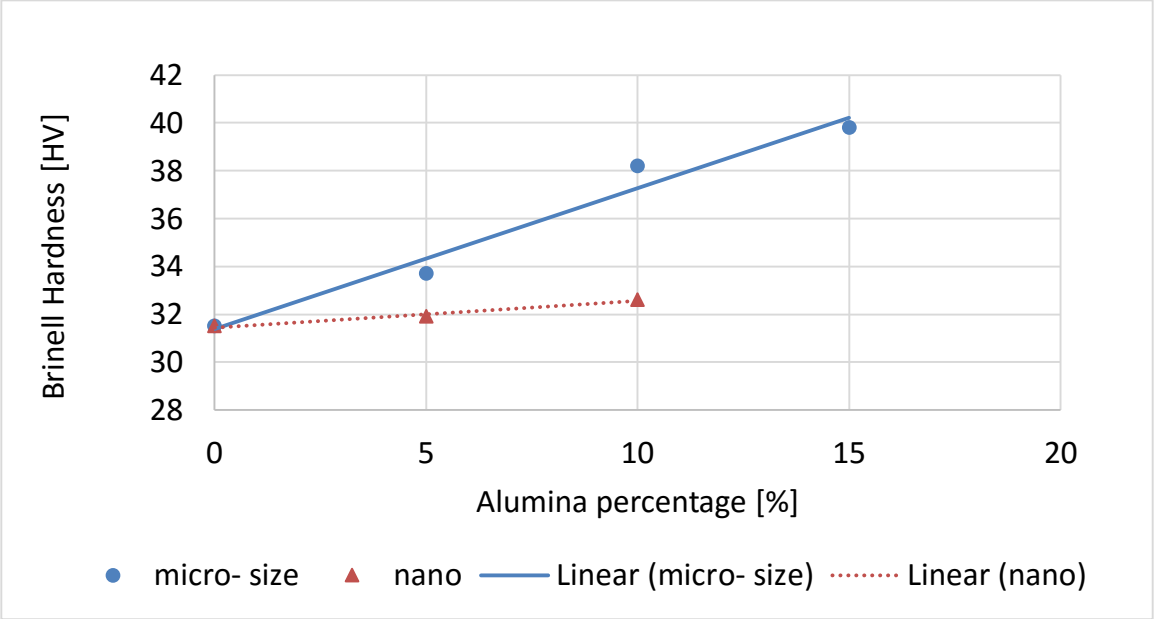

Figure 54. Brinell hardness for aluminum alumina composite

This behavior may result from the fact that small alumina particles tend to locate at the grain boundaries, thus decreasing its energy and decreasing its effect in blocking dislocations from slipping. This leads to two opposite effects by adding Nano alumina, softening and hardening, but hardening effect is a little higher than softening, that is why the hardness is increased a little. On the other hand, the micron size alumina particles composite has grain boundaries with higher energy and more hardening effect.

CHAPTER 4

Mathematical Formulation and Implementation

4.1 SPS process (Multiphysics)

SPS process is an electric, thermal, and mechanical process. When electric current passes through the system, heat is generated in the material due to Joule heating effect. Stress is developed in the sintered powder due to the applied pressure from upper and lower punches, and also from the thermal expansion. When the values of these two parameters start to rise up (temperature and stress), powder consolidate and the density increases with process time. Density of the powder is represented by

$$\rho = \rho_{th}\, \rho_r = \rho_{th}(1 - \theta) \qquad 4\text{-}1$$

Where ρ_{th} is the theoretical density of the material and ρ_r is the ratio between the current density of the sample ρ and the theoretical density of the material. ρ_r can be represented in terms of porosity θ.The evolution of porosity is based on the mass conservation equation [27] and can be represented by

$$\dot{\theta} = (1 - \theta)\dot{e} \;=\; (1 - \theta)\,(\dot{\varepsilon_x} \;+ \dot{\varepsilon_y} \;+ \dot{\varepsilon_z}\,) \qquad 4\text{-}2$$

Where $\dot{\theta}$ is the rate of change of porosity, and $\dot{e}$ is the shrinkage rate which is the sum of strain rates in all three directions. The strain rate is a function of temperature and stress

$$\dot{\varepsilon} = F(T, \sigma) \qquad 4\text{-}3$$

For the temperature field in the powder the joule heating can be expressed by:

$$Q = J * E \qquad 4\text{-}4$$

Where Q is the power per unit volume, and J is the current density, E is the electric field strength.

The heat equation implemented by

$$\rho C_p \frac{\partial T}{\partial t} - \nabla.(k\nabla T) = Q \qquad 4\text{-}5$$

Where ρ is the density of the material, C_p is the heat capacity, T is temperature, t is time,$(-k\ \nabla T)$ is the heat flux where k is the thermal conductivity.

In case of SPS process stress should be calculated considering plastic deformation because temperature goes high and sometimes reaches more than 0.75 of the melting temperature of the material [44], and yielding strength become very low [45], which means plastic deformation is present in the process, Even the strain hardening profile change [46] , also thermal expansion increased[47].

4.2 Constitutive behavior

In this work we consider the strain rate in only one direction, which is the direction of the applied pressure [27], the strain rate considered in this work is a sum of four densification mechanisms

$$\dot{\varepsilon}_x = \dot{\varepsilon}_{crx} + \dot{\varepsilon}_{gbx}^{dl} + \dot{\varepsilon}_{gbx}^{em} + \dot{\varepsilon}_{gbx}^{st} \qquad 4\text{-}6$$

Where $\dot{\varepsilon}_{crx}$ is power law creep strain rate, $\dot{\varepsilon}_{gbx}^{dl}$ is strain rate resulting from diffusion under load, gb subscript refers to the grain boundary diffusion, $\dot{\varepsilon}_{gbx}^{em}$ is the electro-migration strain rate, and $\dot{\varepsilon}_{gbx}^{st}$ is the surface tension strain rate

4.2.1 Power-law Creep

Power-law Creep consists of dislocation glide and climbing over microstructural obstacles as shown in Figure 55 below.

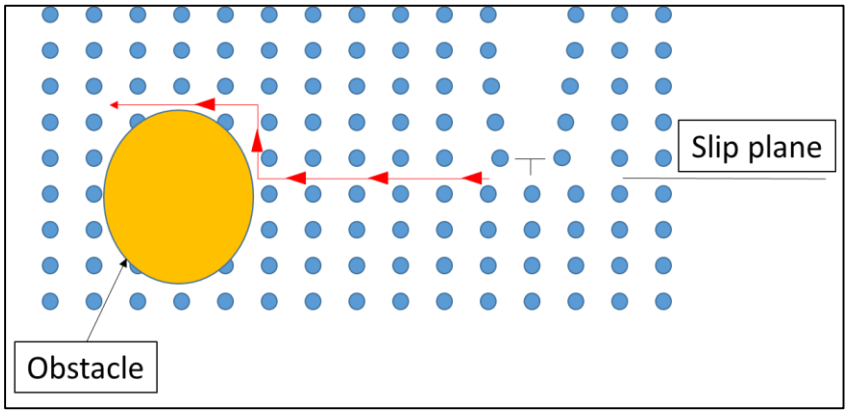

Figure 55. Dislocation Creep (power law creep)

Dislocation glide happen on slip planes, and climbing happened around the obstacles by means vacancy diffusion, Rate of this creep is determined by the lesser of glide and climb rates, in most cases climb rate

From reference [41]

$$\sigma_{ij} = A\, W^{m-1}\left[\varphi\dot{\varepsilon}_{ij} + \left(\psi - \frac{1}{3}\varphi\right)\dot{e}\ \delta_{ij}\right] + P_L\delta_{ij} \qquad 4\text{-}7$$

Where σ_{ij} is the externally applied stress tensor, the equivalent strain rate is W, φ and ψ are the normalized shear and bulk viscosity, $\dot{\varepsilon}_{ij}$ is the component of strain rate, Kronecker's delta is δ_{ij} and the effective sintering stress is P_L.

$$\varphi = \left(1 - \theta\right)^2 \qquad 4\text{-}8$$

$$\psi = \frac{2}{3}\frac{\left(1 - \theta\right)^3}{\theta} \qquad 4\text{-}9$$

$$P_L = \frac{2\alpha}{r_0}\left(1 - \theta\right)^2 \qquad 4\text{-}10$$

Where α is the sintering stress, and r_0 is the average particle e size.

The equivalent strain rate can be represented as:

$$W = \frac{1}{\sqrt{1-\theta}}\sqrt{\varphi\dot{\gamma} + \psi\dot{e}} \qquad 4\text{-}11$$

Where the shape change rate can be represented by:

$$\dot{\gamma} = \sqrt{2\left(\dot{\varepsilon}_{xy}^2 + \dot{\varepsilon}_{xz}^2 + \dot{\varepsilon}_{yx}^2\right) + \frac{2}{3}\left(\dot{\varepsilon}_x^2 + \dot{\varepsilon}_y^2 + \dot{\varepsilon}_z^2\right) - \frac{2}{3}\left(\dot{\varepsilon}_x\dot{\varepsilon}_y + \dot{\varepsilon}_x\dot{\varepsilon}_z + \dot{\varepsilon}_y\dot{\varepsilon}_z\right)} \qquad 4\text{-}12$$

One direction only $\dot{\varepsilon}_x$ is considered, which is the direction of the uniaxial pressure

In reference [48] a semi-empirical relationship to represent the steady state creep rate $\dot{\varepsilon}_s$ as can be represented as following:

$$\frac{\dot{\varepsilon}_s\, k\, T}{DGb} = A_{cr}\left(\frac{\sigma_{PLC}}{G}\right)^n \qquad 4\text{-}13$$

Where G is the shear modulus, b is Burgers vector, A_{cr} and n are material properties, σ_{PLC} is the applied stress, k is the Boltzman's constant, and D is the diffusivity which can be presented as:

$$D = D_o\, e^{-\frac{Q_{cr}}{RT}} \qquad 4\text{-}14$$

Where D_o is the diffusivity constant, Q_{cr} is the activation energy for power law creep, R is the gas constant and T is temperature. Substituting the diffusivity expression in the steady state creep rate expression and rearranging yields:

$$\sigma_{PLC} = \dot{\varepsilon}_s^m\, A \qquad 4\text{-}15$$

Where A is:

$$A = \left(\frac{kTG^{1/m}}{D_o \, e^{-\frac{Q_{cr}}{RT}} GbA_{cr}} \right)^m = \tilde{A} \, T^m e^{\frac{mQ_{cr}}{RT}} \qquad 4\text{-}16$$

Where $\tilde{A}$ depends on material properties:

$$\tilde{A} = \left(\frac{kG^{1/m}}{D_o \, GbA_{cr}} \right)^m \qquad 4\text{-}17$$

Olevsky [27] describe the strain rate resulting from power law creep as;

$$\dot{\varepsilon}_{crx} = \left\{ \left(\frac{3\theta}{2} \right)^{\frac{3}{2}} \left[\frac{3\alpha}{2G} (1-\theta)^2 - \sigma_{PLC} \right] / A(1-\theta)^{\frac{5}{2}} \right\}^{\frac{1}{m}} \qquad 4\text{-}18$$

Where G is the average grain size, α is the surface tension, σ_{PLC} is effective external stress in the considered uniaxial direction, in case of SPS it is compressive, A is the power law frequency factor which according to Ashby [26] can be written as

$$A = A_o \exp\left(\frac{Q_{cr}}{RT} \right) \qquad 4\text{-}19$$

Where $A_o$is the power law creep frequency factor constant, Q_{cr} is activation energy for power law creep, m is the power law creep exponent, R is ideal gas constant, T temperature.

4.2.2 Surface Tension

The surface tension of the powder acts as driving force for a diffusion process towards the contact regions between the particles to reduce the free surface area of the material. This diffusion can take many paths as discussed in the introduction, and in this work only the grain boundary diffusion is considered by using the model of grain boundary diffusion in sintering under applied pressure developed by Olevsky [49, 27] on which strain rate results from surface tension is expressed by:

$$\dot{\varepsilon}_{gbx}^{st} = -\frac{3\delta_{gb}D_{gb}}{kT}\frac{\Omega}{(G + r_p)^2}\frac{\alpha}{G}\left[\frac{1}{r_p} - \frac{1}{2G}\right] \qquad 4\text{-}20$$

Where $\delta_{gb}D_{gb}$ is grain boundary diffusion frequency factor, Ω is atomic volume, k is the Boltzmann constant, and r_p is the pore size which decreases when density increases. This relationship could be represented as

$$r_p = G\sqrt[3]{\theta/[6(1-\theta)]} \qquad 4\text{-}21$$

4.2.3 Diffusion under Load

When the load is applied on the crystalline material, atomic diffusion process occurs on the grain boundaries in the same direction of the applied load. Coble creep [50] is a form of diffusion creep that describes this phenomenon (Figure 56). Strain rate resulting from

diffusion under load is described on the grain boundary diffusion model of Olevsky [49, 27] as:

$$\dot{\varepsilon}_{gbx}^{dl} = \frac{\delta_{gb} D_{gb}}{kT} \frac{\Omega}{(G + r_p)} \frac{\bar{\sigma}}{G^2} \qquad 4\text{-}22$$

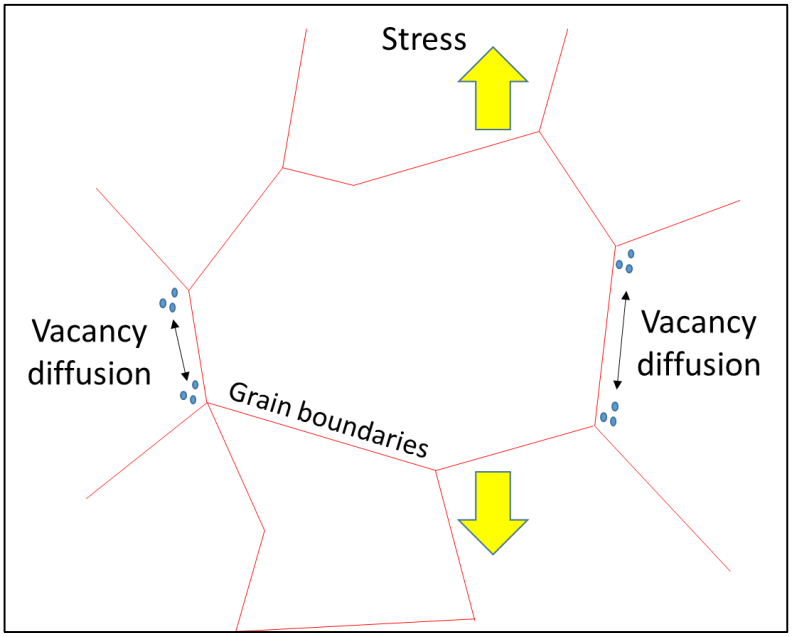

Figure 56. Diffusion under load

4.2.4 Electro-migration

High direct current pass on a conductor may result in material diffusion in the conductor [51]. Material is transport due to the gradual movement of ions because of momentum transfer between conducting electrons and diffusing metal atoms. The effect of electro-migration is of great importance when high direct current densities are used like in SPS. Electro-migration also induces stresses in the sintered material [52]

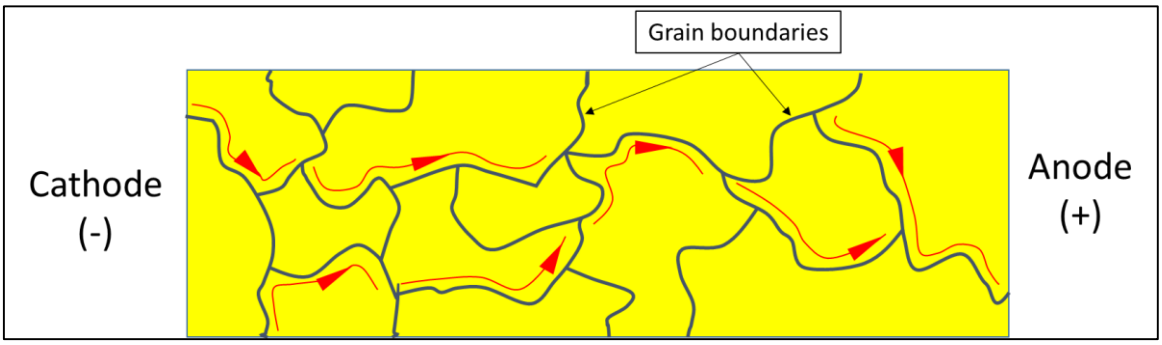

Figure 57. Electro-migration

Strain rate resulting from electro-migration diffusion on grain boundaries in SPS process can be expressed as [27]:

$$\dot{\varepsilon}_{gbx}^{em} = -\frac{\delta_{gb} D_{gb}}{kT} \frac{Z * e_q}{(G + r_p)^2} \frac{U}{l} \qquad 4\text{-}23$$

Where Z Represent the valence of a migrating ion, e_q is the electron charge, $Z * e_q$ is the effective charge, U is the electric potential, and l is the characteristic length.

4.3 Implementation in Comsol

Figure 58 shows the Multiphysics modeling, and how model inputs are defined. Also, the material properties depend on temperature in the case of graphite and depend on temperature and porosity in the case of aluminum. In Comsol environment, four different physics are used. All these physics are coupled directly together. Input voltage is applied in electric currents physics module, and in heat transfer module. All thermal boundary

conditions are applied, and the coupling between these two physics results in the temperature field. The applied SPS pressure and all mechanical boundary conditions are implemented in solid mechanics module. The stress developed in the sintered sample from the applied pressure and the thermal expansion is determined in this physics module. The densification process is simulated in domain ODEs and DAEs physics module by coupling electric field, temperature field, and stress field in the global variable module, and use them to simulate densification resulting from power law creep, diffusion under load, surface tension, and electro-migration.

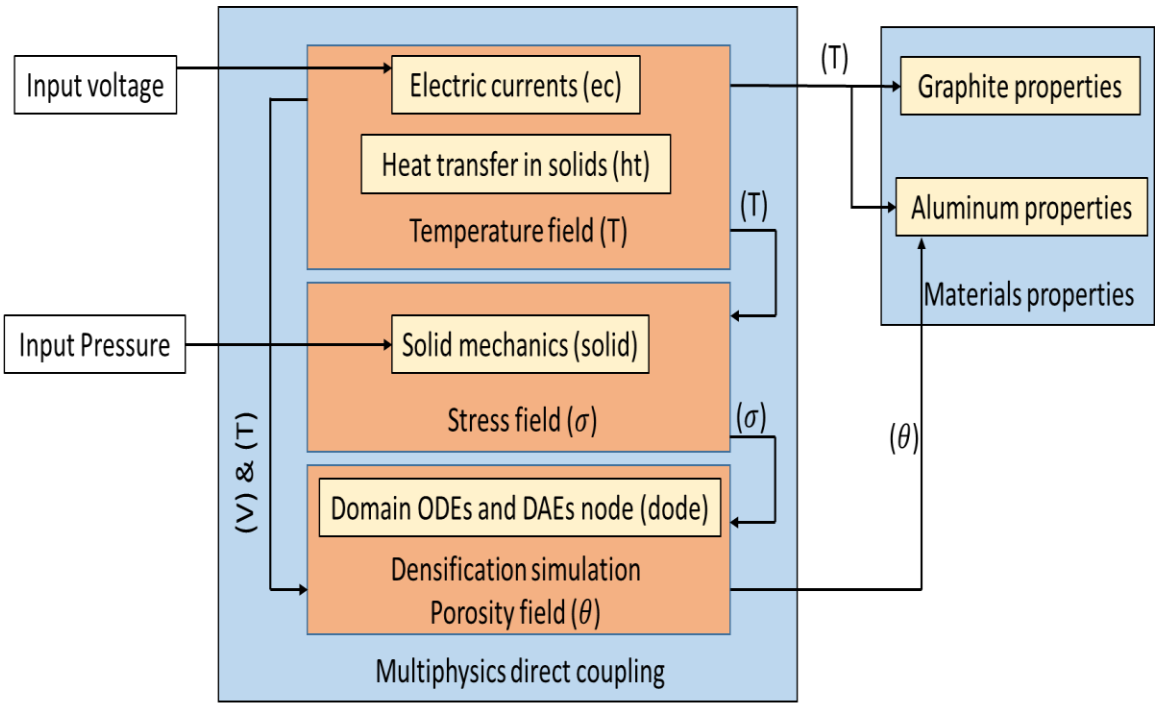

Figure 58. Implementation in Comsol Multiphysics, (V) represent the electric potential field

4.3.1 Geometry, inputs, and Assumptions

Axisymmetric formulation is used in this case because voltage, pressure, geometry, boundary conditions, and material are axisymmetric. Upper and lower punches are made from graphite, and the powder material is aluminum. Figure 59 shows the assembled geometry as well as the material associated with each part. Table 7 shows the dimensions of the parts.

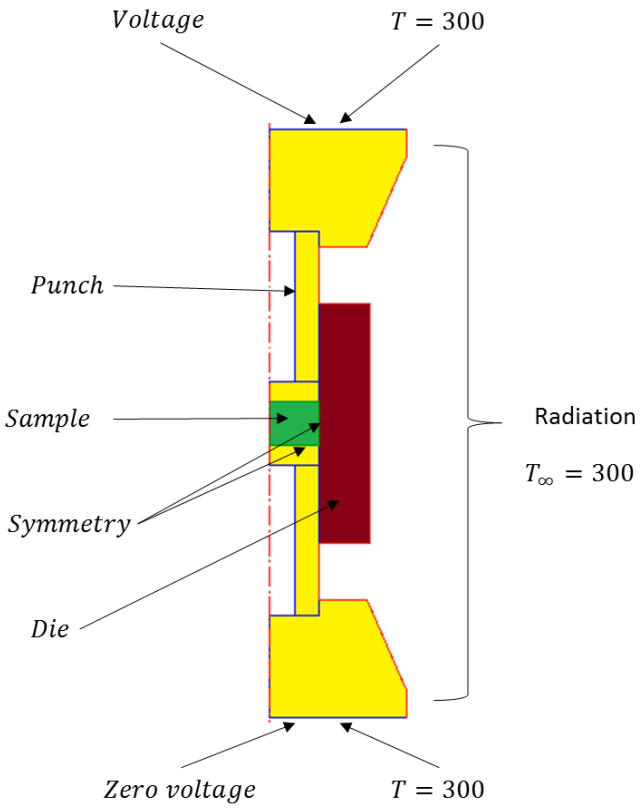

Figure 59. Geometry and boundary conditions

Voltage input was extracted from the experimental voltage profile and applied to the upper surface of the upper punches, whereas a zero voltage is applied to the lower surface of the lower punch. This way, pulsed direct current passes through the whole system causing it to heat up. Since upper punch moves downward in the SPS machine, and the lower punch is fixed during the process, the load profile (pressure vs. time) is applied on the upper surface of the aluminum powder. Figure 60 shows the pressure profile as recorded from the SPS machine in addition to a drop to zero pressure at the end of the process. Mechanical contact between punches and the sample is assumed to be perfect, and the same is assumed for thermal and electrical contact.

Table 7. Geometry dimensions

	Inner diameter [mm]	Outer diameter [mm]	Height [mm]
Die	20	40	48
Punch	-	20	34
Trapezoid Part	-	55	23.5
Sample	-	20	8.5

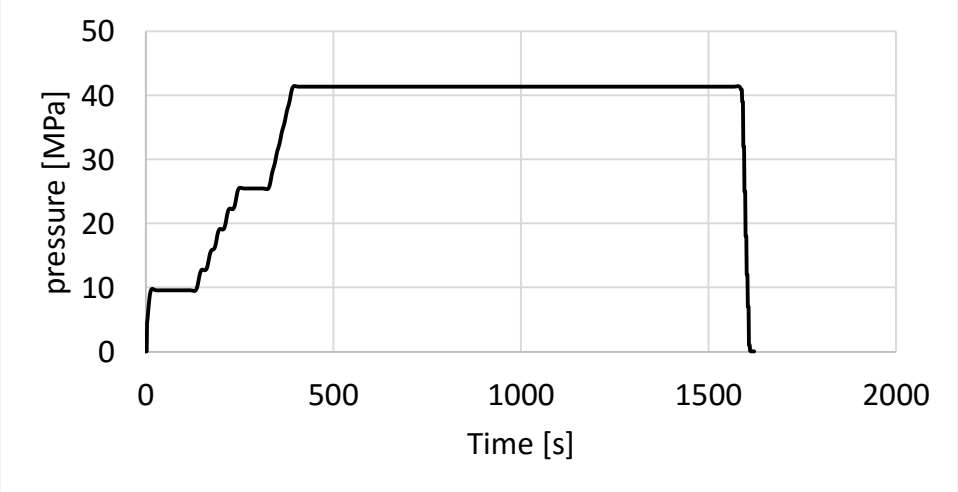

Figure 60. The Applied load including releasing the load

4.3.2 Boundary Condition

Heat is dissipated during the process to surrounding vacuum chamber by means of radiation, with surface emissivity 0.8 [40] heat loss by radiation is written as

$$q_r = \sigma * \varepsilon_r * (T^4 - T_\infty^4) \qquad 4\text{-}24$$

Where σ is the Stefan Boltzman's Constant and ε_r is the emissivity constant, (T_∞). Upper and lower punches are in contact with rams which conduct the direct current and deliver pressure to the upper punch, these rams are continuously cooled by cold water during the process, there is a big chiller unit attached to the SPS machine to cool this water. As heat is dissipated to the cooling water, a convection heat flux is applied to surfaces of the punches. At the contact surfaces between the powder and die, powder is not allowed to move in a direction normal to this surface, the same condition between powder and lower punch. Thus, asymmetric condition is applied to aluminum sample at these surfaces, the equation governing this condition is written as

$$n \,.\, u = 0 \qquad 4\text{-}25$$

Where (u) is the velocity, and (n) is the normal unit vector. The total time of the process is about 1900 seconds, a 0.7-time stepping is used so that any sharp changing in the results can be captured, for instance in the heating period big changes happen in the values of temperature and porosity, and this period is small (about 200 seconds)

4.4 Model Calibration and Validation

The first step in the model is to predict the right temperature field resulting from joule heating phenomena, and the stress field, second step is to capture the densification happened at the end of the process.

4.4.1 Temperature Field

The thermocouple measurement point is located at a distance of approximately 14 mm from the center. This point (Figure 61) is used to control the process by the SPS controller, and the graphite properties are adjusted until the simulated temperature at the same point shows good agreement with the experimental temperature. These material properties depend greatly on the temperature [40]. Properties values before calibration are taken from die manufacturing company.

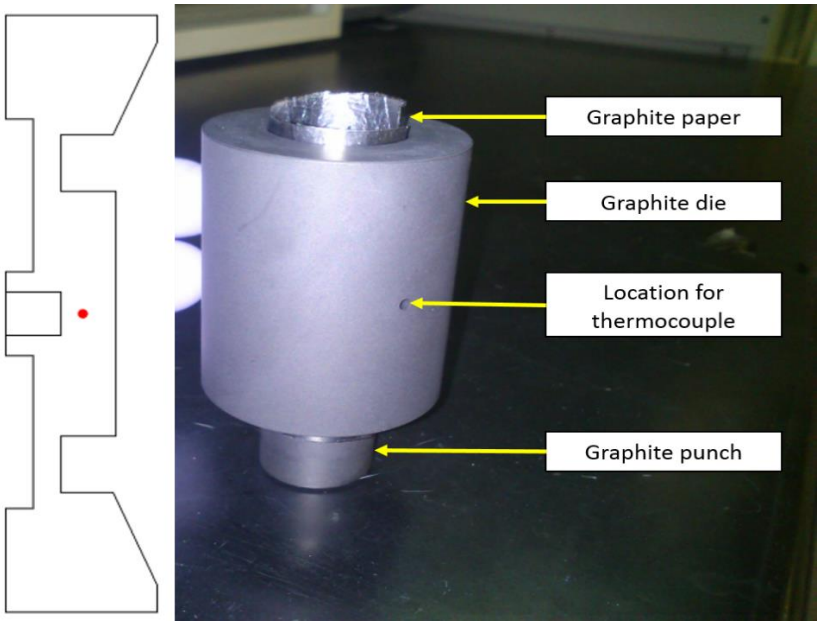

Figure 61. Location of measuring temperature

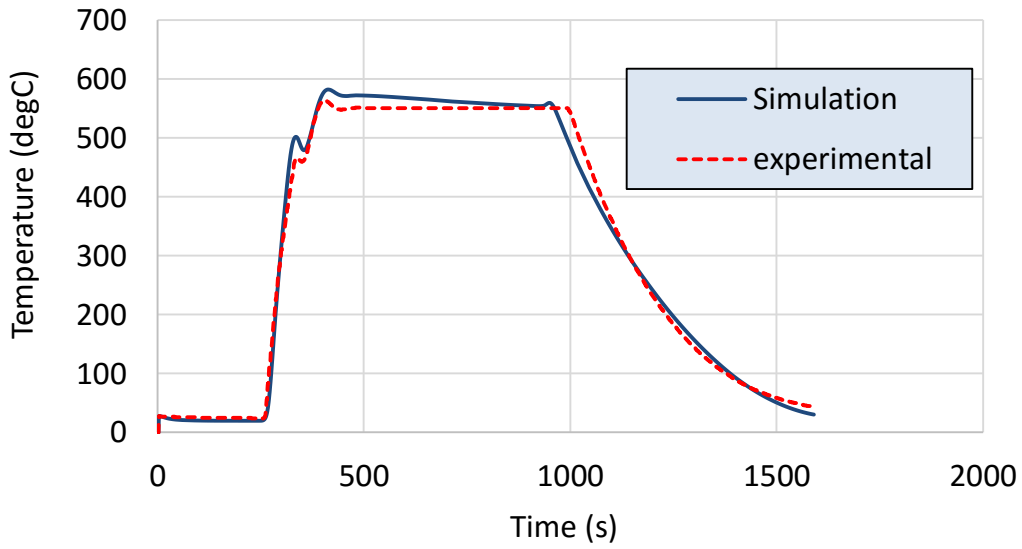

Figure 62. Temperature calibration

As shown in Figure 62 the calibrated graphite properties (Table 8) give reasonable agreement with experimental measurement.

Table 8. Graphite properties after calibration

Property	Value	unit
Heat capacity (C_p)	7.191*T + 1713.9 [T < 793 K] 4700 [T > 793 K]	J/kg.K
Thermal conductivity (k)	-0.026*T + 129.3 [T < 1500 K] 90.5 [T > 1500 K]	W/m.K
Electrical conductivity	$-6E\text{-}15*T^6 + 6E\text{-}11*T^5 - 3E\text{-}07*T^4 + 0.0007*T^3 - 0.9683*T^2 + 761.34*T - 152095$	S/m

4.4.2 Porosity

The resulted average porosity from the simulation is 5.1% when applying the process parameters of case-1, (41 MPa pressure, and 550℃). Measurements of porosity for the same case using Archimedes principle is 5.87%, which shows good agreement between the model and the experimental results.

CHAPTER 5

Results and discussion

5.1 Temperature

Results show that temperature field is highly affected by the shape of the system components, and the boundary conditions. Mainly the region where the powder is located at the center has higher temperature than other regions most of the time.

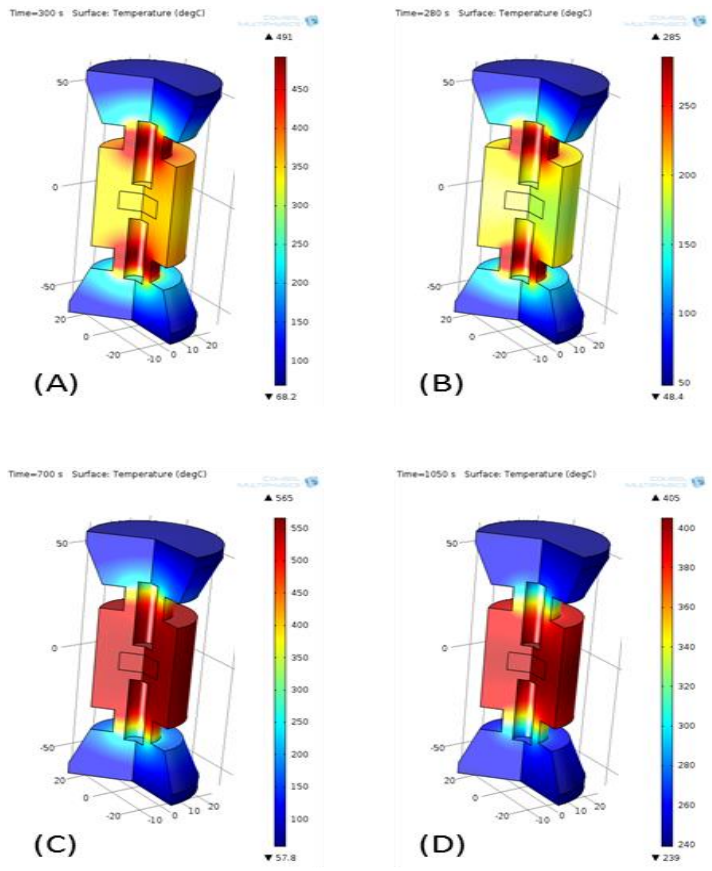

Figure 63. Temperature: (A) after 280 seconds, (B) after 300 seconds, (C) after 700 seconds, (D) after 1050 seconds

Temperature distribution after 280s which is the beginning time of heating period is shown in Figure 63 A, temperature is higher at the small cross-section area of upper and lower punch. When the process is just about entering holding period, in (B) temperature start to increase more in the location of the sample until it becomes the highest temperature in the holding time as shown in (C) and (D)

5.2 Porosity

Figure 64 shows model results for porosity at the end of the process. This variation trend captured by the model is very close to the experimental measurement (Figure 39) as it has lower value at the center of the sample and increasing towards the outer radius.

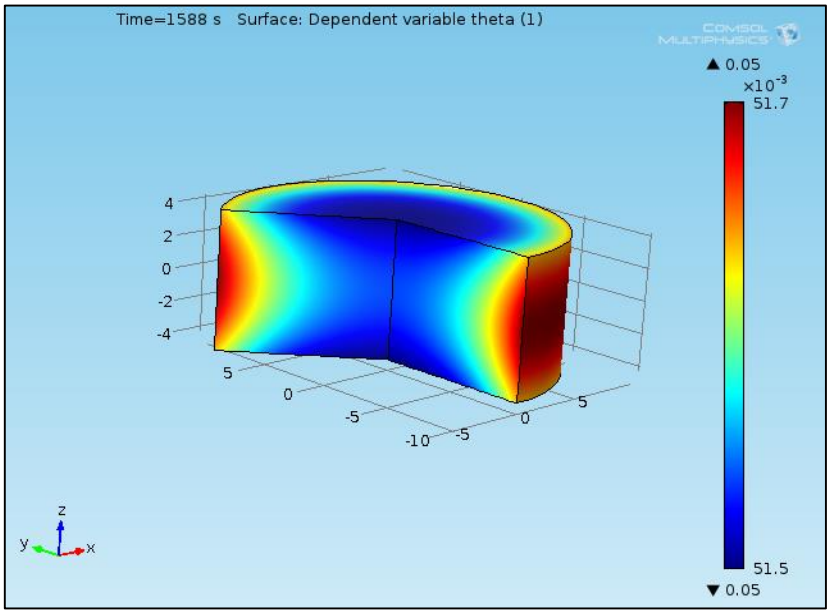

Figure 64. Porosity at the end of the process

The parameter that has the most effect on porosity variation is temperature, below is a brief description of the simulated temperature profile in the sample through the process and its relation to porosity evolution during the process time.

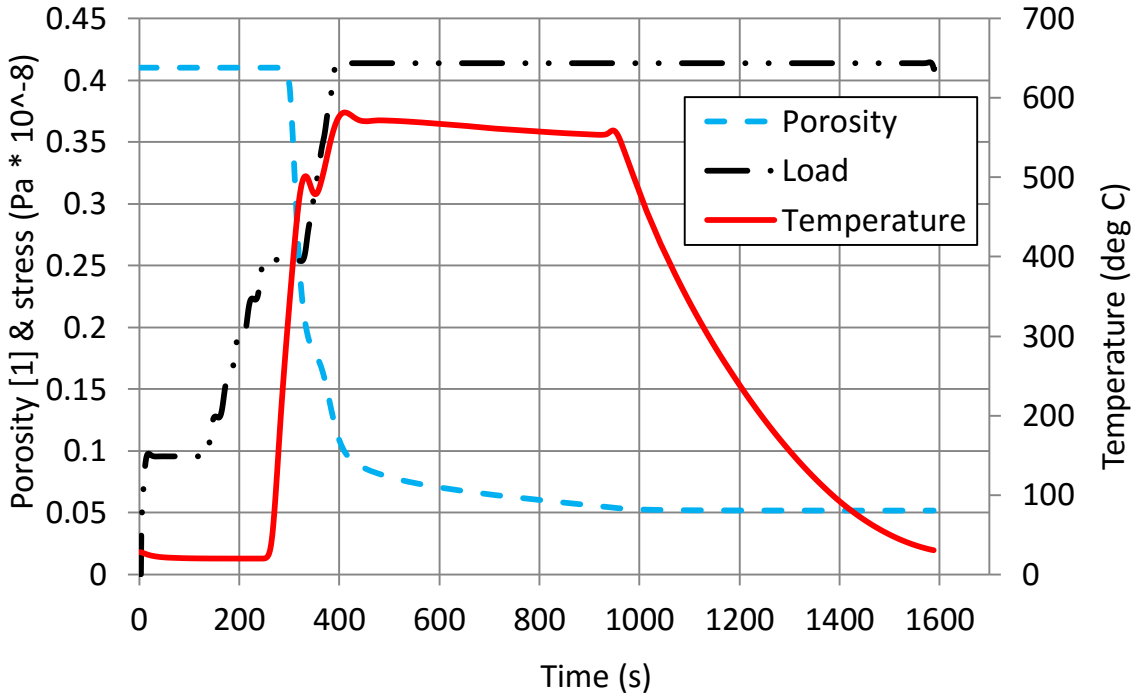

Figure 65. Pressure, temperature, and porosity during the process

Blue line in Figure 65 represent porosity value at the center of the sample, the green line is the applied pressure, and the red line represents the temperature at the same point in the center of the sample. Most of the porosity reduction happened in the period between 284 and 400 seconds after beginning the process which is a heating period. Porosity reduced from 41 % to 11 %, this period is shown by two vertical black lines in the figure. Temperature gradient inside the sample at this period is relatively high when compared to gradient at other time in the process, difference between maximum and minimum reach

3℃ because heating rate is high and temperature cannot reach equilibrium that fast. Also heat generates in the aluminum sample with different rate than it does in the graphite punches and die, and heat is conducted between the two materials through the surface on contact. Figure 66 shows this variation. When comparing it with porosity variation measured at the end of the process (Figure 64), an obvious relation can be deduced, places where the temperature is high porosity is low at the center and vice versa.

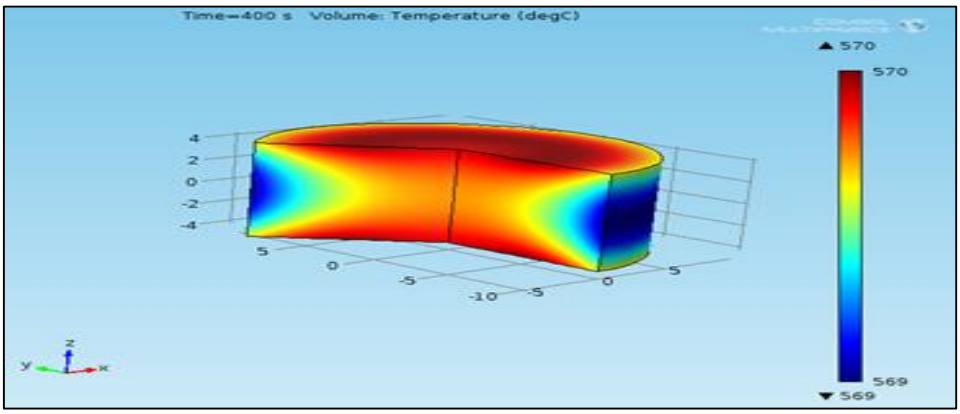

Figure 66. Temperature profile during heating period

In the holding period when temperature is maintained at the highest value, there is almost no variation, because temperature had reached equilibrium. Although the temperature is high, but porosity decreased from 11 % to 5.8 %, this reduction is small when compared to the heating period, because rate of change in porosity reduced when porosity itself reduced as shown in equation (4-2). Heating period has significant effect on porosity gradient because most of the porosity change happened in this period (85.5 % of total porosity reduction, and Temperature variation is high ($up\ to$ 3 ℃) compared to the rest of the process time which is less than 1 ℃.

5.3 Densification mechanisms contribution

In this study, the model is used to study the contribution of each densification mechanism on porosity reduction. This is done by simulating the process parameters of case-1 considering only power law creep, then creep and electro-migration, then adding surface tension, and finally the diffusion under load. Final porosity is measured at the end of the process after each simulation to evaluate how much each mechanism contributes to the densification process. Results show that the total contribution of creep is the main mechanism in the process as shown in Figure 67. Since electro-migration has considerable effect on densification, its contribution is also studied as it changes with the process time. Figure 68 shows the contribution of creep and electro-migration separately as well as combined. It is clear that creep dominates the behavior and therefore it is reasonable to only consider creep.

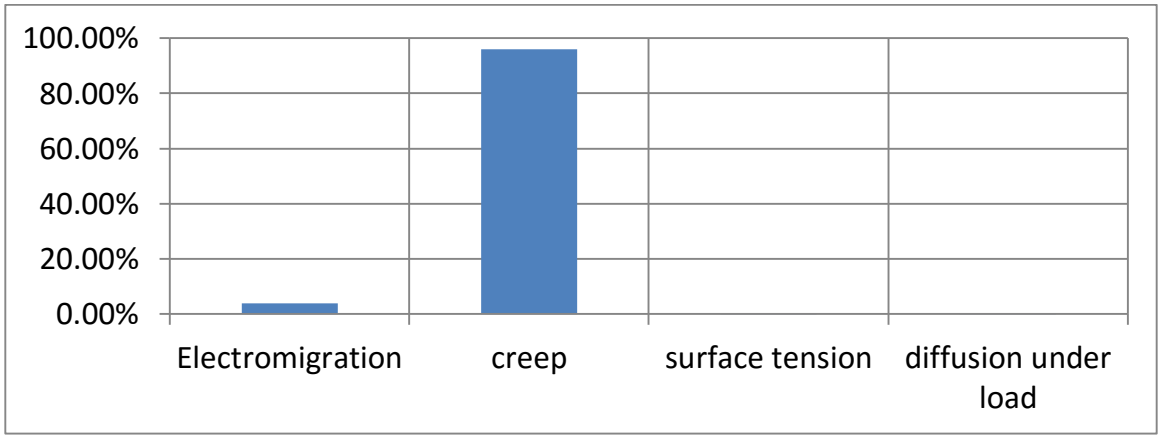

Figure 67. Densification mechanisms contributions

Electro-migration has a total contribution of 3.84% and it is uniformly distributed during the whole process time. In the heating period, electro-migration has no contribution as all

densification results from creep. In the holding period, electro-migration has more effect than the heating period as it contributes with 22% from the densification occurring in the holding period.

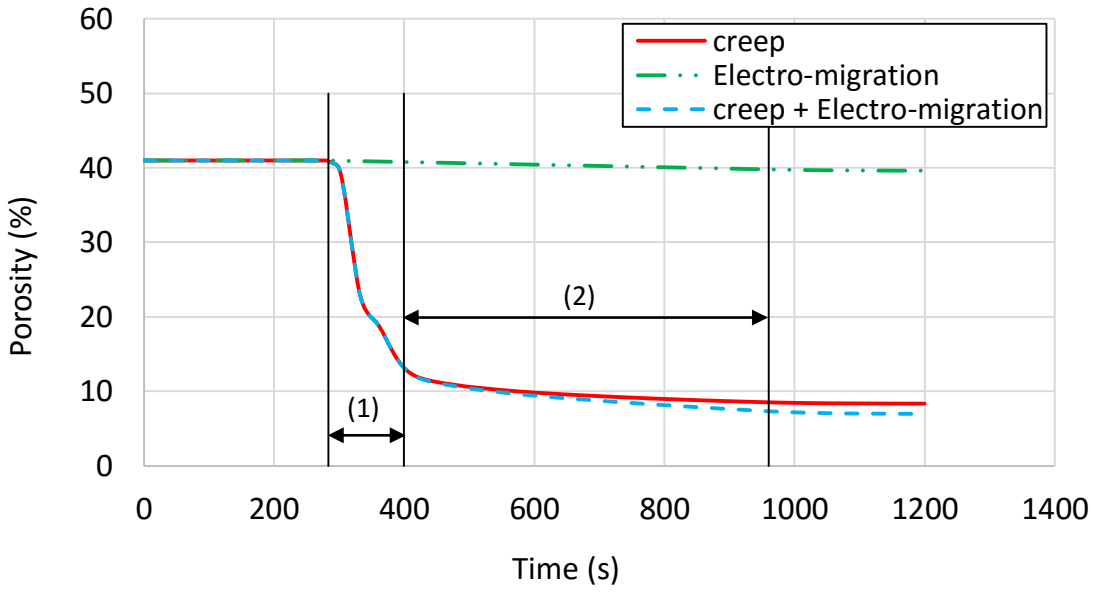

Figure 68. Electro-migration and creep contributions to densification (1) represent heating period & (2) holding period

5.4 Parametric study

We used different parameters [holding temperature and holding pressure] and we checked the simulated porosity and compare it with an experimental measurement using Archimedes principle. Two temperatures and two pressures were considered as follows

Table 9. Experimental validation for the parametric study results

	Temperature (℃)	Pressure (MPa)	Experimental Porosity (%)	Simulation Porosity (%)
Case-1	550	41	5.87	5.1
Case-2	550	25	7.78	8.35
Case-3	450	41	11.2	11.24

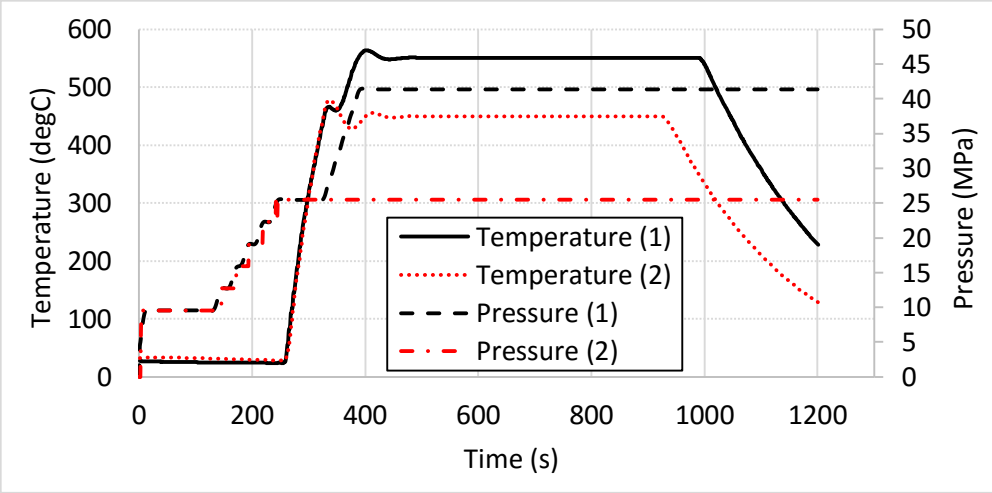

Figure 69. The temperatures and pressures profiles used for the parametric study

In this part of the study, the holding temperature and pressure are varied to examine their effect. The simulated porosity is compared with experimental measurements using Archimedes principle. Figure 69 shows the two temperature and pressure profiles considered for this study. Three different combinations are considered. Table 9 shows the three combinations along with a comparison of the computational and experimental results. As expected, by reducing temperature from 550°C to 450℃, porosity increased to 11.24% from 5.1% (Figure 70). Also reducing the pressure by an amount of 16 MPa causes the porosity to increase up to 8.35%. All the results matches well with the

experimental values. One can conclude the temperature has higher impact on porosity than pressure.

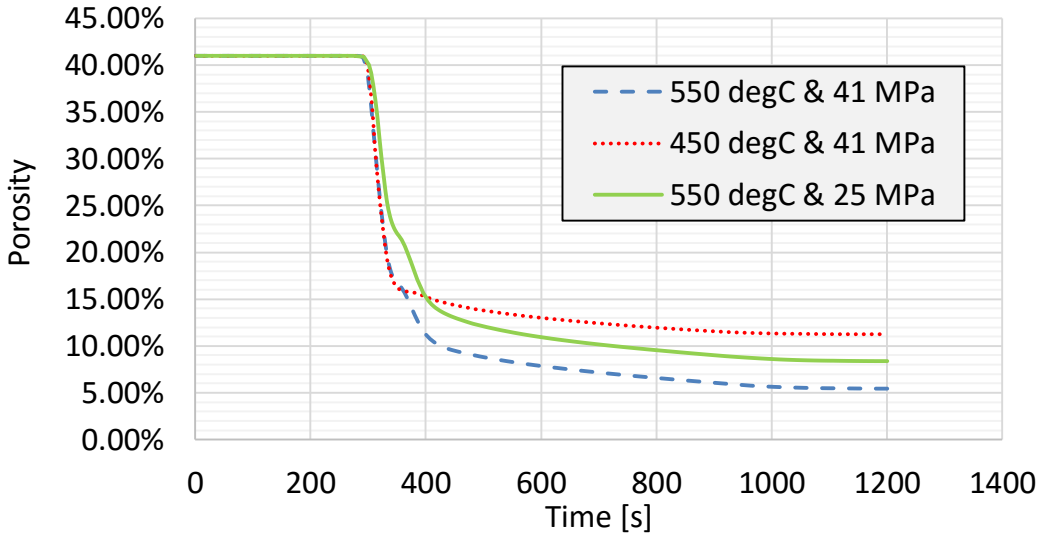

Figure 70. Porosity evolution for the three cases

The model showed that most of the porosity reduction occurred during the heating period as shown in Figure 70. To check this experimentally, one sample with temperature 495 ℃ and pressure of 41 MPa with zero holding time was produced. In this case, all porosity reduction occurred in the heating period. The experimental measurement of porosity was 13.8 %, and the simulation gave a porosity of 13.56 % as shown in Figure 71. By comparing this case with case-3, porosity increased from 11.24% to 13.56%, because of the effect of the holding time. Although, the maximum temperature in case-3 is 480℃ which is less than the maximum temperature used in zero holding time case by 15℃.

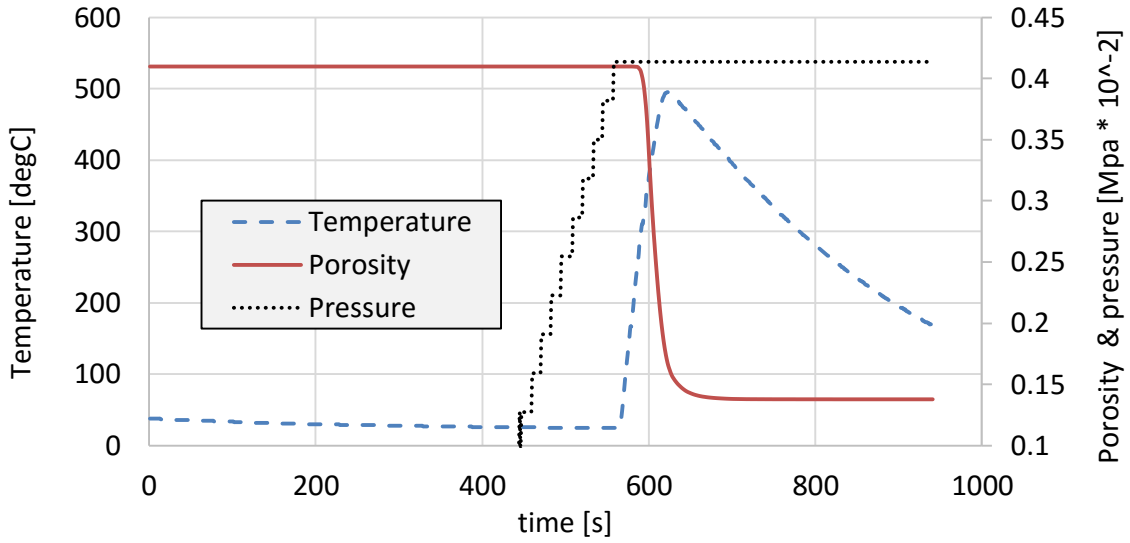

Figure 71. Zero holding time case

5.5 Stress

Stresses developed in the aluminum sample during the process show that stress in Z direction is following the pressure applied by the upper punch. There is a difference between the stress values of r & θ component, both of them increased when temperature increased due to the thermal expansion. At the highest temperature, material become soft, resulting in decreasing the r & θ stresses -22.9 MPa. Z stress component remain high -41 MPa, although temperature is high and the material is soft because of the uniaxial load in Z direction from the punches, which is compressive load. The same behavior is shown by Wang and Casolco [29], the material simulated in that work is copper

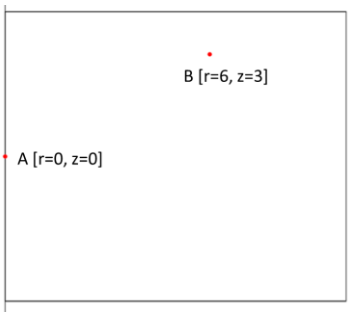

Figure 72. Two points on the section of the sample (distances in mm)

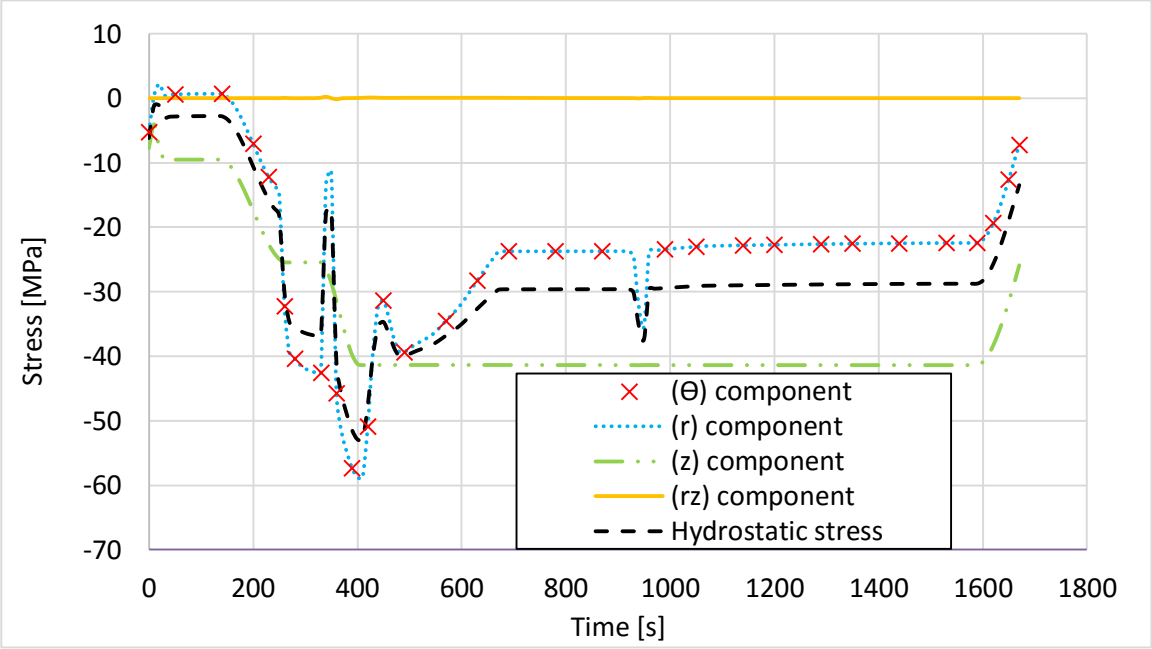

Figure 73. Radial (r), hoop (phi or θ), axial (z), (hydrostatic stress), and (rz) stress components at the center of the sample (Point A)

The spatial distribution of these stresses components shows non-symmetrical behavior in the axial direction because the upper punch is moving while the lower punch is fixed. The stress affects the resulted microstructure and porosity variation in the sample, but in the mathematical model adopted in this work consider the effects of axial stress only on the densification. The radial and hoop stress are fluctuating during the heating period,

because of the difference in the initial yield strength and hardening function of the aluminum at room temperature and elevated the temperature.

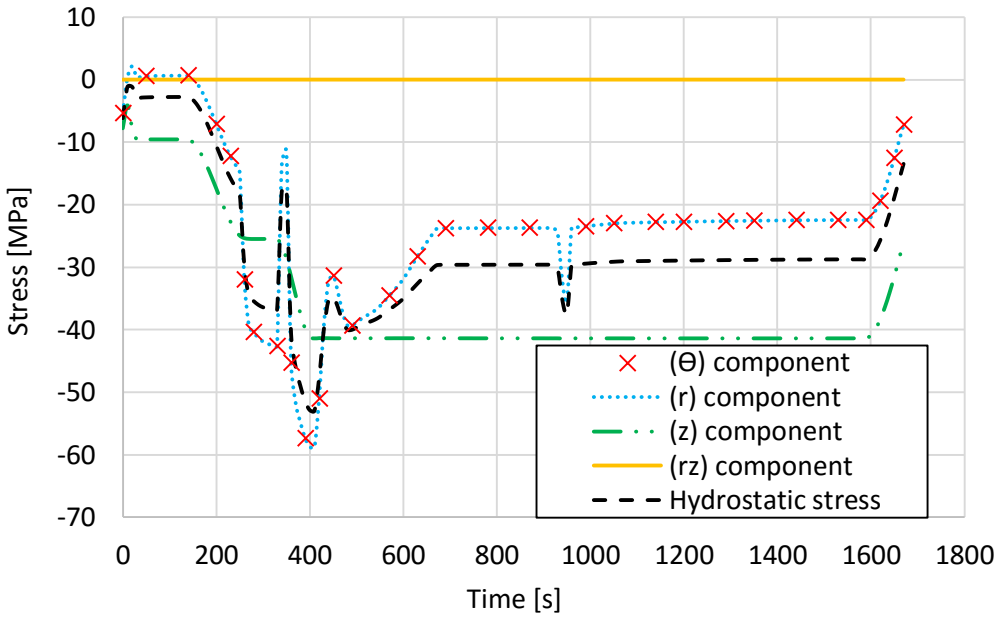

Figure 74. Radial (r), hoop (phi or θ), axial (z), (hydrostatic stress), and (rz) stress components at the center of the sample (Point B)

Aluminum has high thermal expansion, material is displaced more towards the outer radius of the sample hence resulting in more compressive stresses in the radial and hoop stresses, during cooling period r & θ stress components shows a transition from compressive to tension, this can be explained by the fact that material shrink at this period, a tension radial stress are reported by Wang et al. [30]. The rz stress component is not exactly zero but has very small value about 0.035 MPa during the holding time period (Figure 75). The variation in all stress components is very small in the sample, almost less than one MPa, because of the simple disc shape and the size of the sample is very small. Figure 73 and Figure 74 show that at the end of the process there is residual stress,

especially radial and hoop stresses -7 Mpa. The hydrostatic stress which is the part of the stress responsible for the change in the volume is a good analysis criterion, as it involves all the three stress component z, r, and θ, in this case residual stress value at the end of the process is about -12 MPa, the highest residual stress is the axial stress component.

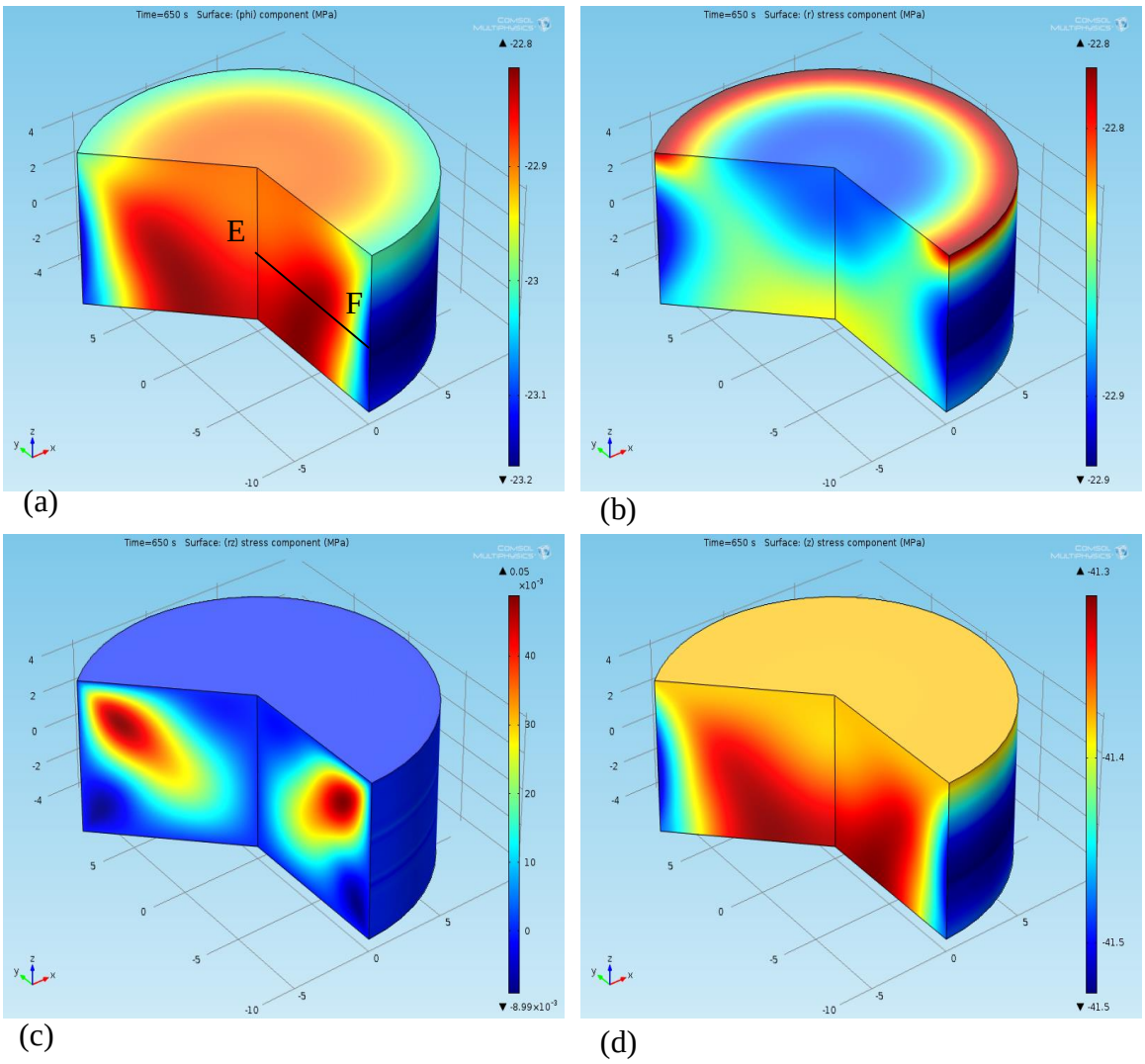

Figure 75. Stress components after 650 seconds in the holding time (a) hoop stress, (b) radial stress, (c) [rz] stress component, (d) axial stress

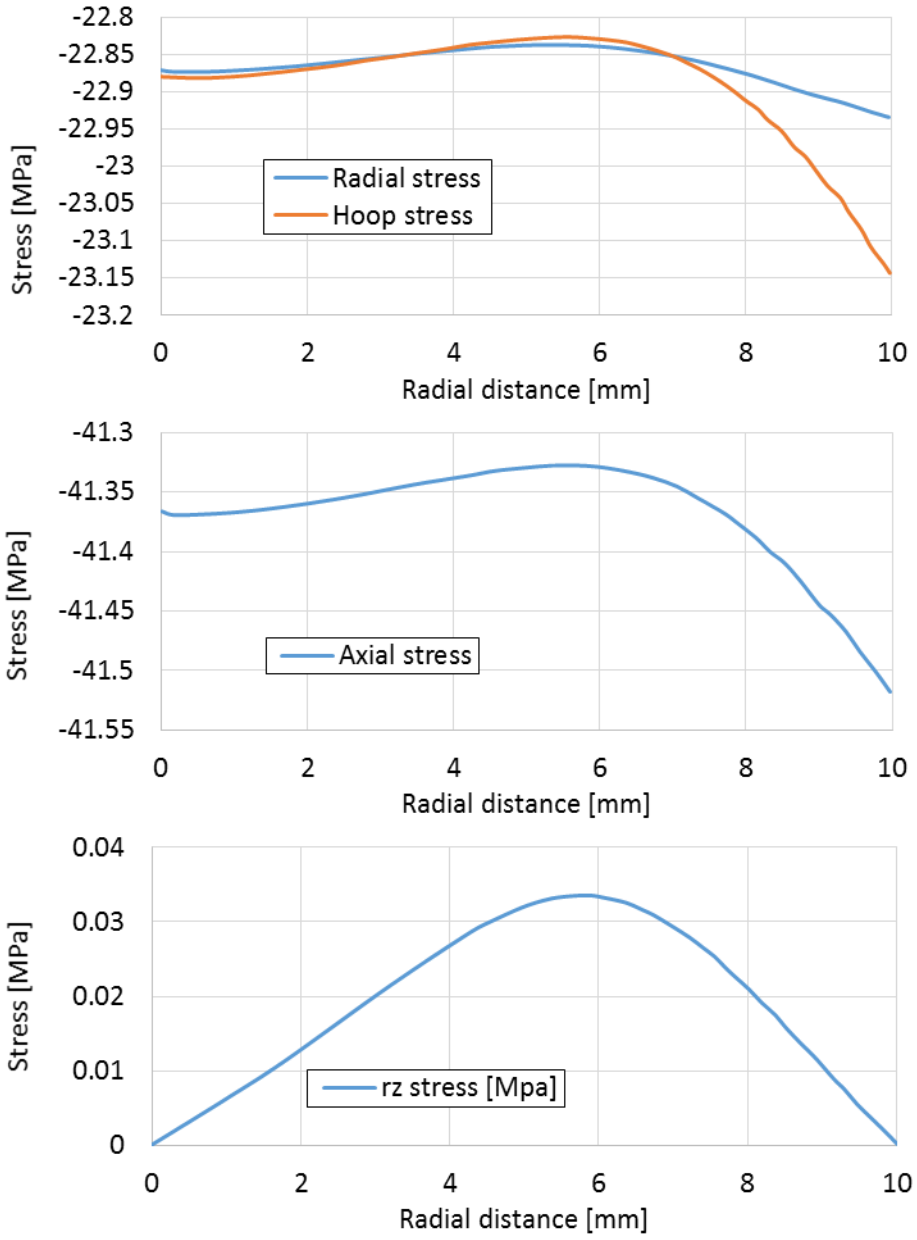

Figure 76. Different stress components along (E-F) line after 650 seconds of the beginning of the process

Axial stress result show higher compressive stress at the outer radius of the sample. The same trend is observed in radial and hoop stress as shown in Figure 76. And this is due to the assumption that the die is rigid

5.6 Conductive material and non-conductive material

In this part of the study, the model is utilized to simulate the densification of alumina, which is an electrical insulator with a thermal conductivity of 30 W/(m·K), and compare it with aluminum. Aluminum thermal conductivity is much higher than alumina with a value of 237 W/(m·K). A temperature of 1300 ℃ is used for sintering alumina because it has a high melting temperature of 2072 ℃. A maximum pressure load of 41 MPa was used for both materials (Figure 77).

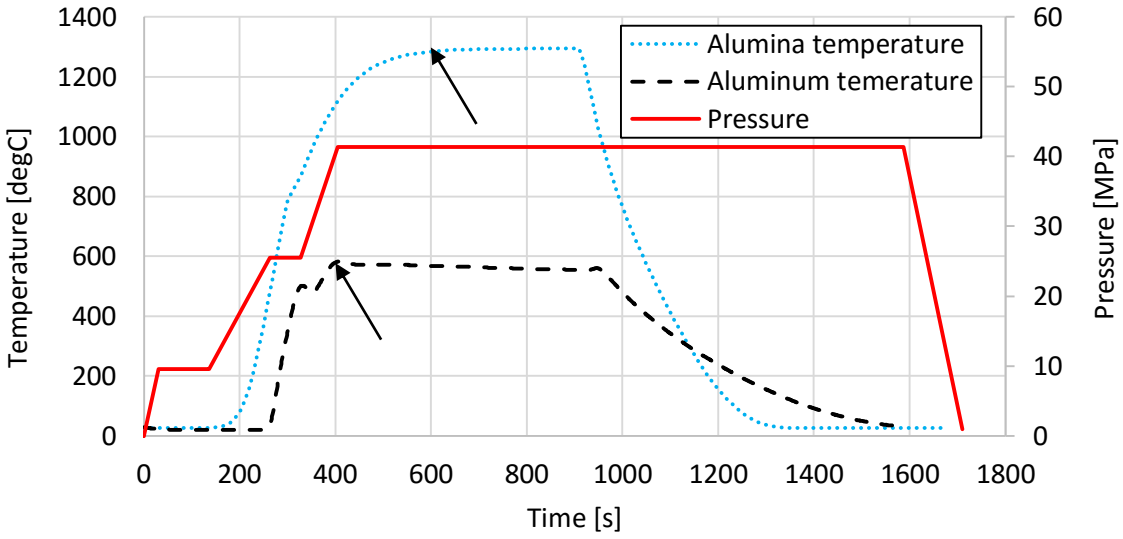

Figure 77. Process parameters for aluminum and aluminum (the two arrows indicate the moments at which we compare porosity when reaching maximum temperature in each case)

Porosity variation at the moment when the temperature is near its maximum value, which is around 410 seconds for aluminum (Figure 78) and 600 seconds for alumina (Figure 79) show different patterns in aluminum and alumina. Aluminum has low porosity at the center and lower porosity at the outer radius. On the other hand, the alumina sample has the opposite pattern that is higher porosity at the center and lower porosity at the outer

radius. Alumina has a porosity variation at the beginning of the holding time of 0.2%. This range is reduced to 0.03% during the holding time and the cooling time. This means the porosity field became more uniform with time. The pattern of porosity also changed during the process. On the other hand, aluminum porosity is almost uniform from the beginning of the process until the end of the process with a range of 0.03%, and the porosity field pattern is also the same during the process as the center of the sample is more dens than the outer radius.

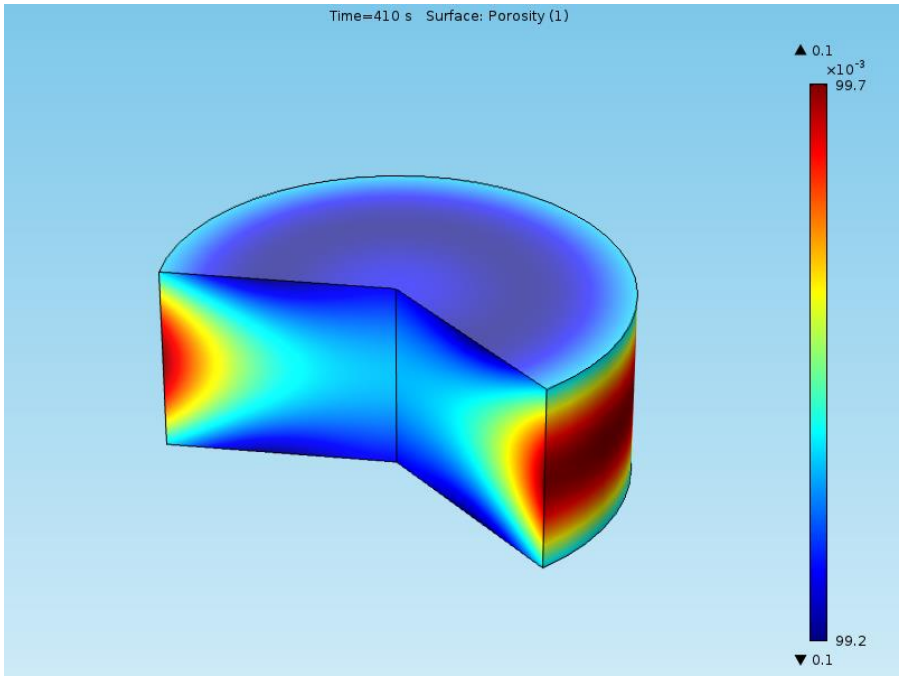

Figure 78. Aluminum porosity at 410 s (when temperature reaches maximum level)

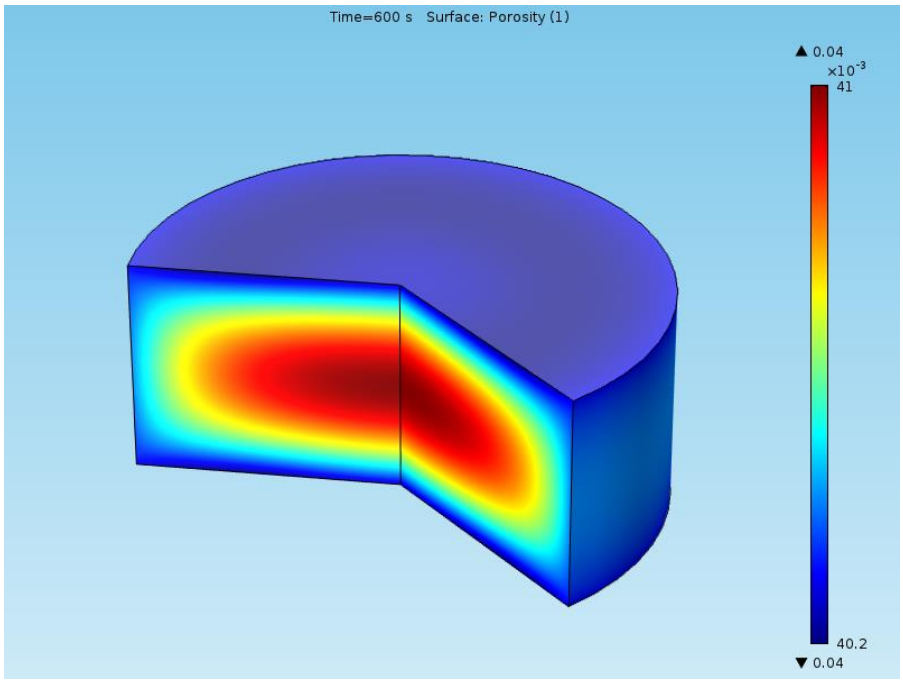

Figure 79. Alumina Porosity at 600 s (when temperature reaches maximum level)

One of the main reasons for the two different patterns is the temperature gradient and variation pattern for each sample, during the period between the moment when temperature start to rise up, and the moment of reaching the maximum temperature. Figure 80 shows the temperature gradient at different times.

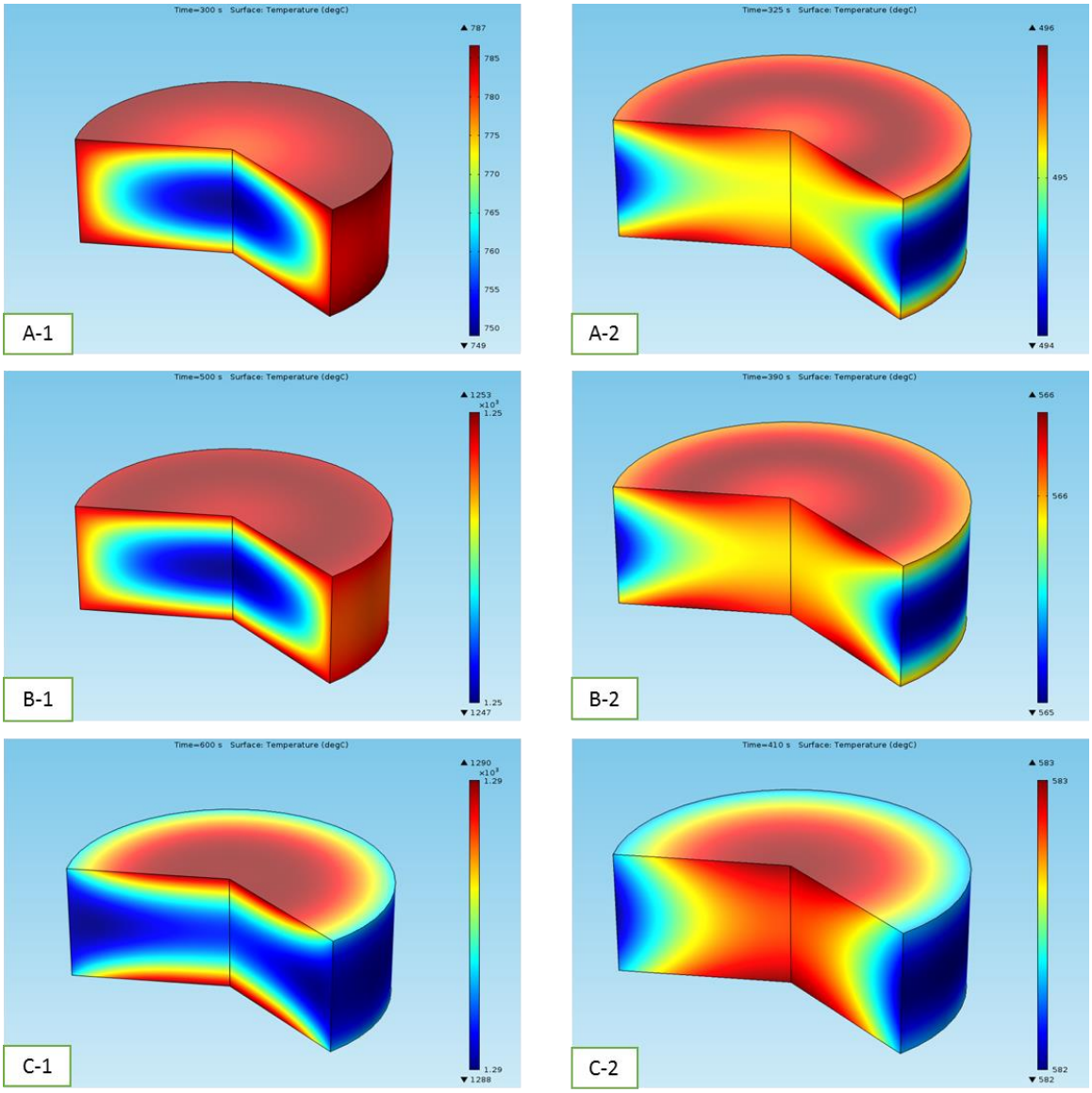

Figure 80. Temperature (℃) (A-1, B-1, C-1) is the temperature of alumina after (300 s, 500 s, 600 s), (A-2, B-2, C-2) is the temperature of aluminum after (325 s, 390 s, 410 s)

For aluminum most of the time temperature at the center is higher than the outer radius, that's why porosity is high at the center. This temperature has this pattern because aluminum is electrically and thermally conductive, so the heat is generated inside the sample due to the passage of electric current and also the heat generated in the die rapidly is conducted to the sample, this causes the low-temperature gradient (the maximum

difference is 3℃). On the other hand, temperature pattern in alumina is different, higher temperature on the outer surface of the sample and lower temperature in the center of the sample, because electric current is almost not passing in the sample, and that is why the heat is not generated inside the sample. But heat is generated in the die and the punches, for this reason the outer surface of the sample has high temperature. Moreover, the thermal conductivity of alumina is lower than that of aluminum, so the heat is not easily conducted from the outer surface to the center of the sample. As a result, a high temperature gradient is observed, difference between maximum and minimum temperature in the sample reach more than 10 ℃. In the case of alumina, the holding time is important, because it allows the temperature gradient to be minimized as the temperature has the time to be conducted from the outer surface to the sample core. The second parameter which affecting porosity is the axial stress since the mathematical assumption adopted in this work consider the stresses only in the direction of the uniaxial load, which is the axial stresses. Figure 81, and 82 below show the axial stress in aluminum and alumina at the moment when the temperature reaches maximum level. Results show very small variation, difference between maximum and minimum value is about 1 Mpa.

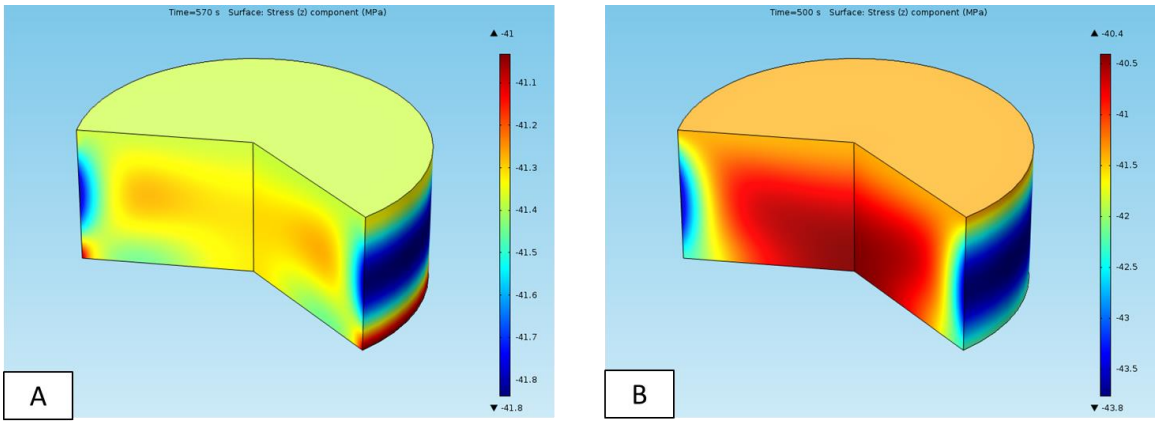

Figure 81. Axial stress in alumina sample during the heating period, (A) after 570 seconds, (B) after 500 seconds

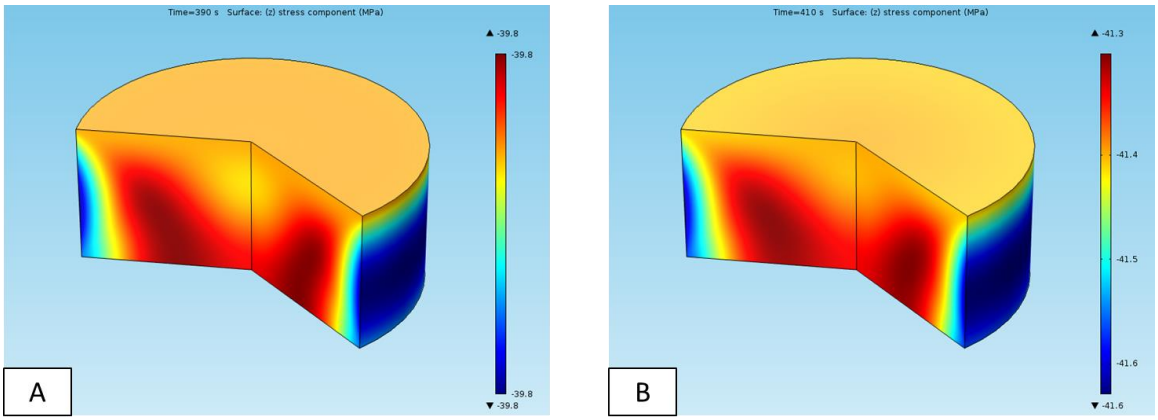

Figure 82. Axial stress in aluminum sample during the heating period, (A) after 390 seconds, (B) after 410 seconds

Porosity variation pattern is affected by temperature field more than the stress field during heating period. Because axial stress is the component which affecting porosity according to the assumptions of the mathematical model, and it is almost uniform in both cases, aluminum and alumina, due to the uniform cross section.

5.7 Shape effect (Sample, die and punches

In this study, the model is used to analyze the SPS process for another sample shape. The sample considered for this part is a cutting tool insert made by Kennametal which is an American supplier of tooling and industrial materials. Figure 83 shows the insert tool geometry.

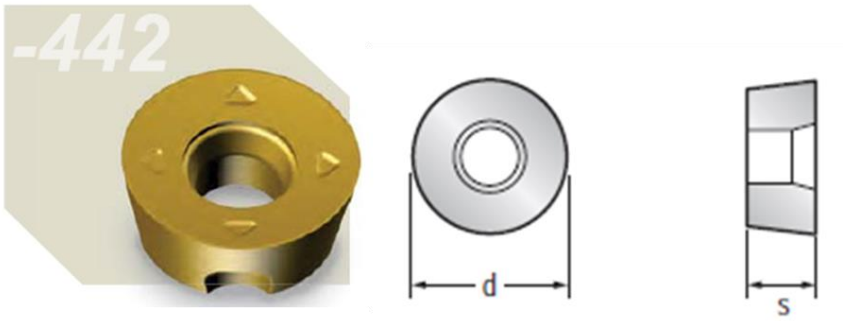

Figure 83. Positive geometry minimizes the pressure from the chip

The circular shape of the sample makes it possible to use an axisymmetric model as was done in the previous analysis of this work. A system of die and punches, as shown in Figure 85, is used to produce this shape using SPS. The small angle on the lateral surface of the tool makes it difficult to produce the shape directly by SPS, and therefore some machining is required after SPS is performed. The shape could be produced directly using metal injection mold technique with minimum machining required after the production of the shape. In SPS, machining is required as mentioned, so the suggested initial shape is illustrated in Figure 84.

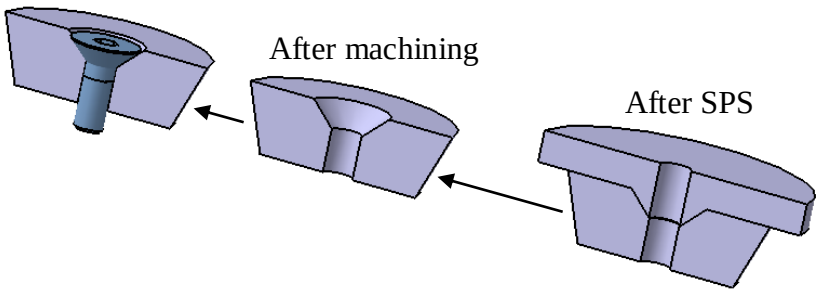

Figure 84. Producing the final shape steps

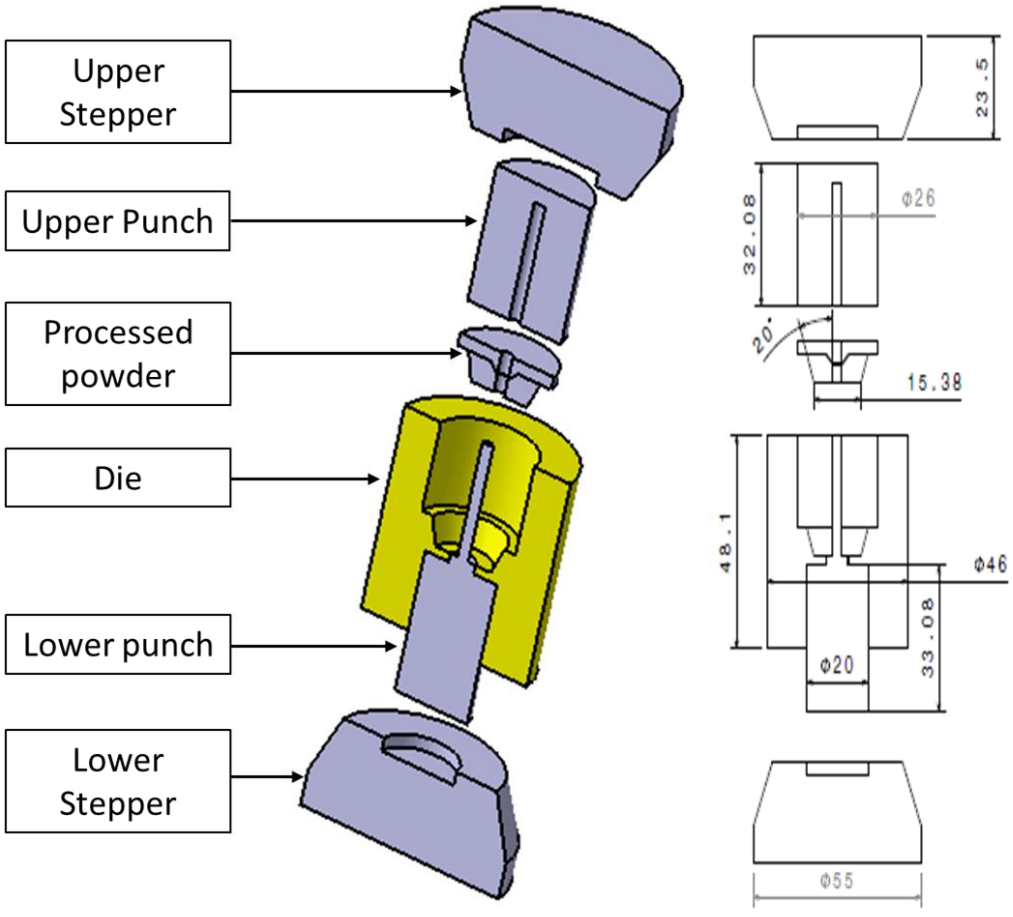

Figure 85. Die, punches and stepper to produce the tool shape [all dimensions are in mm]

The holding temperature used to analyze this geometry measured at the thermocouple location is 450 ℃ on average, holding pressure is 41 MPa. The temperature variation in the sample (Figure 86) is found to be much higher than the simple disc shape, because of sample shape itself, as well as the shape of the die and the punches, and the difference in the thermal properties of the two materials.

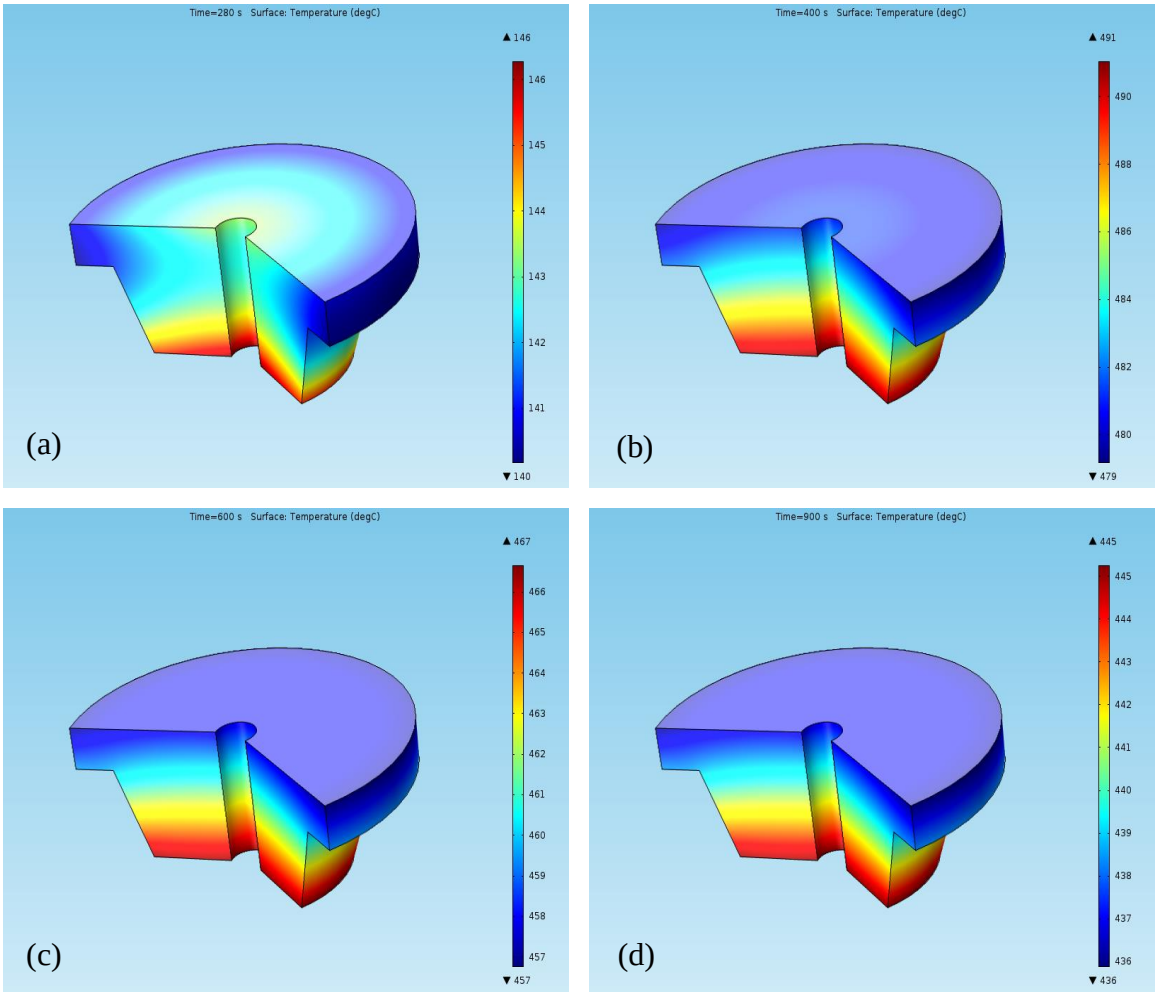

Figure 86. Temperature [degC] (a) after280 seconds, (b) after 400 seconds, (c) after 600 seconds, (d) after 900 seconds

When starting heating period after 280 seconds the difference between the maximum and the minimum temperature in the sample is about 6 ℃. The outer radius of the upper flange has the lowest temperature. During most of the heating and dwelling periods the variation become even higher, as the difference inside the sample reach more than 10 ℃, and the whole upper flange has the least temperature. Figure 87 shows the line (a-b) on which, temperature, axial stress, and porosity are plotted to study the vertical variation.

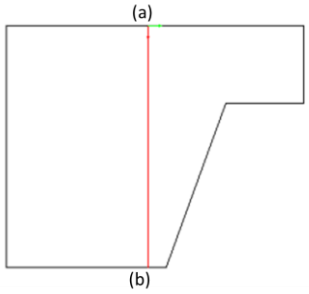

Figure 87. Line (a-b)

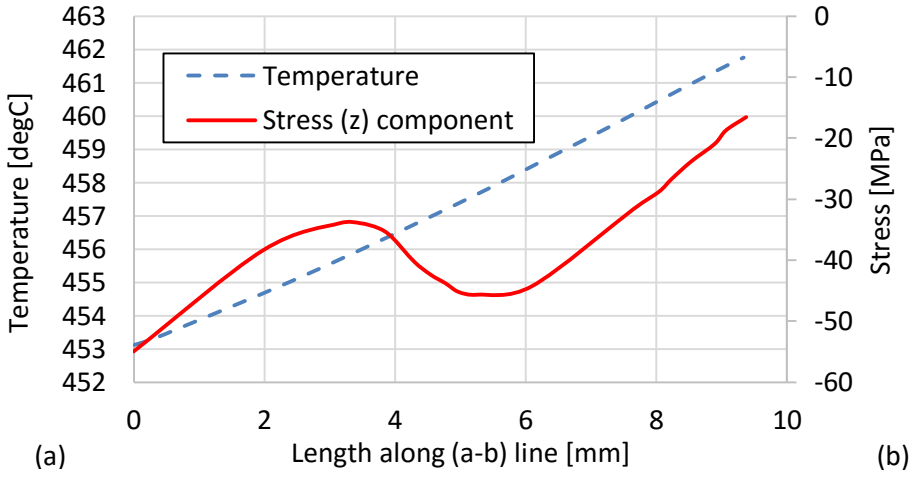

Figure 88. Temperature and stress (z) component distribution along line (a-b)

The temperature is lower in the upper flange and increasing towards the bottom surface of the tool insert. On the other hand, there is a higher compressive axial stresses in the upper flange than the lower surface, this difference reach more than 38 MPa as shown in Figure 88. It is expected that the temperature and axial stress will affect the densification in the sample thus making porosity variation (Figure 89) which leads to mechanical properties variation.

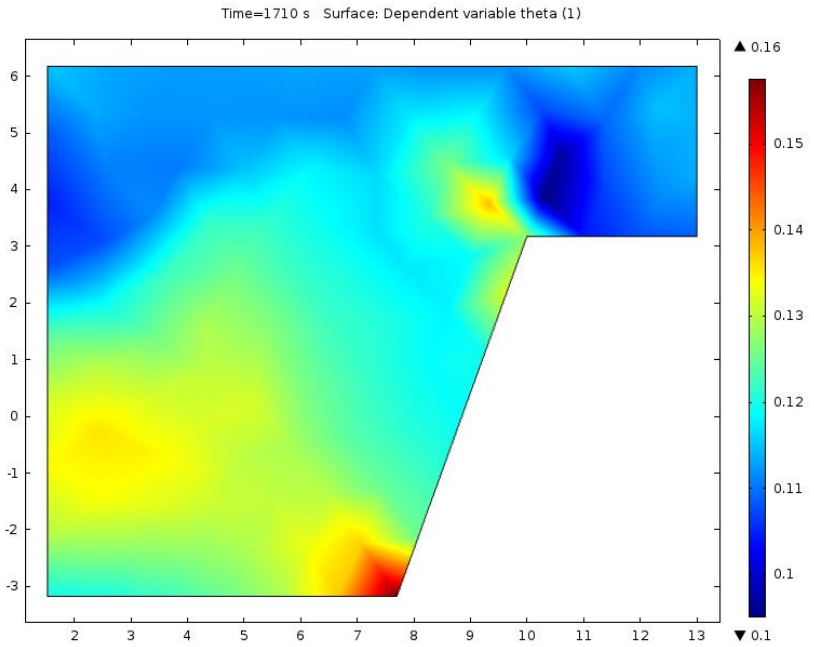

Figure 89. Porosity variation in the sample at the end of the process

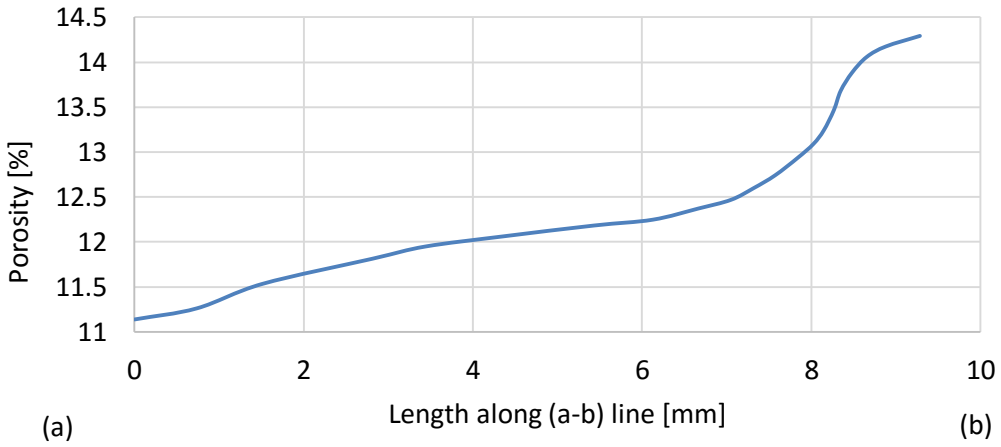

Figure 90. Porosity variation along line (a-b)

Results show that there is a higher porosity in the lower surface of the tool and higher porosity in the upper flange (Figure 90), it is clear that the effect of the axial stress variation, in this case, is higher than the effect of the temperature variation. Because the axial stress variation is relatively high, about 38 MPa, and temperature variation is about 10 ℃.

CHAPTER 6

Conclusions & Recommendations

6.1 Conclusions

The study was carried out to explore the SPS process and find out, to what extent, a numerical modeling for the process itself, could be reliable and useful to study the process and enhance the products. Or design the process parameters to achieve certain product properties. In this work, a multi-physics computational model that can capture densification during the SPS process is developed. Joule heating effect of the direct electric current is considered, and the model simulates densification during the process resulting from four different mechanisms. These mechanisms are power law creep, electro-migration, surface tension, and diffusion under load. The model is utilized to simulate the SPS process on aluminum powder with average size of 30 µm to produce a simple disc shape. The microhardness profile in the section of the sample is mapped experimentally using Vickers hardness test. Porosity profile in the section is also mapped experimentally using SEM Images. The model is used to investigate the production of a cutting tool insert. The effect of the material properties is investigated using the model too. The main findings from this work can be summarized as follows:

- A numerical model is developed for the process, with the ability to simulate the temperature, stresses, and porosity fields and how they evolve with time. The model is reliable to a good extent as the resulted porosity field is validated

experimentally using SEM images for an aluminum sample having a disc shape. the center of the disc has a higher density than the outer radius, this pattern is caused mainly by the temperature field, the effect of the stress field on the density variation, in this case, is very small, because the shape is disc and the stress field is almost uniform.

- Microhardness is evaluated on the section of the sample using Vickers hardness, and results show that the region where the microhardness is higher, is the same region where the numerical model shows higher density.
- The optical microscope is used to evaluate the microstructure on the sample section, images show that small grains are resulting from the process in the regions where the density is higher as expected by the model.
- The model is used to conduct a parametric study to achieve the desired porosity value by changing the maximum temperature and pressure, the results of the parametric study are also validated experimentally with good agreement.
- The model is used to compare the electrically conductive material and non-conductive material, by simulating the process for alumina and aluminum with the same process parameters, except the maximum temperature, because it should be higher for alumina than for aluminum. Results show that conductive sample tends to have a higher density in the center of the sample than the outer surfaces of disc shape. On the other hand, the non-conductive material has the opposite trend, higher density in the outer surfaces of the sample than the center.
- The model is used to study the shape effect on product quality, by simulating two different shapes for the same material (aluminum), and with same parameters. In

this case, the new shape has a non-uniform cross-section, this results in high-stress gradient. Because of this gradient, stresses affected the resulted density more than the effect of the temperature field.

- The simulated stress at the end of the process shows a compressive residual stress with a range of -7 MPa to -20 MPa in different stress components. This may be an advantage for the SPS process because compressive residual stresses may act to close the internal cracks in the material, thus enhancing the lifetime of the product.
- Experimental measurement of residual stress is done using hole drilling method, the resulted values is in the range -30 MPa to -50 MPa, these measured stresses are in the plane of the sample, so It represent stresses like radial stress and hoop stress which have almost similar values in the case of the disc shape .

The developed model in this work shows good results with aluminum mainly and alumina. The model could be used especially with the machine owned by the cent lab (research institute at King Fahad University of Petroleum and Minerals) as the calibration of the model is done based on this machine. Some studies showed that a specific porosity value in an object could enhance its lifetime and fracture toughness, so defining the process parameters to produce the desired Porosity could be one the usage of the model, also, the model could be used to study and to better understand the SPS process.

6.2 Recommendations

The model could be enhanced in many ways to give more accurate results, also to ease the usage for certain purposes, some of these enhancement ideas are listed below:

- Considering the contact resistance could enhance the results quality, namely thermal contact, Electrical contact, and mechanical contact. As they are assumed to be perfect in this model.
- Considering the thermal expansion and stresses in the die and the punches would be a good idea, because the thermal expansion of the die and the punches is affecting the stress field in the sample. Another benefit could be evaluating the stress field in the die and the punches, and avoiding their failure, which is a common problem usually happen during the SPS process.
- Adding a PID controller to the model in order to control the voltage and the pressure load, to achieve a defined temperature profile and defined density value at the end of the process.
- The mathematical model adopted in this study is considering only the densification in the uniaxial direction of the applied pressure. Results show very good accuracy when compared with experimental measurements, but can be enhanced by considering the densification in all directions.
- Experimental microstructure study shows that, the grains are aligned and elongated in one direction normal to the applied pressure direction, which may result in orthotropic properties. Further experimental investigation is needed to study this effect.

Overall the developed model could serve the research activities and reduce the number of needed experiments to achieve a certain goal, as usually models and simulations cannot substitute experiments totally.

References

[1] P. Ramakrishnan, "History of powder metallurgy," *Indian journal of history of science*, vol. 18, no. 1. pp. 109–114, 1983.

[2] M. F. Ashby, "A first report on sintering diagrams," *Scr. Metall.*, vol. 7, no. 10, p. xiv, 1973.

[3] D. Demirskyi, H. Borodianska, D. Agrawal, A. Ragulya, Y. Sakka, and O. Vasylkiv, "Peculiarities of the neck growth process during initial stage of spark-plasma, microwave and conventional sintering of WC spheres," *J. Alloys Compd.*, vol. 523, pp. 1–10, May 2012.

[4] H. Djohari and J. J. Derby, "Transport mechanisms and densification during sintering : II . Grain boundaries," vol. 64, pp. 3810–3816, 2009.

[5] E. A. Olevsky, S. Kandukuri, and L. Froyen, "Consolidation enhancement in spark-plasma sintering: Impact of high heating rates," *J. Appl. Phys.*, vol. 102, no. 11, pp. 0–12, 2007.

[6] D. M. Hulbert, A. Anders, J. Andersson, E. J. Lavernia, and A. K. Mukherjee, "A discussion on the absence of plasma in spark plasma sintering," *Scr. Mater.*, vol. 60, no. 10, pp. 835–838, May 2009.

[7] M. Suárez, a Fernández, J. L. Menéndez, R. Torrecillas, H. U. Kessel, J. Hennicke, R. Kirchner, and T. Kessel, "Challenges and Opportunities for Spark Plasma Sintering : A Key Technology for a New Generation of Materials," *Sinter. Appl.*, pp. 319 –342, 2013.

[8] R. Orrù, R. Licheri, A. M. Locci, A. Cincotti, and G. Cao, "Consolidation/synthesis of materials by electric current activated/assisted sintering," *Mater. Sci. Eng. R Reports*, vol. 63, no. 4–6, pp. 127–287, 2009.

[9] D. Leguillon and R. Piat, "Fracture of porous materials – Influence of the pore size," *Eng. Fract. Mech.*, vol. 75, no. 7, pp. 1840–1853, May 2008.

[10] R. E. Cooper, "TOUGHNESS - POROSITY PHENOMENA.pdf." Waterloo, CANADA, pp. 809–819, 1977.

[11] M. Hoffman, B. D. Flinn, R. K. Bordia, T. Chuang, and E. R. F. Jr, "Fracture of Alumina with Controlled Pores," vol. 57, pp. 2449–2457, 1998.

[12] R. L. Coble, "Diffusion models for hot pressing with surface energy and pressure effects as driving forces," *J. Appl. Phys.*, vol. 41, no. 12, pp. 4798–4807, 1970.

[13] R. L. Coble, "Sintering Crystalline Solids. I. Intermediate and Final State Diffusion Models," *J. Appl. Phys.*, vol. 32, no. 5, p. 787, 1961.

[14] F. B. Swinkels and M. F. Ashby, “A second report on sintering diagrams,” *Acta Metall.*, vol. 29, no. 2, pp. 259–281, 1981.

[15] S. J. Park, P. Suri, E. Olevsky, and R. M. German, “Master sintering curve formulated from constitutive models,” *J. Am. Ceram. Soc.*, vol. 92, no. 7, pp. 1410–1413, 2009.

[16] A. Jacota and P. R. Dawson, “Micromechanical unit problems for sintering and traction induced deformation,” vol. 36, no. 9, pp. 2551–2561, 1988.

[17] A. Jagota and P. R. Dawson, “Simulation of the Viscous Sintering of Two Particles,” vol. 77, pp. 173–177, 1990.

[18] J.Pan and A.C.F.Cock, “A numerical technique for the analysis of coupled surface and grain-boundary diffusion,” *Acta Mater.*, vol. 43, no. 4, pp. 1395–1406, 1994.

[19] J. Martínez-Herrera and J. Derby, “Viscous sintering of spherical particles via finite element analysis,” *J. Am. …*, 1995.

[20] H. Djohari, “A finite element model for the sintering of crystalline particles via vacancy diffusion,” University of M innesota, 2004.

[21] A. L. Maximenko and E. A. Olevsky, “Effective diffusion coefficients in solid-state sintering,” *Acta Mater.*, vol. 52, no. 10, pp. 2953–2963, 2004.

[22] Y. U. Wang, “Computer modeling and simulation of solid-state sintering: A phase field approach,” *Acta Mater.*, vol. 54, no. 4, pp. 953–961, 2006.

[23] M. M. Ristić and S. D. Milosević, “Frenkel’s Theory of Sintering,” *Sci. Sinter.*, vol. 38, no. 1, pp. 7–11, 2006.

[24] H. Djohari, I. M. Jorg, and J. J. Derby, “Transport mechanisms and densification during sintering- I Viscous flow versus vacancy diffusion,” *Chem. Eng. Sci.*, vol. 64, pp. 3799–3809, 2009.

[25] J. Bruchon, D. Pino-Muñoz, F. Valdivieso, and S. Drapier, “Finite Element Simulation of Mass Transport During Sintering of a Granular Packing. Part I. Surface and Lattice Diffusions,” *J. Am. Ceram. Soc.*, vol. 95, no. 8, pp. 2398–2405, Aug. 2012.

[26] E. a. Olevsky, “Theory of sintering: from discrete to continuum,” *Mater. Sci. Eng. R Reports*, vol. 23, no. 2, pp. 41–100, 1998.

[27] E. Olevsky and L. Froyen, “Constitutive modeling of spark-plasma sintering of conductive materials,” *Scr. Mater.*, vol. 55, no. 12, pp. 1175–1178, 2006.

[28] Z. a. Munir, U. Anselmi-Tamburini, and M. Ohyanagi, “The effect of electric field and pressure on the synthesis and consolidation of materials: A review of the spark plasma sintering method,” *J. Mater. Sci.*, vol. 41, no. 3, pp. 763–777, Feb. 2006.

[29] X. Wang, S. R. Casolco, G. Xu, and J. E. Garay, “Finite element modeling of

electric current-activated sintering: The effect of coupled electrical potential, temperature and stress," *Acta Mater.*, vol. 55, no. 10, pp. 3611–3622, 2007.

[30] C. Wang, L. Cheng, and Z. Zhao, "FEM analysis of the temperature and stress distribution in spark plasma sintering: Modelling and experimental validation," *Comput. Mater. Sci.*, vol. 49, no. 2, pp. 351–362, Aug. 2010.

[31] D. Tiwari, B. Basu, and K. Biswas, "Simulation of thermal and electric field evolution during spark plasma sintering," *Ceram. Int.*, vol. 35, no. 2, pp. 699–708, 2009.

[32] P. Mondalek, L. Silva, and M. Bellet, "A numerical model for powder densification by SPS technique," *Adv. Eng. Mater.*, vol. 13, no. 7, pp. 587–593, 2011.

[33] J. Zhang and A. Zavaliangos, "Discrete finite-element simulation of thermoelectric phenomena in spark plasma sintering," *J. Electron. Mater.*, vol. 40, no. 5, pp. 873–878, 2011.

[34] B. McWilliams and A. Zavaliangos, "Multi-phenomena simulation of electric field assisted sintering," *J. Mater. Sci.*, vol. 43, no. 14, pp. 5031–5035, 2008.

[35] E. A. Olevsky, V. Tikare, and T. Garino, "Multi-scale study of sintering: A review," *J. Am. Ceram. Soc.*, vol. 89, no. 6, pp. 1914–1922, 2006.

[36] B. McWilliams, J. Yu, and A. Zavaliangos, "Fully coupled thermal???electric-sintering simulation of electric field assisted sintering of net-shape compacts," *J. Mater. Sci.*, vol. 50, no. 2, pp. 519–530, 2014.

[37] C. Wolff, S. Mercier, H. Couque, and A. Molinari, "Modeling of conventional hot compaction and Spark Plasma Sintering based on modified micromechanical models of porous materials," *Mech. Mater.*, vol. 49, pp. 72–91, 2012.

[38] M. Lugman, "MULTIPHYSICS MODELING OF THE SPARK PLASMA SINTERING (SPS) PROCESS," king fahad university of petroleum & minerals, 2014.

[39] K. Sairam, J. K. Sonber, T. S. R. C. Murthy, C. Subramanian, R. K. Fotedar, P. Nanekar, and R. C. Hubli, "Influence of spark plasma sintering parameters on densification and mechanical properties of boron carbide," *Int. J. Refract. Met. Hard Mater.*, vol. 42, pp. 185–192, Jan. 2014.

[40] E. a. Olevsky, C. Garcia-Cardona, W. L. Bradbury, C. D. Haines, D. G. Martin, and D. Kapoor, "Fundamental Aspects of Spark Plasma Sintering: II. Finite Element Analysis of Scalability," *J. Am. Ceram. Soc.*, vol. 95, no. 8, pp. 2414–2422, Aug. 2012.

[41] D. Giuntini, E. A. Olevsky, C. Garcia-Cardona, A. L. Maximenko, M. S. Yurlova, C. D. Haines, D. G. Martin, and D. Kapoor, "Localized overheating phenomena and optimization of spark-plasma sintering tooling design," *Materials (Basel).*,

vol. 6, no. 7, pp. 2612–2632, 2013.

[42] B. Berger, “the Importance and Testing of Density / Porosity / Permeability / Pore Size for Refractories,” *Refractories*, pp. 111–116, 2010.

[43] A. Kurşun, E. Bayraktar, and H. Enginsoy, “Experimental and Numerical Study of Alumina Reinforced Aluminium Matrix Composites: Processing, Microstructural Aspects and Properties,” *Compos. Part B*, no. January, 2016.

[44] A. H. Clausen, T. Børvik, O. S. Hopperstad, and A. Benallal, “Flow and fracture characteristics of aluminium alloy AA5083-H116 as function of strain rate, temperature and triaxiality,” *Mater. Sci. Eng. A*, vol. 364, no. 1–2, pp. 260–272, 2004.

[45] E. Semb, “Behavior of Aluminum at Elevated Strain Rates and Temperatures,” no. June, 2013.

[46] J. R. P. CARREKER and J. W. R. HIBBARD, “TENSILE DEFORMATION OF ALUMINUM AS A FUNCTION OF TEMPERATURE, STRAIN RATE, AND GRAIN SIZE.” 1955.

[47] J. E.hatch, *Aluminum, prperties and physical metallurgy*, Subsequent. Ohaio: American society for metals International, 1984.

[48] M. Deighton, *Deformation and fracture mechanics of engineering materials*, 5th editio., vol. 5, no. 4. Wiley & sons, 1984.

[49] E. a. Olevsky *, B. Kushnarev, a. Maximenko, V. Tikare, and M. Braginsky, “Modelling of anisotropic sintering in crystalline ceramics,” *Philos. Mag.*, vol. 85, no. May 2013, pp. 2123–2146, 2005.

[50] R. L. Coble, “A Model for Boundary Diffusion Controlled Creep in Polycrystalline Materials,” *J. Appl. Phys.*, vol. 34, no. 6, p. 1679, Jun. 1963.

[51] S. T. Pai and J. P. Marton, “Electromigration in metals,” *Can. J. Phys.*, vol. 55, no. 2, pp. 103–115, Jan. 1977.

[52] M. Lin and C. Basaran, “Electromigration induced stress analysis using fully coupled mechanical-diffusion equations with nonlinear material properties,” *Comput. Mater. Sci.*, vol. 34, no. 1, pp. 82–98, 2005.

[53] H. J. Frost and Michael F Ashby, *Deformation-Mechanism Maps, The Plasticity and Creep of Metals and Ceramics*, 1st ed. Pergamon Press, 1982.

[54] S. Doi, “the Mechanical Properties of Porous Aluminum Using,” vol. 1580, 2013.

Appendices

Appendix A: Material properties

Table A - 1. Alumina properties

Property	value	unit
Electrical conductivity	$1 * 10^{-8}\left(\frac{1-\theta}{1+2\theta}\right)$	S/m[40]
Thermal conductivity	$\left(\frac{65181330.4+T}{-669628.8+8175.85T}\right)(1-1.5\theta-0.5\theta^2)$	W/(m.K) [40]
Heat capacity	$\left(\frac{777.025T}{249.4+T}+\frac{790.15}{249+T}+0.008T\right)(1-\theta)$	J/(kg.K) [40]
Density	$4000(1-\theta)$	Kg/m^3 [40]
Surface energy	1.12	J/m^2 [40]
Atomic volume	$4.25*10^{-29}$	m^3[40]
Activation energy for power-law creep	330	kJ/mol[40]
Power-law creep exponent	0.333	1[53]

Table A - 2. Aluminium properties

Property	value	unit
Electrical conductivity	$(80.632 * \mathrm{T}^2 - 140325\mathrm{T} + 7 * 10^7)(-0.616\theta^2 - 0.3995\theta + 1.013)$	S/m[47]
Thermal conductivity	$-4 * 10^{-10}\mathrm{T}^4 + 10^{-6}\mathrm{T}^3 - 0.0012\mathrm{T}^2 + 0.5307\mathrm{T} + 161$	W/(m.K)[47]
Heat capacity	$(0.5077 * \mathrm{T} + 746.13)(1 - \theta)$	J/(kg.K)
Density	$2700(1 - \theta)$	Kg/m^3 [54]
Surface energy	1.12	J/m^2[27]
Atomic volume	$1.66*10^{-29}$	m^3[27]
Activation energy for power-law creep	120	kJ/mol[27]
Power-law creep exponent	0.227	1[53]

Appendix B: Matlab code

Matlab code for evaluating porosity value from SEM image

```
% binary image tester
A=imread('A88.jpg');
nopi=im2bw(A);
[rows columns numberOfColorChannels] = size(nopi);
nop = rows*columns*numberOfColorChannels;
%AW=imread('A11W.jpg');
%AWA = im2bw(AW,0);
%CC=bwarea(AWA);

for i=0.311:0.001:0.319
   B = im2bw(A,i);
   redAndBlueChannel = 255 * uint8(B);
   greenChannel = 255 * ones(size(B), 'uint8'); % Green Everywhere.
   rgbImage = cat(3, redAndBlueChannel, greenChannel, redAndBlueChannel);
   figure, imshow(rgbImage)
   C=bwarea(B);
   greenarea=nop-C;
   porosity=greenarea/nop;
   title(i)
   xlabel(porosity)
   ylabel('A8')
```

```
    % save the figure
    %baseFileName = sprintf('Figure %d',i);
    % Specify some particular, specific folder:
    %fullFileName = fullfile('D:\KFUPM LAST DESKTOP\kfupm\TERM
151\Experimental study\porosity images\S1 - 3 - p1 - 3\CUT\A66', baseFileName);
    %figure; % Activate the figure again.
    %saveas(figure,i.tif); % Using export_fig instead of saveas.
end
figure, imshow(A)
```

Vitae

Name	:Mohamed Abdelmageed Mohamedzein Abdelhameed
Nationality	:Sudanese
Date of Birth	:3/20/1985
Email	:mageedoo@windowslive.com
Address	:KFUPM, AL-Dhahran, 31261, Saudi Arabia
Academic Background	:B.Sc in mechanical engineering from university of khartoum

Research papers

1- A. Yousif, **M. A. M. Zein**, M. E. A. Elsayed, "Computational Analysis of a Truss Type Fuselage", Applied Mechanics and Materials, Vol. 225, pp. 183-188, 2011 **(Presented)**

2- Abul Fazal M. Arif, **Mohamed Abdelmageed**, Homam Jumaa, "Multi-physics modeling of densification during CAPAD/SPS process" in Proceedings of the 2016 International Mechanical Engineering Congress & Exposition IMECE2016, Phonex, AZ, USA, November 11-17-2016 **(Accepted)**